Evaluation and method establishment of biological and ecological effects of DDT: Imaging technique and molecular analysis approach

（殺虫剤 DDT の生体・生態影響評価とその手法の確立：イメージングと分子解析アプローチ）

Kodai Motohira

Table of contents

Investigation of dichlorodiphenyltrichloroethane (DDT) on xenobiotic enzyme disruption and metabolomic bile acid biosynthesis in DDT-sprayed areas using wild rats

Comparison of micro-computed tomography (micro-CT), multiomic analysis, and classical methods for evaluating hepatomegaly induced by phenobarbital

The evaluation of DDT's effect using rats of three generations based on DDT-sprayed areas

Abbreviations

8-OHdG	8-hydroxydeoxyguanosine
Abcb	ATP binding cassette subfamily B member 11
Abcc2	ATP binding cassette subfamily C member 2
Actb	beta actin
AhR	aryl hydrocarbon receptor
AOP	adverse outcome pathway
Baat	bile acid CoA:amino acid N-acyltransferase
Bax	BCL2 associated X
BUN	blood urea nitrogen
CAR	constitutive androstane receptor
Cat	catalase
Ccnb	cyclin B
cDNA	complementary DNA
Cer	ceramide
CL	cardiolipin
Cpt1a	carnitine palmitoyltransferase 1A
CRE	creatinine
CT	computed tomography
CV	coefficient of variation
CYP	cytochrome P450
DBIL	direct bilirubin
DDD	dichlorodiphenyldichloroethane
DDE	dichlorodiphenyldichloroethylene
DDT	dichlorodiphenyltrichloroethane
DDTs	DDT, DDE and DDD
DG	diacylglycerols
DIABLO	Data Integration Analysis for Biomarker discovery using Latent variable approaches for Omics studies
DNA	deoxyribonucleic acid
ECD	electron capture detector
ESI	electrospray ionization
FA	fatty acids
Fasn	fatty acid synthase
FDR	false discovery rate

GC-MS/MS	gas chromatography with mass spectrometer
GOT	aspartate aminotransferase
GPT	alanine transaminase
Gpx1	glutathione peroxidase 1
HDLC	high-density lipoprotein cholesterol
HE stain	hematoxylin and eosin staining
HexCer	hexosylceramides
Hmox1	heme oxygenase 1
HPLC	high performance liquid chromatography
HPLC-qToF/MS	HPLC with Time-of-flight mass spectrometer
HSD	hydroxysteroid dehydrogenase
IARC	International Agency for Research on Cancer
IRS	indoor residual spray
KEGG	Kyoto Encyclopedia of Genes and Genomes
LOESS	locally estimated smoothing function
MB-PLS	multiblock partial least squares regression
MC	measuring cylinder
MEGA	Molecular Evolutionary Genetics Analysis
NADH	nicotinamide adenine dinucleotide
NADPH	nicotinamide adenine dinucleotide phosphate
NCBI	National Center for Biotechnology Information
NOAEL	no-observed-adverse-effect-level
Nrf2	nuclear factor erythroid 2-related factor 2
PA	phosphatidic acid
PC	phosphatidylcholine
PC1	first principal components
PC2	second principal components
PCA	principal component analysis
PC-O	ether-linked phosphatidyl-cholines
PCR	polymerase chain reaction
PE	phosphatidylethanolamine
Pemt	phosphatidylethanolamine N-methyltransferase
PE-O	ether-linked phosphatidyl-ethanolamine
PEtOH	phosphatidylethanol
PI	phosphatidylinositol
PMDA	Pharmaceuticals and Medical Devices Agency

PMeOH	phosphatidylmethanol
POPs	persistent organic pollutants
PPAR	peroxisome proliferator-activated receptor
PXR	pregnane X receptor
QA	quality assurance
QC	quality control
qPCR	quantitative polymerase chain reaction
Rela	RELA proto-oncogene, NF-kB subunit
RNA	ribonucleic acid
RNS	reactive nitrogen species
ROS	reactive oxygen species
RSD	relative standard deviation
SD	standard deviation
Sod1	superoxide dismutase 1
sPLS	sparse partial least squares regression
Srebp1	sterol regulatory element binding protein-1
SULT	sulfotransferase
T11	11^{th} thoracic vertebrae
TBIL	total bilirubin
TCHO	total cholesterol
TCMX	2,4,5,6-tetrachloro-m-xylene
TCPOBOP	4-bis[2-(3,5-dichloropyridyloxy)]benzene
TG	triglyceride
Tgfb1	transforming growth factor, beta 1
Txnrd1	thioredoxin reductase 1
UGT	uridine diphosphate glucuronosyltransferase
UV	ultraviolet
WHO	World Health Organization
ww	wet weight
YAP	Yes-Associated Protein

Notes

List of publications related to the dissertation

1. Motohira K, Yohannes YB, Yoshinori Ikenaka Y, Eguchi A, Nakayama SMM, Wepener V, Smit NJ, van Vuren JHJ, Ishizuka M. Investigation of dichlorodiphenyltrichloroethane (DDT) on xenobiotic enzyme disruption and metabolomic bile acid biosynthesis in DDT-sprayed areas using wild rats, J Vet Med Sci, in press.

2. Motohira K, Yohannes YB, Ikenaka Y, Ogawa T, Nakayama SMM, Wepener V, Smit NJ, van Vuren JHJ, Ishizuka M. Gene expression profile of sex-linked metabolic enzyme in rats inhabiting dichlorodiphenyltrichloroethane (DDT)-sprayed areas of South Africa, Jpn J Vet Res, in press.

Preface

In this thesis, the toxicity of dichlorodiphenyltrichloroethane (DDT) was evaluated using field samples where DDT is currently sprayed along with an *in vivo* animal study, and a new strategy to evaluate its hepatic toxicity was developed.

DDT is well known pesticide which was used worldwide. However, owing to its toxicity to the environment and several animal species, DDT use has been banned in many countries. Currently, only few developing countries are using DDT for vector control against malaria. High environmental persistence has been reported for DDT and filed surveys have revealed bioaccumulation of DDT in various animal species. However, DDT use is essential to control malaria in some countries. Therefore, both the benefits and risks of DDT need to be carefully considered. However, several concerns need to be noted: i) although the benefits (vector control) of DDT are well-understood, risk assessments in wild animals remain limited, ii) novel toxicities overlooked by classical toxicity tests are still being revealed, iii) and effective biomarkers reflecting the health conditions under DDT toxicity remain lacking.

Therefore, in my PhD thesis, I aimed to (1) evaluate the biological and ecological effect of DDT in the sprayed areas, (2) develop a new method development to evaluate toxic chemicals *in vivo* using imaging and molecular techniques, (3) apply the developed method to study DDT-induced toxicity *in vivo*, and (4) summarize the risks of DDT use and the future prospects.

Chapter 1 of this thesis describes the history of DDT, focusing on its benefits and risks in the environment and human life, and introduces the methodology for evaluating chemical toxicity. Further, the main purpose, goal, and expected outcome of this thesis are included at the end of this chapter.

Chapter 2 describes the evaluation of DDT-induced environmental effects and its metabolites using molecular analyses of wild rodents living in a DDT-sprayed area in South Africa. This is discussed in two thematic areas. ***2.1***. The accumulated DDT levels in wild rodents are revealed. I then describe the assessment of DDT-induced ecological effects on sex-linked gene expression in wild rats. ***2.2***. I further investigated the biological

effects of DDT and candidate biomarkers in wild rats using quantitative PCR and metabolome analysis. (Motohira K et al, J Vet Med Sci, and Motohira K et al,.Jpn J Vet Res, in press.)

In Chapter 3, I suggest a new methodology for evaluating liver toxicity using computed tomography (CT) and multiomics analysis *in vivo* using an animal model.

In Chapter 4, I describe the effect of DDT on rat liver in multigeneration and DDT-sprayed field-reflecting *in vivo* experimental analyses.

Chapter 5 summarizes all the studies in this thesis and provides future perspectives based on the findings presented in this thesis.

Chapter 1:

General Introduction

Chapter 1: General Introduction

1. Positive and Negative Impact of Environmental Pollution

Environmental pollution is one of the biggest concerns facing humanity today. Further, environmental pollution has been considered to contribute to 9 million premature deaths in 2015. Most damages are considered to occur in developing countries (Landrigan et al., 2018). Human activity significantly effects environmental pollution directly; however, the lockdown imposed during the COVID-19 pandemic significantly improved environmental quality and reduced NO_2 (air pollutant) levels (Muhammad et al., 2020). However, the problems of environmental pollutants are complicated because they have both risks and benefits to humans.

I consider pesticides as the typical case to discuss the duality of pollutants. Pesticides are chemicals used to protect agricultural produce and public health by repelling or killing pests (Alavanja, 2009). Thus, the benefits of pesticides are obvious. With the increasing global population, the demand for food production is also increasing. However, in 20 years from 1990, the forest area has decreased significantly, and further generation of new cultivation regions using natural areas is not desirable for protecting biodiversity. In such a situation, pesticides are crucial for ensuring a stable food supply as they increase agricultural production remarkably (Crist et al., 2017; Tudi et al., 2021). Loss of fruits and vegetables was estimated to reach 78% and 54%, respectively, when grown without pesticides. Further, prohibition of pesticides can decrease agricultural production, and eliminate more than 100,000 jobs in the USA (Zhang et al., 2011).

Pesticides are not only used in agriculture but also to control infectious diseases. Vector-borne diseases such as malaria and dengue are still raging, especially in developing countries; thus, vector control is more effective than human medicine to control these diseases. Pesticides play an important role in vector control (Wilson et al., 2020). Owing to these advantages, the amount of pesticides consumption has dramatically increased between 1960 and 2000 (Zhang et al., 2011). Contrary to these beneficial effects of pesticides, many researchers have alerted their risks to both human and environmental health (Tudi et al., 2021; Zhang et al., 2011). However, most pesticide users do not mind the risks to both human health and the environment in some countries. Thus, inappropriate

use of pesticides is considered to increase its adverse effects in developing countries (Sharma Msc et al., 2012).

Overall, although pesticides have obvious benefits to human society, they pose a potential risk to human and environmental health. As pesticide use is necessary, the balance between their benefits and risks needs to be discussed in detail for their appropriate use.

2. Discovery and Spread of DDT

DDT is an organochlorine with chlorine-substituted aliphatic or aromatic rings in its structure and was discovered its insecticidal efficiency in the 1930s (Jayaraj et al., 2016; Sharma et al., 2020). Since the development of synthesized organic pesticides, they were mainly categorized as carbamates, organophosphates, and organochlorides (Zhang et al., 2011). DDT kills various pest species by attacking the sodium channels and is widely used because of its high insecticidal efficiency and low cost (Sharma et al., 2020; World Health Organization, 1979). DDT was first commercially sold in 1945 and its use dramatically spread in many countries. In 1974, DDT production was recorded to be 6,000 tons worldwide (World Health Organization, 1979).

The first effect of DDT on the human society was improved human hygiene. The history of DDT use for infectious disease control is quite long; in the second world war, DDT was used to repel lice and prevent the spread of typhus. At this time, DDT was directly applied all over the human body (Bailey, 2022). The effect of DDT on disease control was highly appreciated; Paul Müller, who discovered the high insecticidal efficiency of DDT, was thus awarded the Nobel Prize for Physiology and Medicine in 1958 (Yang et al., 2017). One of the most famous achievements of DDT is its role in malaria control worldwide. The effectiveness of DDT on malaria control has been reported in many countries including, South-Africa (Channa et al., 2012), Sri Lanka (Simac et al., 2017), Italy (Benjamin Roche et al., 2018). DDT is used for controlling anopheline mosquitoes, which transmit malaria, and remains the main pesticide used for spraying operations (studied between 2010 and 2019) (van den Berg et al., 2021, 2017).

3. Environmental Contamination of DDT

DDT is metabolized into DDE and DDD, and all of them persist in both the environment and animal bodies (Eskenazi et al., 2018; Kitamura et al., 2002). The DDE/DDT ratio is useful to understand recent exposure; a high DDT concentration reflects current exposure. DDE is biomagnified as the food chain advances; thus, top consumers are likely to accumulate high concentrations of DDE (Deribe et al., 2013). Regardless of the current DDT use, many countries and areas have reported DDT and DDE contamination in human and environmental samples. When focusing on human blood levels at a global scale, DDE can reach up to 300 ng/g lipid weight, depending on countries, even though countries banned the usage of DDT in the 1970s, but its concentration has decreased compared with that in 1950–1969. However, the available information in malaria endemic countries is limited, and the DDE concentration and its transition in humans in these countries remains unclear (Koureas et al., 2019). The situation of limited information in malaria endemic countries is also applicable to wild animals. A previous study showed that most surveys of raptors on DDT only covered North America and Europe (Padayachee et al., 2023). However, among malaria endemic countries, South Africa has published several surveys related to DDT contamination using wide variety of samples from water (Barnhoorn et al., 2009), fish (Gerber et al., 2016) amphibians (Viljoen et al., 2016), birds (Bouwman et al., 2019), and humans (Channa et al., 2012). Most surveys indicate high DDT concentrations in South Africa and indicate concerns regarding its risk to the environment and humans. These wide surveys from the same area can help understand DDT biomagnification and reveal the source of DDT contamination in humans and animals.

4. Toxicity of DDT

Section 2 briefly summarized the effectivity of DDT for infectious disease control. However, contrary to its benefits, the environmental problems of DDT started to raise concerns in the 1960s. The publication of *Silent Spring* in 1962 presented the environmental risks associated with pesticides and accelerated studies related to environmental pollutants. DDT was one of main topics in *Silent Spring*. Sweden began analyzing DDT early, in 1964, for studying its environmental impacts (Bouwman et al.,

2013). As the environmental problems of DDT were revealed along with the emergence of DDT-resistant mosquitoes, its use was gradually prohibited in various countries like Sweden in 1970 and the USA in 1972, followed by many developed counties (Walter J Rogan and Aimin Chen, 2005). Finally, DDT was listed as a persistent organic pollutant (POP) under the Stockholm Convention, and its use was banned globally since 2004 with permitted limited use in indoor residual spraying (IRS) for disease control especially in developing countries (World Health Organization, 2011). However, some countries used DDT illegally even during the ban period. Improper use of agrichemicals such as pesticides has been reported in some developing countries (Jayaraj et al., 2016). Since Sweden started the research program on DDT, its ecological and biological toxicity has been revealed; this section briefly summarizes these effects in birds and mammals.

DDT and DDE have a wide range of toxicity affecting the immune system, apoptotic pathways and so on, but one of the most well-known effects on both the environments and humans is endocrine disruption. DDE is an androgen receptor antagonist that induces alterations in steroid hormones such as testosterone and estradiol (Bornman et al., 2018; Burgos-Aceves et al., 2021). The effect of DDT on birds and fish has been long studied; for example, a report in 1947 indicates the relationship between disturbed bird populations and DDT in DDT-sprayed areas (George and Mitchell, 1947). The estrogenic effect of *o,p'*-DDT (an isomer of DDT) causes reproductive disorders such as eggshell thinning in birds (Kamata et al., 2020), and this phenomenon was widely observed in DDT-sprayed regions (Bouwman et al., 2019). In experimental animals, several toxicities have been reported, including reproductive developmental and neurodevelopmental changes including acute toxicity and necrosis as well as hypertrophy and tumors in the liver in chronic toxicity (Agency for Toxic Substances and Disease Registry, 2022). DDT is a known carcinogen, and the International Agency for Research on Cancer (IARC) has classified DDT under Group 2A, which is probably carcinogenic to humans. However, the evaluation of DDT toxicity remains ongoing. As of 2015, the IARC has not suggested any association between breast cancer and DDT concentration (International Agency for Research on Cancer, 2015). However, after the IARC report, several studies have discussed the relationship between breast cancer and DDT (Krigbaum et al., 2020; Samira and Kadmiri, 2021). Epidemiological studies targeting humans have shown various possible DDT toxicities; however, inconsistent findings have

been reported among studies, and several reviews suggest that speculating the role of DDT to cancer development would be premature (Agency for Toxic Substances and Disease Registry, 2022; Beard, 2006; Samira and Kadmiri, 2021).

5. Various Methods and Markers to Evaluate Chemical Toxicity

Nowadays regulatory toxicology is crucial for the management and safe use of chemicals; toxicity tests evaluate their adverse effects (Fischer et al., 2020). Since the 1970s, various studies have reported several toxicities of DDT. However, more than 50 years after the publication of *Silent Spring*, new toxicities of DDT are still being found. For example, a mutigenerational exposure test of DDT showed that even though rats were not directly exposed of DDT, ancestral DDT exposure induced disease in their sexual organs and caused obesity in experimental rats. Epigenetic changes were considered the possible mechanism for this effect (King et al., 2019). Although the concept existed previously, the epigenetics boom began during the 1990-2000s (Peixoto et al., 2020). Thus, the effect of DDT on epigenetics was not considered during era of *Silent Spring* when DDT was actively used. In another example of pesticide, no-observed-adverse-effect-level (NOAEL), and even lower concentration of clothianidin (neonicotinoid pesticides) altered mouse behaviors in several tests including open field and elevated plus maze tests (Kubo et al., 2022).

Recently, new findings of effects undetected by classical methods have been revealed. In 40 years, toxicological risk assessment has not changed drastically; thus, the current animal-based toxicity test might provide false-positive or false-negative results along with statistically and biologically incorrect results (Fischer et al., 2020). Thus, new approaches or alternative methods for evaluating chemical toxicities have been investigated, such as *in vitro* cell models (Astashkina et al., 2012), *in silico* computational methods, deep learning (Mayr et al., 2016; Raies and Bajic, 2016), and real-time imaging (Hirai et al., 2022; Shuhendler et al., 2014). For example, the combination of fluorescence resonance energy transfer and chemiluminescence resonance energy transfer revealed chemical induced hepatotoxicity in mice by allowing visualization of reactive oxygen species (ROS) and reactive nitrogen species (RNS) in real-time (Shuhendler et al., 2014). These approaches also contribute directly to the three Rs (Reduce, Refine, Replace) in

animal experimentation and need to be accelerated in the field of toxicology.

Especially, in the case of evaluating environmental pollutants, the biomarkers reflecting their health effects are useful for evaluating the effects of chemicals and biomonitoring surveys. For example, blood acetylcholinesterase levels and 8-hydroxydeoxyguanosine (8-OHdG) have been used for assessing the effects of organophosphates and genotoxic chemicals, respectively. Various biomarkers have already been developed for assessing environmental pollution in humans and for environmental biomonitoring (Lionetto et al., 2019). Currently, metabolomics approaches have accelerated the discovery of new candidate biomarkers. Metabolomics can comprehensively visualize the changes in metabolites caused by chemical exposure in the body (Ramirez et al., 2013). Several reviews have already reported the candidate biomarkers associated with environmental pollutants in humans and experimental animals (Dai et al., 2020; Sun et al., 2022).

6. Benefits and Risks of DDT

This thesis targets the pesticide DDT, which has a long usage history in the control of infectious diseases; its positive impact has been evaluated in many countries. In particular, South Africa experienced that stopping the use of DDT increased the number of malaria patients, whereas its reintroduction recovered the malaria situation (Channa et al., 2012). Simultaneously, the biological and ecological toxicity of DDT is of significant concern worldwide as mentioned above. DDT has both benefits (for controlling malaria) and risks (toxicity to the environment, humans, and animals). Thus, I consider DDT to be the best model chemical to discuss appropriate chemical use and develop methods for toxicity evaluation.

The purpose of this thesis

This thesis aimed to evaluate the biological and ecological effects of DDT, to establish new approaches to evaluate chemical toxicity using imaging and molecular analysis, and to reevaluate DDT toxicity using the newly developed method. I approached these goals using wild rats collected in a field survey of a DDT-sprayed area and experimental rats exposed to DDT and phenobarbital. Phenobarbital is a sedative and antiseizure drug (https://pubchem.ncbi.nlm.nih.gov/) and was used as an additional model chemical for method evaluation. Thus, the main objectives of this thesis were as follows:

1. Elucidation of the DDT pollution levels in each organ and disturbance in the mRNA expression of sex-linked cytochrome P450 families in wild rats living in a DDT-sprayed area in South Africa

2. Investigation of mRNA expression related to bile acid biosynthesis and steroidogenesis, as well as plasma metabolome levels such as bile acid to reveal the effect of DDT as an endocrine disrupter using wild rats in a DDT-sprayed area.

3. Demonstration of the utility of micro-CT in toxicity testing to evaluate chemical-induced hepatomegaly and finding a biomarker to help reveal the biological process using multiomics analysis in experimental rats (Wistar rat) exposed to phenobarbital.

4. Demonstration of the effects of DDT using the newly developed method in 3 and using multiple generations of Wistar rats exposed to low concentrations of DDT.

The goal of this thesis and expected outcome

The benefits of DDT are well-known, but the evaluation of its risk remains under progress worldwide. This study will provide crucial information about the current DDT pollution levels and its effect on mammals in DDT-sprayed areas. This research will also reveal the effects of DDT at a molecular level using DDT-accumulated wild rats. These data are essential for understanding the condition of in mammals in the field and the adverse outcome pathway (AOP) of DDT. This molecular study also facilitates further approaches to find possible biomarkers reflecting DDT toxicity in sprayed areas. Further, this study uses wild rodents living in South Africa, and such samples and data are valuable to discuss proper vector control strategies in malaria endemic countries. This study also presents a new toxicity test using the techniques of CT and multiomics analysis. This approach in the evaluation of chemical toxicity is pioneering and enables toxicity testing throughout the lifetime of an experimental animal. My approach can be applied for DDT as well as other pesticides with toxic effects in mammals. As these techniques are not common in the field of toxicology, this study provides new insights into the fields of toxicology and pharmacology. Finally, this study provides initial results connected to developing new standards for sustainable toxicity testing and the safe use of chemicals.

Chapter 2.1:

Gene expression profile of sex-linked metabolic enzyme in rats inhabiting dichlorodiphenyltrichloroethane (DDT)-sprayed areas of South Africa

Gene expression profile of sex-linked metabolic enzyme in rats inhabiting dichlorodiphenyltrichloroethane (DDT)-sprayed areas of South Africa

Highlight

- Tissue distribution of DDT and its metabolites were investigated in wild rats living in a DDT-sprayed area in South Africa.
- The liver had a unique ratio of DDT and its metabolites compared with that in other organs.
- Quantitative PCR revealed that DDTs affect sex-linked metabolic enzymes, especially in females.
- This research assessed DDT toxicity using wild rodents; these findings might augment *in vivo* studies on DDT.

Abstract

Dichlorodiphenyltrichloroethane (DDT) is still used in some developing countries to control vectors such as malaria, despite being highly toxic to humans and animals. Cytochromes P450 (CYPs) are enzymes that break down xenobiotics such as DDT. However, only few studies have investigated DDT effects on biological organisms. We collected wild rats in DDT indoor sprayed (IRS) and non-IRS residential areas in the KwaZulu-Natal province in South Africa, and several organs, including the liver, kidney, brain, spleen, and lung, were collected. DDT levels were determined using GC-ECD, and their effects on 12 metabolic enzymes in the liver were assessed using qRT-PCR. The liver showed the highest total median concentrations of DDT and its metabolites. Sex-linked gene expression differences disappeared in the IRS region, but the same difference was seen in the rat livers in the non-IRS region, with female rats having low expression levels, suggesting that DDT may affect the expression of some CYP genes in different ways depending on the extent of exposure. As only a few studies have investigated gene expression patterns of metabolic enzymes in terrestrial mammals, the findings of this study will be useful for future *in-vivo* studies employing rats and field samples.

Keywords: DDT, CYP, South Africa, sex-linked, nuclear receptor

1. Introduction

Dichlorodiphenyltrichloroethane (DDT) is a pesticide used in developing countries with certain restrictions owing to environmental persistence and its adverse effects on mammals, including humans, and the environment. The Republic of South Africa, where our study was conducted, still uses DDT in indoor residual spraying (IRS) (Wolmarans et al., 2021). However, various investigations have indicated DDT toxicity in mammals, and DDT has been classified as a carcinogen and an endocrine disruptor (Water J Rogan and Aimin Chen, 2005). In 2015, the International Agency for Research on Cancer (IARC) re-evaluated the carcinogenicity of DDT and categorized it into Group 2A (probably carcinogenic to humans). Higher testosterone and estradiol levels and decreased follicle-stimulating hormone levels were found in the blood of highly DDT exposed males in a field study conducted in the Republic of South Africa (Bornman et al., 2018). Although DDT is required in some countries to control mosquito-borne diseases, the advantages and risks to human health and the environment should be carefully considered (Water J Rogan and Aimin Chen, 2005).

DDT can be metabolized into dichlorodiphenyldichloroethylene (DDE) and dichlorodiphenyldichloroethane (DDD), both of which have high potential to accumulate in animals, humans, and the environment over time and can travel vast distances in the upper atmosphere (Agency for Toxic Substances and Disease Registry, 2002; Kitamura et al., 2002). While microorganisms are responsible for the environmental DDT degradation, DDT has a long half-life and persists in the environment for a long period (Agency for Toxic Substances and Disease Registry, 2002). Previous studies have employed wild rodents to assess the likely exposure levels on individuals living in IRS areas in countries where DDT is used as a malaria vector control (Motohira et al., 2019; Yohannes et al., 2017). As rodents commonly share habitats with people, especially in houses, it is assumed that they have human-like exposure patterns, including exposure to high amounts of DDT in IRS areas. Previous studies have reported high concentrations of DDTs in house rats from IRS areas, and *para*, *para*-isomers (*p,p′*-DDT, *p,p′*-DDE, and *p,p′*-DDD) were found at higher liver tissue concentrations than *ortho*, *para*-isomers (*o,p′*-DDT, and *o,p′*-DDD) (Motohira et al., 2019; Yohannes et al., 2017).

Phase 1 metabolic enzymes, such as cytochrome P450 (CYP), and phase 2 metabolic enzymes, such as uridine 5'-diphospho-glucuronosyltransferase (UGT) and sulfotransferase (SULT), are involved in the metabolism and excretion of numerous exogenous chemicals (Foti and Dalvie, 2016). These enzymes also play roles in homeostasis, such as regulating the levels of activated hormone concentration in mammalians (You, 2004). However, several chemical compounds can easily and significantly upregulate these enzymes. Evidence from various studies implies that DDT activates metabolic enzymes and their activity (Chanyshev et al., 2014; Harada et al., 2016; Mrema et al., 2013). By activating these metabolic enzymes, human or animal bodies can oxidize or conjugate exogenous chemicals and excrete them from their bodies. However, it has been noted that inducing these enzymes can have negative health consequences. For example, overexpression of CYP2B can produce reactive oxygen species that potentially exacerbate tumors in the liver (Hrycay and Bandiera, 2015). These biological processes, in turn, are mediated by nuclear receptors such as the constitutive androstane receptor (CAR), pregnant X receptor (PXR), peroxisome proliferator-activated receptor alpha (PPARa), and transcription factor like aryl hydrocarbon receptor (AhR) (Hakkola et al., 2020; Meech et al., 2019).

Male rats or mice have mostly been used for toxicity tests as the sexual cycle can cause larger variations in female rats. However, one study found that after exposure to 100 mg/kg DDT, males and females had distinct reactions, such as a larger induction of CYP3A1 in females (31.9-fold) than in males (1.3-fold). However, the trend of CYP2B1 upregulation was the same for females and males at 19.3- and 19.4-fold induction, respectively (Sierra-Santoyo et al., 2000). These disparities highlight the importance of considering toxicity for both sexes. This study focuses on wild rats living in DDT-sprayed areas. It aims to investigate if there are links between DDT pollution levels and gene expression of nuclear receptors and metabolic enzymes in both males and females.

2. Materials and Methods

2.1 Sample collection and preparation

Rats from a sample set collected in South Africa that has been described in a previous paper were used (Yohannes et al., 2017). Briefly, eight and ten rats were captured

using gauze traps with food as bait in residential areas in the KwaZulu-Natal province from IRS and non-IRS areas in April 2014, respectively. The sampling area is provided in the previous paper (Yohannes et al., 2017). The application of DDT in the IRS program areas was within the target range set by the IRS program: 75% DDT wettable powder was applied at a dosage of 2 g active ingredient per square meter. Following capture, the rodents were euthanized, their body weight and sex were determined, and were subsequently dissected to collect the brain, lung, spleen, liver, and kidney, which were stored at −20℃ until DDT analysis. For RNA extraction, a small portion of the liver was excised and kept in RNAlater (Sigma-Aldrich, Saint Louis, MO, USA). The eyes were recovered and preserved in formalin to determine age.

2.2 Extraction and analysis of DDT and its metabolites

Analytical methodology, including the use of chemicals and reagents, instrumental analysis, and quality control procedures, are described in detail in Yohannes et al. (2013). Approximately 1–5 g of each tissue was mixed with anhydrous sodium sulfate, spiked with 10 ng of PCB77, and extracted with hexane/acetone (3:1, v/v) using a Soxtherm extractor (S306AK, Gerhardt, Germany). To obtain DDT and its metabolites (DDE and DDD), the extracts were concentrated and subjected to a Florisil (5% deactivated) glass column, with elution carried out by hexane:dichloromethane (7:3, v/v). The eluate was then concentrated to near dryness under a gentle nitrogen stream and redissolved in 100 μL n-decane. Before instrumental analysis, all extracts were treated with 2,4,5,6-tetrachloro-m-xylene (TC*m*X). DDTs (DDT, DDE, and DDD) were analyzed using a Shimadzu 2014 gas chromatography model equipped with a 63 Nickel μ−electron capture detector (ECD) and an ENV-8MS capillary column (30 m x 0.25 mm i.d. x 0.25 μm film thickness). The DDTs were identified by comparing their retention time with the corresponding standard. The correlation coefficients (r^2) of the calibration curves were all greater than 0.990. The mean DDT recovery for the spiked blanks was 60%. Thus, the DDT concentrations were calculated and corrected based on the recovery rate. Concentrations of DDTs were expressed as nanogram per gram of wet weight (ng/g ww).

2.3 Species identification and age estimation of wild rodents

Wizard® Genomic DNA Purification Kit (Promega Corporation, Madison, WI, USA) was used to recover genomic DNA from wild rodent liver tissues. Species were identified following the method of Robins et al. (2007), with some modifications. The cytochrome b-containing genome region was amplified using PrimeSTAR Max (Takara Bio Inc., Shiga, Japan) and the following primers (forward primer 5′-GGTGAAGGCTTCAACGCCAACCCTA-3′ and reverse primer 5′-TAGAATATCAGCTTTGGGTGTTGATGG-3′). Molecular Evolutionary Genetics Analysis (MEGA) 7 software was used to perform maximum-likelihood analyses on these sequences. *Rattus tanezumi* was the subject of this study.

Measuring the lens weight of rodents has provided researchers with a reliable indicator of their age. Thus, the formalin-preserved lens from each eye was dried for 48 hr at 50℃ and then weighed in pairs to estimate the rat's age using the equations [log Y = 1.00 + 0.023X] for male and [log Y = 1.05 + 0.023X] for female animals, where Y is the age in days and X is the total weight of both lenses in milligrams based on Tanikawa's protocol (Tanikawa, 1993). This protocol was developed for *Rattus rattus*, a species closely related to *R. tanezumi*, aged 20 to 1121 days. Commonly, both species are referred to as "black rats" (Lack et al., 2012). This study thus classified *R. tanezumi* as a "black rat" in our data analysis.

2.4 RNA extraction, cDNA synthesis, and quantitative real-time PCR

Total RNA was extracted from the liver samples of *R. tanezumi* using the Nucleospin RNA kit (Macherey-Nagel Düren, Germany) and the quality and amount of the extracted RNAs were evaluated using a Nanodrop-1000A spectrophotometer (Delaware, USA). The ReverTra Ace qPCR RT Kit (Toyobo, Osaka, Japan) was used to synthesize first-strand cDNA from RNA according to the manufacturer's protocol. Quantitative real-time PCR analysis of 12 metabolic enzymes and three nuclear receptor genes was performed on StepOne Plus Real-Time PCR system (Applied Biosystems) using cDNA and Fast SYBR Green master mix (Applied Biosystems, CA, USA). The primers used for the amplification are summarized in Table 2.1.1. Some of the primers used in this study were those used in previous studies (Asaoka et al., 2010; Kawase et al.,

2008; Liu et al., 2011; Luvizotto et al., 2010; Mei et al., 2004; Miksys et al., 2000; Petersson et al., 2007; Sonneveld et al., 2007). A 10 μL reaction mixture containing 5 μL Fast SYBR Green master mix, 300 nM forward and reverse primers, and 20 ng of cDNA was used for the PCR. The PCR protocol was 95°C for 20 s, followed by 40 cycles of 95°C for 3 s, and 60 °C (for all genes) for 30 s. The specificity of the reaction was verified by melt curve analysis. For each sample, the amount of gene expression was normalized against the housekeeping gene, *beta-actin*, and relative expression was calculated using the comparative CT method (ΔΔCT method). The lowest expressions of each gene in all rats were assigned a value of one and served as reference samples for calculation. Expression levels not identified and out of the range of primer efficiency were set to 0.5.

2.5 Statistics

JMP 16 (SAS Institute, NC, USA) software was used for all the statistical analyses, with a significant threshold of $p<0.05$. Both parametric and non-parametric approaches were used according to the sample size and normality of the data. Wilcoxon's test was used to compare DDT concentrations between sexes. For age differences between areas and sexes, both parametric (Tukey-Kramer's HSD test) and non-parametric (Steel-Dwass test) statistical analyses were performed. To bring the distribution of gene expression closer to normal, the natural logarithm was applied. Both parametric (Welch's t-test) and non-parametric (Wilcoxon's exact test) statistical analyses were used to compare gene expression between sexes. We used $p<0.05$ from both analyses as significance. The significance of the correlative analysis between nuclear receptor and metabolic enzymes gene expression was tested using Spearman's correlation test.

3. Results

The information on the sex, weight, age, and collected area for each *R. tanezumi* rat is summarized in Table 2.1.2. There were eight male and ten female rats in total and their age ranged from 39–356 days. Ten rats were collected from the IRS area and eight from the non-IRS area. Tukey-Kramer's HSD and Steel-Dwass tests revealed that the ages did not differ significantly among all the pairs of sexes and areas with the lowest *p*-value 0.26 detected between male rats in non-IRS and IRS area by Tukey-Kramer's HSD test.

The bioaccumulation of DDTs in tissues of wild rodents by sampling area is depicted in Figure 2.1.1 and Table 2.1.3. The levels of DDTs in all tissues in the IRS area were significantly higher than those in the non-IRS area ($p<0.05$). The median concentration of sum of *p,p'*-DDE, *p,p'*-DDD, and *p,p'*-DDT ranged from 723.9 ng/g ww in the brain to 5053.1 ng/g ww in the liver in the IRS area and from 9.7 ng/g ww in the spleen to 189.3 ng/g ww in the liver in the non-IRS area. DDTs residues were found almost in all samples, indicating that distribution is ubiquitous in the study area, even in the non-IRS areas. In this study, no sex differences were observed in any of the DDT concentration levels.

The composition profiles of DDT and its metabolites in each of the tissues analyzed in the present study are shown in Figure 2.1.2. Except for the liver, all organs from the same site had similar patterns. The brain, lung, spleen, and kidney had the highest abundance of *p,p'*-DDT in the IRS area, with ratios of 62%, 76%, 78%, and 76%, respectively, compared to only 12% in the liver. The liver had a substantial amount of *p,p'*-DDD, a metabolite of *p,p'*-DDT, with a ratio of 73%. The accumulation profile of DDTs in the IRS area was DDT > DDD ≈ DDE, reflecting that *p,p'*-DDT was still used. The most common DDT metabolite, *p,p'*-DDE, was predominantly detected in most tissues from the non-IRS area (Figure 2.1.2). The brain, lung, spleen, kidney, and liver all had high levels of *p,p'*-DDE, at 74%, 64%, 63%, 54%, and 39%, respectively. The parent chemical *p,p'*-DDT was also detected in the non-IRS area.

Quantitative PCR was used to assess changes in gene expression between males and females in both areas. Both Welch's t-test and Wilcoxon's exact test were used for statistical analyses as the sample number in this study was small and it was impossible to

ensure that the samples followed a normal distribution. In this study, the results of significance from both parametric and non-parametric analyses were taken as significant (p<0.05) to prevent loose significance. Figures 2.1.3 and 2.1.4 show the natural logarithm of calculated expressions using the ΔΔCT method. The expression of nuclear receptor genes in both sexes and sampling areas is shown in Figure 2.1.3. There was a significant difference (p<0.05) in *PXR* and *PPARa* gene expression between the sexes in the non-IRS area. Compared to female rats (*PXR* range: 1.0–1.96; median: 1.40 and *PPARa* range: 1–2.29; median: 1.98), male rats had higher expression levels of *PXR* (3.14–4.05; 3.23) and *PPARa* genes (3.04–4.98; 3.75). However, this significant difference was not seen in the IRS area, where female rats had slightly higher median *PXR* and *PPARa* expression than male rats. Female rats showed a modest difference in gene expression between areas (p = 0.07 for both genes) for *PXR* and *PPARa*. No significant differences were found in both comparisons for *AhR*.

The mRNA expression profiles of 12 metabolic enzymes are shown in Figure 2.1.4. Significant sexual differences (p<0.05) in mRNA expression levels were seen in the non-IRS area for *Cyp2a2*, *Cyp3a2*, and *Cyp3a18*. Male rats had significantly higher medians for *Cyp2a2*, *Cyp3a2*, and *Cyp3a18* than female rats. In the IRS area, however, the median of *Cyp3a18* expression in female rats (26.5) was slightly higher than that in male rats (22.2), indicating that high levels of DDTs seemed to eliminate the sexual difference in this gene. This difference seemed to be derived from the high expression of *Cyp3a18* in females rather than the change of expression in males. Even though *Cyp3a1* had the same propensity as *Cyp3a18*, there was no discernible difference between the IRS and non-IRS areas. For the other genes, in both areas, there were no significant differences in gene expression between males and females. Many genes, such as *Cyp2c11* and *Cyp7a1*, had similar patterns in both areas, indicating that male or female dominance in the non-IRS area was maintained in the IRS area. The dominance revealed in the non-IRS area of some genes such as *Cyp2a1* and *Ugt2b1* was reversed in the IRS area.

Table 2.1.4 shows the correlation between nuclear receptors and metabolic enzymes as determined by Spearman's correlation test using entire group (both males and females). Even though sex specific Spearman's correlation tests were conducted, the tendency in highly associated gene pairs remained unchanged. The highest Spearman's

rank correlation coefficient (ρ = 0.77) was found in *AhR* and *Ugt2b1*. There were many gene expression pairs with significant correlations (p<0.05), indicating interactions between nuclear receptors and metabolic enzymes such as *Cyp2b1*, *Cyp3a2*, *Cyp3a18*, and *Ugt2b1*. In contrast, *Cyp2c11*, *Cyp3a1*, *Cyp7a1*, and *Sult1e1* showed no strong correlation with nuclear receptors. The correlation between gene expression and DDTs concentration was also investigated and is shown in Table 2.1.5. Some pairs showed rather high correlations, for example, the correlation coefficient between *p,p'*-DDT and *Cyp3a2* in females was 0.9.

4. Discussion

The levels of DDTs measured in different tissues of the captured rodents reflect the widespread occurrence of these compounds in the environment. This study found that the concentrations of DDTs in each organ of wild rodents from the IRS area were significantly higher than in those from the non-IRS area. The liver was the primary organ for DDTs accumulation, followed by the kidney. This result revealed that the IRS program in residential areas for malaria vector control routinely exposed rodents to high concentrations of DDT. However, the accumulation of DDTs was low in the brain, which could be due to the protective role of the blood-brain barrier, which prevents xenobiotics from entering the cerebral compartment (Agúndez et al., 2014).

The composition analysis of DDT showed that *p,p'*-DDD accumulated predominantly in the liver, both in IRS and non-IRS areas. This could reflect the liver's high metabolic capacity or the direct ingestion of DDD from the field. In the presence of nicotinamide adenine dinucleotide (NADH) or nicotinamide adenine dinucleotide phosphate (NADPH), *p,p'*-DDT is generally converted to *p,p'*-DDD in rat liver microsomes (Kitamura et al., 2002). Furthermore, non-enzymatic metabolism involving the heme group of hemoglobin produces *p,p'*-DDD in the blood (Kitamura et al., 2002; Sugihara et al., 1998). The high level of *p,p'*-DDD accumulation in the liver was unique, as *p,p'*-DDT and *p,p'*-DDE were the most abundant compounds in the other organs. Our findings agree with previous study (Harada et al., 2016). DDE has higher persistency in the environment and living organisms than DDT and is more resistant to degradation and elimination from the body (Eskenazi et al., 2018). All investigated organs had a larger

DDE to total DDT ratio in non-IRS areas as compared with IRS areas in this study. This result could derive from the high persistency of DDE. Various effects of DDE as endocrine disruptor have been reported (Burgos-Aceves et al., 2021). Thus, even if the use of DDTs has been banned, DDE effects, especially on endocrine disruption, persist in the environment for a long time in areas that were sprayed with DDT in the past.

In the IRS area, female rats lost their sexual differences in some gene expressions of metabolic enzymes and transcription factors. In the non-IRS area, the studied nuclear receptors, PXR and PPARa, were significantly different between male and female rats. These nuclear receptors are responsible for the induction of CYP450 gene expression, such as CYP2, CYP3, and CYP4 families (Bougarne et al., 2018; Hakkola et al., 2020). Previous studies have shown a difference by sex in nuclear receptor activity or CYP enzyme induction in response to chemical exposure (Hernandez et al., 2009; Ledda-Columbano et al., 2003; Xiang et al., 2020). There have only been a few studies on nuclear receptor mRNA levels that focused on sexual differences. Nuclear receptor gene expression in mouse liver was studied extensively, and many of them, including *PXR* and *PPARa*, exhibited no sexual differences (Rando and Wahli, 2011). However, in the case of rats, *PPARa* showed sexual differences (Jalouli et al., 2003).

Unlike *Rattus norvegicus,* which is a commonly used species in experimental trials, the metabolic ability of *R. tanezumi* has yet to be studied. As a result, it was not possible to determine whether the variation in the non-IRS area was due to the effects of pollutants or natural species-specific characteristics. The specificity of *R. tanezumi* could explain some mismatched gene expression patterns between sexes, such as higher *Cyp2a1* expression in males than females in the non-IRS area and a modest sexual difference in *Cyp2c11*. Therefore, an *in vivo* investigation including *R. tanezumi* and *R. norvegicus* is required to understand the process of sexual differentiation elimination in the IRS area.

In rats, distinct sexual differences in metabolic enzymes have been reported (Kato and Yamazoe, 1992). For example, Asaoka et al. (2010) reported that for Sprague-Dawley rats, juvenile males have a higher expression of *Cyp3a1, Cyp3a2* and *Cyp3a18* than female juveniles. An *in vivo* study by Sierra-Santoyo et al. (2000) found higher expression of CYP3A1 and CYP3A2 in basal males than females, as well as a notable induction of CYP3A1 and CYP3A2 in female rats after a single DDT exposure. In this

study, the female-specific response to DDT exposure was also observed in some metabolic enzymes. One of the key mechanisms involved in CYP sexual morphism is thought to be the growth hormone. In rats, episodic growth hormone influences male-specific CYP expression, and many studies have reported a relationship between growth hormone and CYP expression in rat liver, occasionally with a hypophysectomized operation (Thangavel et al., 2006; Waxman et al., 1991). Hypophysectomized female rats, for example, had a high level of *Cyp3a2* mRNA, similar to male rats, but growth hormone restoration fully repressed *Cyp3a2* induction and restored female expression (Pampori Nisar A., 1996).

Many previous reports have revealed female-specific responses to CYP induction by chemical exposure. In fetal female rats, prenatal monocrotaline exposure significantly increased *Cyp3a* gene expression and protein levels (Xiang et al., 2020). A prenatal-retrorsine-exposure animal experiment significantly upregulated CYP3 protein and *Cyp3a1* expression in female rat liver (Dai et al., 2021). Sex-dependent upregulation patterns were also seen in the CYP2B family in rodents after exposure to nicardipine, nifedipine, and TCPOBOP (Konno et al., 2004; Ledda-Columbano et al., 2003). However, this study did not reveal the mechanism of the female-specific impact of DDTs. It is probable that the endocrine disturbance produced by DDTs, which targets growth hormone, affects the gene expression of CYP. More hormone profiles could reveal the mechanism through which DDTs affect sex-linked CYP expression. Another possible mechanism is that DDTs could disrupt CYP expression via up- or down-regulation of nuclear receptors' mRNA levels. The same tendencies were observed when comparing nuclear receptors and some CYPs, such as *PXR* and *Cyp3a18* from IRS and non-IRS areas. The overexpression of nuclear receptors by DDTs in females may have induced some CYP expressions as shown by the significant correlation between nuclear receptors and some metabolic enzymes in this study. DDT-induced CYP induction has already been reported and CYPs are involved in xenobiotic metabolism and maintaining homeostasis (Harada et al., 2003; You, 2004). For a better understanding of the effect of DDTs on animals, the toxicity of DDTs on metabolic enzymes should be carefully monitored. The human residents in the current research area may be contaminated with the same level of DDTs, but the effect of DDTs on metabolic enzymes in humans in this area is still unclear. Several studies have reported alterations in the blood metabolome of humans and

experimental animals due to DDT exposure (Hu et al., 2020; Salihovic et al., 2016). Discovery of an effective biomarker that can be applied in sprayed areas and used across various mammals is desirable in addition to molecular analyses.

The small number of rats in the sample was a weakness of this study. The main issue with this sample size was that it was difficult to use only one type of statistical analyses. For some gene expressions, even natural log-transformed relative gene expression showed a non-normal distribution. Moreover, at such a small sample size, non-parametric statistical tests were inappropriate. Thus, to ensure the statistical power of our results, we performed both parametric and non-parametric analyses. In addition, the present sample size did not allow us to analyze the age groups separately. Thus, determining the precise effect of DDT on gene expression based on sex and age was difficult. Moreover, previous studies have suggested that other environmental pollutants such as chlordane and polychlorinated biphenyls contaminate the environment in KwaZulu-Natal Province (Batterman et al., 2009; Wolmarans et al., 2021). Wild rats in the area are likely to be also exposed to these various other toxic chemicals; thus, exposure experiments using experimental rats need to be performed to evaluate the individual effect of DDT. However, this type of research, particularly with wild animals, is rare. Therefore, despite the small sample size, the findings of this field study are relevant for augmenting *in vivo* studies of DDT.

In conclusion, even though global usage of DDTs is declining, some developing countries still use DDTs for vector control of mosquito-borne diseases. Our results showed that gene expression varied between sexes in the non-IRS area but not in the IRS area, indicating that high DDT levels might disrupt CYP genes expression levels in both sexes. As replicating DDT-sprayed environments in animal experiments is difficult, this study will encourage further field studies in a DDT-sprayed areas and the use of wild rodents to assess DDT toxicity. The data from this study may open up the environment-based evaluation of DDT toxicity in this area and help researchers in assessing the toxicity of chemicals in the field.

Figures and Tables

Table 2.1.1. Primer and amplicon information of target and reference genes for qPCR.

Gene	5′-forward primer-3′	5′-reverse primer-3′	Size (bp)
Beta-actin	GGTCCACACCCGCCACCAGTT	ACCCATACCCACCATCACACCCTG	169
AhR	AAACCAAAGACACGGGATAAACTC	TCGGACTCTGAAACTTGCTTAGG	179
PXR	GCGTCATCAACTTCGCCAAA	CCAGGTTCCTGTTTCCGTGT	140
PPARa	ACTAGCAACAATCCGCCTTTTG	GGACCTCTGCCTCCTTGTTTTC	115
Cyp2a1	GAGGCGAACAGGCTACCTACA	CGCTCCCCACTGCTGAAT	67
Cyp2a2	TACCTGAGCAAAACAGTCTCCA	TCGATCATCTCCAACAGTGACAA	101
Cyp2b1	GCTCAAGTACCCCCATGTCG	ATCAGTGTATGGCATTTTACTGCGG	109
Cyp2c11	CGCACGGAGCTGTTTTTGTT	GCAAATGGCCAAATCCACTG	115
Cyp3a1	GATTCTGTGCAGAAGCATCGA	ATAGGGCTGTATGAGATTCTT	91
Cyp3a2	CGATTCCAACATATGCTCTTCATCA	TTCTCCTTGCTAAACCTTTCTGGAT	85
Cyp3a18	AAGCACCTCCATTTCCTTCATA	TCTCATTCTGGAGTTTCTTTTG	74
Cyp4a1	TCCACCCGCTTCACGGGCAGC	AGCCTTGAGTAGCCATTGCC	120
Cyp7a1	TGACCGGTACCTTGATGAAAG	AAGAGTCTTCCAGGACATATT	120
Ugt1a6	AGTTCTAGGTGACAAGCTGC	CACTAGCACCACAATGTCGT	112
Ugt2b1	CAACCATTTAAAGAGAAGTCCTG	GGTAAGAATGGGTGTGGAAA	143
Sult1e1	GATGAAGAACAATCCATGCACC	CTCCTCAAATCTCTCCCTCAGG	142

Table 2.1.2. Information on rats.

Site	Sex	Weight (g)	Age (day)	Age (month)
IRS	F	135.4	183	6.1
IRS	F	140	274	9.1
IRS	F	47.1	48	1.6
IRS	M	52.6	62	2.1
IRS	M	43.8	40	1.3
IRS	M	149	77	2.6
IRS	M	85.3	78	2.6
IRS	F	82.8	85	2.8
IRS	F	52.3	48	1.6
IRS	F	22	134	4.5
non-IRS	M	101.1	356	11.9
non-IRS	F	70	39	1.3
non-IRS	F	19.5	104	3.5
non-IRS	M	19.5	137	4.6
non-IRS	M	23.6	149	5
non-IRS	F	21.6	135	4.5
non-IRS	M	70.6	62	2.1
non-IRS	F	69.8	55	1.8

Figure 2.1.1. Sum of DDTs concentration (ng/g wet weight) in each tissue in IRS area and non-IRS area.

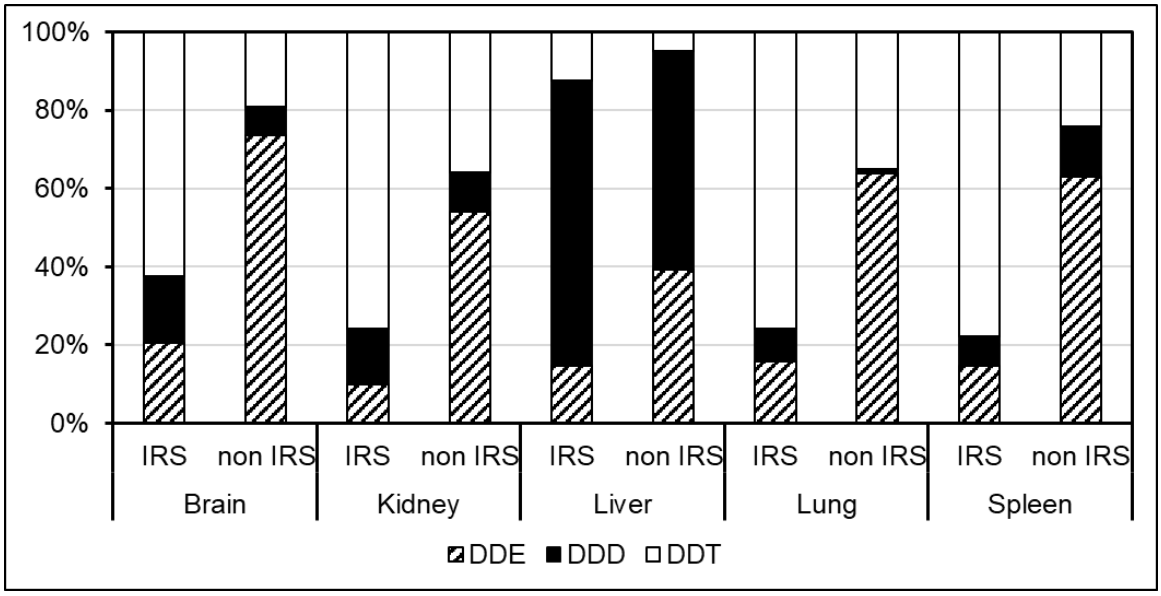

Figure 2.1.2. Percentage composition of DDT metabolites in tissues of rats per area.

Table 2.1.3. Concentration of DDTs in IRS and non-IRS areas.

IRS area		*p,p'*-DDE (ng/g ww)	*p,p'*-DDD (ng/g ww)	*p,p'*-DDT (ng/g ww)	sum of DDTs (ng/g ww)
Brain	Range	23.2- 250.4	31.7-230.4	96.5-649.5	151.4-1057.6
	Median	123.2	101.3	401.8	723.9
Kidney	Range	87.0-818.0	144.0-1207.0	691.0-10491.0	922.0-12516.0
	Median	475.5	485.5	3088.0	4156.5
Liver	Range	163.1-1406.8	1355.8-4828.7	15.8-1278.9	1803.4-7025.6
	Median	543.2	3473.5	282.4	5053.1
Lung	Range	27.5-3406.2	26.8-743.8	277.4-4243.3	331.6-6122.5
	Median	222.7	115.5	1176.1	1478.2
Spleen	Range	43.4-4616.5	9.6-1179.6	224.6-7682.7	277.8-13241.4
	Median	189.3	103.7	2378.9	3547.5

Non-IRS area		*p,p'*-DDE (ng/g ww)	*p,p'*-DDD (ng/g ww)	*p,p'*-DDT (ng/g ww)	sum of DDTs (ng/g ww)
Brain	Range	3.9-31.3	ND-9.3	ND-12.7	11.0-45.4
	Median	24.6	0.4	4.9	28.7
Kidney	Range	3.0-75.0	ND-11.0	2.0-78.0	16.0-157.0
	Median	29.5	4.5	14.0	47.0
Liver	Range	14.2-115.0	42.3-262.7	ND-18.0	113.1-390.6
	Median	77.3	126.7	13.1	189.3
Lung	Range	7.8-81.8	ND-7.8	5.3-35.8	21.2-91.7
	Median	31.2	0.0	14.0	45.7
Spleen	Range	ND-60.9	ND-5.9	ND-3.6	2.3-63.0
	Median	7.9	0.0	2.2	9.7

The concentration of each DDTs was expressed as ng/g wet weight (ww).

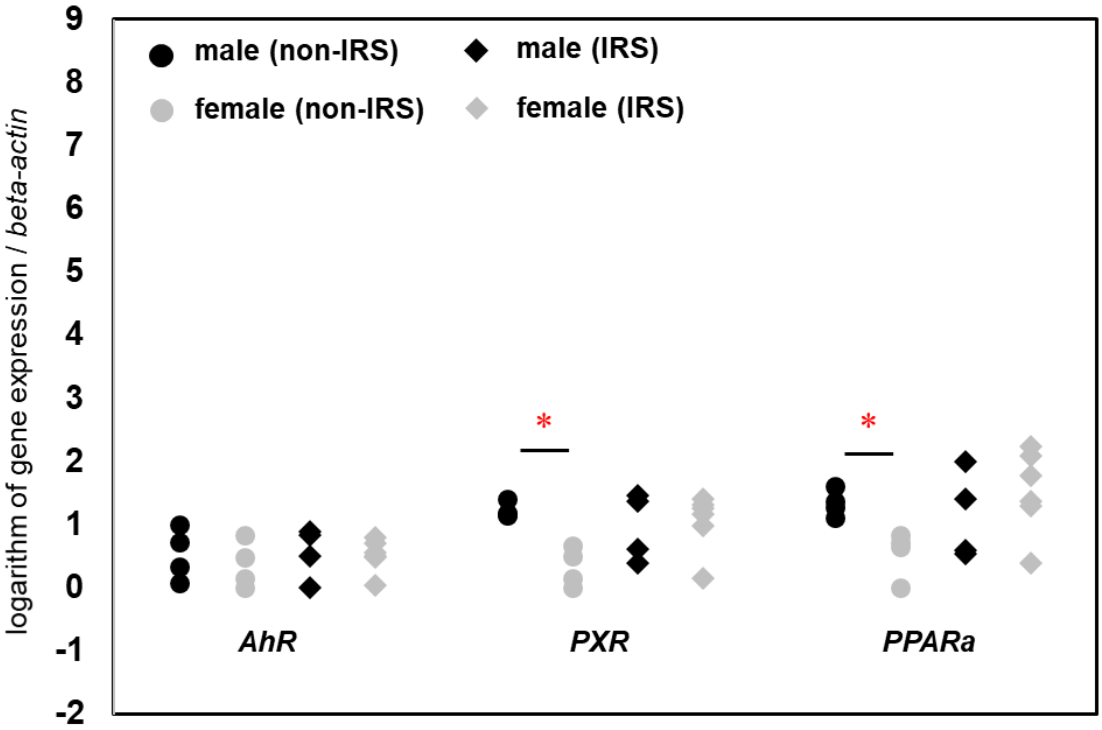

Figure 2.1.3. Gene expression of nuclear receptors. Scatter plots show gene expression of the nuclear receptor in the rat liver. Gene expressions were normalized by *beta-actin* and calculated using the comparative CT method. * Significant differences (p<0.05) between males and females in each group was calculated using both Welch's t test and Wilcoxon's exact test.

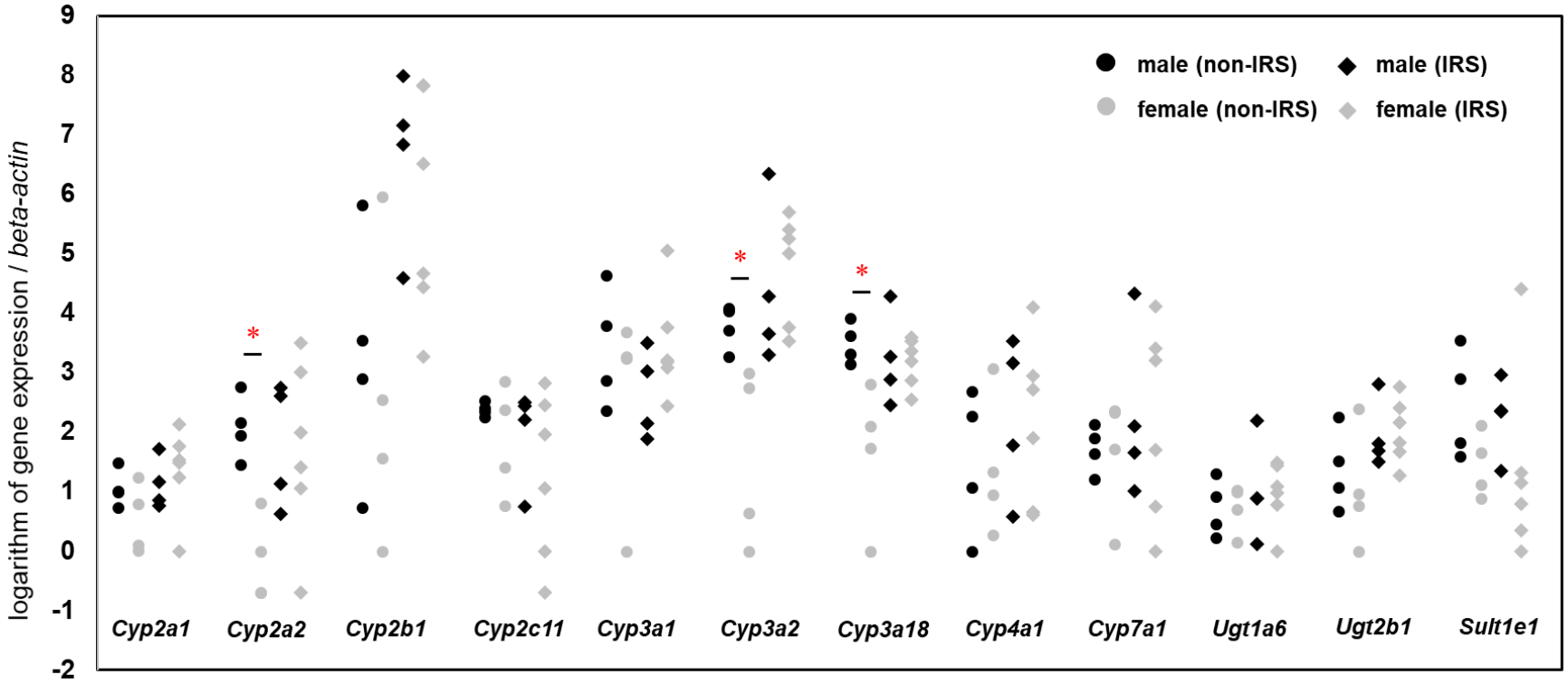

Figure 2.1.4. Gene expression of metabolic enzymes. Scatter plots show gene expression of metabolic enzymes in rat liver. Gene expressions were normalized by *beta-actin* and calculated using the comparative CT method. The lowest expressions of each gene in all rats were defined as 1 and used as a reference sample for calculation. Undetected samples were not included for calculation but defined as 0.5 and added on the figure. * Significant differences (p<0.05) between males and females in each group was calculated using both Welch's t test and Wilcoxon's exact test.

Table 2.1.4. Spearman's correlation analysis between nuclear receptors and metabolic enzymes gene expression level.

	PXR	*PPARa*	*Cyp2a1*	*Cyp2a2*	*Cyp2b1*	*Cyp2c11*	*Cyp3a1*	*Cyp3a2*	*Cyp3a18*	*Cyp4a1*	*Cyp7a1*	*Ugt1a6*	*Ugt2b1*	*Sult1e1*
AhR	0.63*	0.49*	0.33	0.42	0.70*	0.31	0.29	0.19	0.34	0.08	0.02	0.49*	0.77*	0.08
PXR		0.78*	0.47*	0.64*	0.55*	0.16	0.37	0.50*	0.59*	0.43	0.01	0.38	0.57*	0.24
PPARa			0.39	0.61*	0.44	0.16	0.3	0.56*	0.67*	0.49*	0.29	0.47	0.56*	0.23

Male and female rats in IRS and non-IRS areas were combined in this analysis. Each value is the Spearman's rank correlation coefficient between each pair. * Significant correlation ($p < 0.05$).

Table 2.1.5. Correlation of gene expression between each gene expression and DDTs concentration.

Female

	ahr	*pxr*	*ppara*	*cyp2a1*	*cyp2a2*	*Cyp2b1*	*Cyp2c11*	*Cyp3a1*	*Cyp3a2*	*Cyp3a18*	*Cyp4a1*	*Cyp7a1*	*Ugt1a6*	*Ugt2b1*	*Sult1e1*
p,p′-DDE	0.50	0.76	0.75	0.61	0.71	0.84	0.19	0.33	0.68	0.81	0.15	0.49	0.45	0.70	0.09
p,p′-DDD	0.39	0.72	0.81	0.61	0.71	0.72	-0.32	0.15	0.79	0.61	0.47	0.20	0.28	0.62	-0.04
p,p′-DDT	0.33	0.60	0.64	0.42	0.50	0.54	-0.48	-0.05	0.90	0.58	0.39	0.08	0.20	0.55	-0.20
ΣDDTs	0.36	0.70	0.79	0.55	0.57	0.68	-0.31	0.10	0.84	0.60	0.53	0.22	0.22	0.58	0.01

Male

	ahr	*pxr*	*ppara*	*cyp2a1*	*cyp2a2*	*Cyp2b1*	*Cyp2c11*	*Cyp3a1*	*Cyp3a2*	*Cyp3a18*	*Cyp4a1*	*Cyp7a1*	*Ugt1a6*	*Ugt2b1*	*Sult1e1*
p,p′-DDE	0.17	0.00	0.00	0.38	-0.31	0.69	0.14	-0.24	-0.05	-0.12	0.43	-0.31	-0.26	0.40	0.10
p,p′-DDD	0.40	0.17	0.07	0.40	-0.12	0.86	-0.14	-0.48	-0.05	-0.19	0.31	-0.19	-0.02	0.64	-0.21
p,p′-DDT	-0.31	0.07	0.07	-0.17	0.17	0.52	-0.64	-0.40	0.55	0.05	0.29	0.52	0.33	0.24	-0.10
ΣDDTs	0.40	0.17	0.07	0.40	-0.12	0.86	-0.14	-0.48	-0.05	-0.19	0.31	-0.19	-0.02	0.64	-0.21

The correlation between each gene expression and DDT concentration, which was quantified and normalized in Figures 2.1.1 and 2.1.4, in rat liver was evaluated by Spearman's correlation test. Male and female rats were separately analyzed and both IRS and non-IRS areas were combined. Each value is the Spearman's rank correlation coefficient between each pair. Significance was not evaluated owing to the low sample number.

Section bridge

Section 2.1 reveals the possible effects of DDT on sex-linked metabolic enzymes. These metabolic enzymes act on both endogenous and xenobiotic metabolism and maintain homeostasis in mammals. Thus, a disturbance in metabolic enzymes could alter metabolite profiles. The following section presents the plasma metabolome assessment and gene expression analysis using wild rats inhabiting a DDT-sprayed area. The sampling in Section 2.2 was conducted in 2017 whereas that in the previous section was performed in 2014. However, the concentration of DDT was still high in 2017. In addition to Section 2.1, Section 2.2 focuses on the steroid and bile acid biosynthesis pathway and introduces a molecular approach against the ecological effects of DDT.

Chapter 2.2:

Investigation of dichlorodiphenyltrichloroethane (DDT) on xenobiotic enzyme disruption and metabolomic bile acid biosynthesis in DDT-sprayed areas using wild rats

Investigation of dichlorodiphenyltrichloroethane (DDT) on xenobiotic enzyme disruption and metabolomic bile acid biosynthesis in DDT-sprayed areas using wild rats

Highlight

- Wild rodents inhabiting a DDT-sprayed area were collected and the effects of DDT were examined using metabolome analysis and quantitative PCR.
- Metabolome analysis revealed a possible association of DDTs with bile acid; however, the gene expression analysis did not fully reveal strong effects of DDT on bile acid biosynthesis.
- Gene expression analysis of the rat liver showed that DDT may disrupt xenobiotic metabolic enzymes.
- No significant correlation was found between DDT concentration and expression of steroid biosynthesis enzymes in the testis.

Abstract

Dichlorodiphenyltrichloroethane (DDT) is an organochlorine insecticide used worldwide. Several studies have reported the toxic effects of DDT and its metabolites on steroid hormone biosynthesis; however, its environmental effects are not well understood. This study examined wild rats collected in DDT-sprayed areas of South Africa and quantified plasma metabolites using liquid chromatography quadrupole time-of-flight mass spectrometry (LC-Q-TOF-MS). Fold change analysis of the metabolome revealed the effect of DDT on bile acid biosynthesis. Gene expression of the related enzyme in rat liver samples was also quantified. Significant association was found between DDT and gene expression levels related to constitutive androstane receptor mediated enzymes, such as *Cyp2b1* in rat livers. However, current results could not fully demonstrate that enzymes related to bile acid biosynthesis were strongly affected by DDT. The correlation between DDT concentration and gene expression involved in steroid hormone synthesis in testis was also evaluated; however, no significant correlation was found. The disturbance of metabolic enzymes occurred in rat liver in the target area. Current results suggest that DDT exposure affects gene expression in wild rats living in DDT-sprayed areas. Therefore, there is a need for DDT toxicity evaluation in mammals living in DDT-sprayed areas. This study could not find an effective biomarker that could reflect the mechanism of DDT exposure; however, this approach can provide new insights for future research to evaluate DDT effects in sprayed areas.

Keywords

bile acid biosynthesis, DDT, metabolomics, steroid hormone biosynthesis, wild rat

1. Introduction

Dichlorodiphenyltrichloroethane (DDT) was used for agriculture and human hygiene globally until its adverse effects were forewarned in the 1970s. However, selected African countries continue to spray DDT for malaria vector control as indoor residual spraying (IRS) on the recommendation of the World Health Organization (WHO, https://www.who.int/en). DDT spraying has effectively decreased the number of malaria cases worldwide (Water J Rogan and Aimin Chen, 2005). Although, pyrethroids replaced DDT in the Republic of South Africa around 1995, malaria cases have increased since then (Govere et al., 2002). Thus, we need to carefully examine the risk (toxicity on animals and ecosystems) and benefit (vector control) of DDT spraying. DDT persistence has an effect on the ecosystem. DDT and its main metabolites, dichlorodiphenyldichloroethylene (DDE) and dichlorodiphenyldichloroethane (DDD), have a long half-life of elimination and reportedly persist in animal bodies (Eskenazi et al., 2018). Laboratory animal studies and human epidemiological studies have shown the contribution of endocrine disruptor chemicals to obesity, reproductive problems, several cancers, etc.; however some risks are still controversial (Safe, 2020). The effect of DDT as an endocrine disruptor is well known. *o,p′*-DDT (another isoform of DDT) and *p,p′*-DDE exhibit estrogenic effects and antagonistic ability of the androgen receptor, respectively (Kelce et al., 1995). The epidemiological study showed that the alteration or correlation between steroid and thyroid hormones in human plasma are related to the accumulation of DDTs in South Africa, which is my target area (Bornman et al., 2018; Delport et al., 2011). And a review linked DDT to the risk of hepatocellular carcinoma in human. However, inconsistency in the results of these epidemiologic studies was observed (VoPham et al., 2017), and real scenarios in South Africa have not been investigated to date. Therefore, it is crucial to further assess DDT toxicity in the liver and organs involved in steroid hormone biosynthesis in DDT-sprayed areas.

However, it is difficult to access molecular analysis in human studies, such as gene expression levels in organs, to reveal the biological processes affected by DDT due to technical and ethical problems. My previous studies have observed high concentrations of commercially used isoforms: *p,p′*-DDT, *p,p′*-DDE, and *p,p′*-DDD accumulated in rat liver samples in South Africa (sum of DDTs ranging between 18–1452 and 15–1389 μg/kg wet weight in female and male rats, respectively) (Motohira et al., 2019). In

sampling area in South Africa, rats frequently coexist with humans in their environments, particularly in houses, hence it is presumed that they have exposure patterns similar to those of humans, including exposure to high DDT concentrations in IRS areas. Therefore, wild rats can be considered bioindicators to estimate the effects of DDT on human (Motohira et al., 2019).

Metabolomics, the study of small molecules within cells, biofluids, and tissues, has been applied to reveal the modes of action and evaluate the eco-toxicological risk of environmental pollutants, e.g., pesticides, on mammals (Aliferis and Chrysayi-Tokousbalides, 2011; Liu et al., 2022). Furthermore, it can demonstrate the biochemical changes caused by chemicals with molecular pathways and find biomarkers of exposure reflecting chemical responses (Ramirez et al., 2013). Metabolomics utilized analytical techniques such as high-performance liquid chromatography with reverse phase columns for separating chemicals (Issaq et al., 2008). This technique has also been used for the evaluation of DDT toxicity. For example, a metabolomics study using high-resolution liquid chromatography mass spectrometry alerted adverse effects of DDT on fetal development derived from maternal metabolic alterations and of DDE on mitochondrial dysfunction and lipid dysregulation (Hu et al., 2020). Another study identified that fatty acids and glycerophospholipids were associated with plasma DDE concentration in human and indicated to be a possible biomarker to reflect human health disrupted by chemical exposure (Salihovic et al., 2016). A field-based study may reveal further unknown pathways through which DDT affects mammals. To better understand the toxicity of DDT and find biomarkers that reflect its adverse effects, I evaluated the effect of DDT at the molecular level in wild rodents in DDT-sprayed areas.

2. Materials and Methods

2.1 Sample preparation

This study used rat samples from my previous study, conducted in 2019. The wild rats were collected from a sprayed area in the Phongolo River floodplain, South Africa, and DDT concentrations were quantified. Details of the sampling area, physical information, and DDT concentrations in rat livers were provided in a previous study (Motohira et al., 2019). Samples comprised 10 male and 23 female rats (*Rattus tanezumi*).

However, only 31 and 28 rat samples were used in gene and metabolome analyses, respectively, because of a lack of liver RNA or blood volume. This study followed the Hokkaido University Manual for Implementing Animal Experimentation for euthanasia and refinement of wild rats, substituting wild animals for experimental animals.

2.2 Metabolome analysis

Metabolome analysis was performed using 28 samples. The metabolites in rat plasma were extracted using a previously reported method with slight modifications (Eguchi et al., 2017). The mixture of plasma and methanol (4:6, volume ratio) was centrifuged at 3,000 × *g* for 10 min, and 100 μL of supernatant was used for subsequent analysis. I used 100 μL of 100 μM N,N-diethyl-2-phenylacetamide and D-camphor-10-sulfonic acid (Wako Pure Chemical Industries Ltd., Osaka, Japan) as internal standards for the positive and negative ion modes, respectively. The internal standards were added to the supernatant, and then loaded on Amicon® Ultra-0.53 k filter columns (Merck Millipore, Darmstadt, Germany), followed by centrifuged at 14,000 × *g* for 1 hr. Finally, the extracts were transferred to vial, and analyzed using liquid chromatography–quadrupole time-of-flight MS (LC-QTOF/MS). The Nexera liquid chromatography system (Shimadzu, Kyoto, Japan) interfaced with a Triple TOF 5600 (LC-QToF/MS) system, (AB Sciex, Framingham, MA, USA) with electrospray ionization was operated in both positive and negative ion modes. A 3.5 μm XBridge ethylene bridged hybrid amide hydrophilic interaction chromatography column (Waters Corporation, Milford, MA, USA) was used for the separation of metabolites in a HPLC system. Solvents A and B and other parameters used for metabolome analysis were described in Table 2.2.1. The gradient program started at 85% solvent B; then, at t = 4 min: 75% B, t = 17 min: 2% B, t = 17–20: 2% B, t = 21 min: 85% B, t = 21–26 min: 85% B. Acetonitrile and methanol were purchased from Wako Pure Chemical Industries Ltd (Osaka, Japan). Ultrapure water was synthesized using a RFD280NC system (ADVANTEC, Dublin, CA, USA).

Blank (pure water) and quality control (the mixture of each plasma sample, QC) samples were prepared and injected in LC-QToF/MS to identify potential contamination during analyses and evaluate their stability during the sequence. During machine analysis, five QC and five blanks were run with test samples. The metabolites detected in at least 50% of the samples with a coefficient of variation of less than 0.3, were used for statistical

analyses. Metabolites identified at annotation level two were used for data analysis as proposed in a previous report (Schymanski et al., 2014). The extracted metabolites were analyzed using Mass Spectrometry-Data Independent AnaLysis software version 4.60 (http://prime.psc.riken.jp/compms/msdial/main.html). The following libraries were used for peak selection and annotation: RIKEN (Tsugawa et al., 2015), Massbank of North America (https://mona.fiehnlab.ucdavis.edu/), human metabolome database (Wishart et al., 2018), and National Institute of Standards and Technology (2020) tandem mass spectrometry library. The specimen with the highest calculated MS/MS spectra similarity score (at least more than 80) was used for the analyses.

2.3 Gene analysis

The liver and testis from each rat were sampled and preserved in RNAlater (Sigma-Aldrich, St Louis, MO, USA) for gene expression analysis. Gene expression analyses were performed using 9 male and 22 female rats without any reconstruction depending upon the DDT concentrations. The procedures for RNA extraction, complementary DNA (cDNA) synthesis, and real-time PCR are detailed in the previous section (Section 2.1). All primer sets used were obtained from Invitrogen (Carlsbad, CA, USA). The primer data are summarized in Table 2.2.2 and some primers used were based on previous reports (Alsiö et al., 2009; Kawase et al., 2008; Liaset et al., 2009; Liu et al., 2011; Michihara et al., 2011; Miksys et al., 2000; Petersson et al., 2007; Tully et al., 2006; Zhu et al., 2020, 2013). Gene expression was normalized using the housekeeping gene (*beta-actin*) and calculated using the comparative Ct method (ΔΔCT) in both liver and testis. The lowest expression of each gene from all groups was used as a reference control to normalize the comparative Ct method. Undetected samples and those outside the range of primer efficiency were deleted from the dataset. More than 90% individual samples were detected and included in the statistical analysis for all target genes. These results were then analyzed in terms of ΣDDT concentrations (wet weight).

2.4 Statistical analysis

DDT concentrations were described in previous report (Motohira et al., 2019). No remarkable differences in DDT concentrations (ng/g, wet weight) between sexes and phases of sexual development (immature, transitional, and mature) were identified (data is shown in my previous report (Motohira et al., 2019)). Principal component analysis (PCA) was conducted using DDT concentrations and normalized peak height intensity of metabolites by pairwise correlation. After PCA analysis, all samples were divided into four groups depending upon their DDT concentrations. The highest and the lowest 25 percentile were used in metabolome analysis as high contaminated samples (high DDT exposure, n:7) and low contaminated samples (low DDT exposure, n:7). There were four females and three males in the low-exposure group, and five females and two males in the high-exposure group. After normalization with common logarithm, t test was used for comparing metabolome features between the low and high DDT-exposed group. Fold change analysis used the raw mean and median value of each metabolite before normalization and extracted the features with at least a 2-fold difference between the low and high DDT-exposed group. MetaboAnalyst 5.0 (https://www.metaboanalyst.ca/) was used for all statistical analyses targeting metabolome. *p*-values of metabolome analyses were adjusted by controlling the false discovery rate (FDR) (Benjamini and Hochberg, 1995) with a significance threshold of FDR < 0.1.

For gene analysis, Wilcoxon's test was used for comparisons between the sexes. Multiple linear regression was performed to determine the factors that influence gene expression. Firstly, the common logarithm was applied to gene expressions to make the distribution closer to normal except *Ugt1a1* which was normally distributed. Then all the variables of gene expressions, rats ages, and ΣDDT concentrations were normalized using their average and standard deviation and included in multivariate analysis. The correlation between the concentration of DDT and gene expression in testis was assessed using Spearman's rank correlation test. Multiple linear regression analysis at a significant association of $p < 0.1$ and Spearman's rank correlation test at a significance threshold of $p < 0.05$ were conducted using JMP 16 software (SAS Institute, Cary, NC, USA).

3. Results

3.1 Metabolome analysis

Sixty-three and fifty-one metabolomes were extracted from positive and negative ion selection, respectively. High and low DDT accumulated rat liver samples were reconstructed as high and low exposed groups. DDT concentrations were recorded between 90.6 and 1203.1 ng/g wet weight in the low exposed group and between 2586.4 and 5236.9 ng/g wet weight in the high exposed group. Figure 2.2.1 depicts PCA in DDT concentration and metabolome analysis for both sexes using low and high exposed groups. The first (PC1) and second (PC2) principal components accounted for 28.6% and 14.8%, respectively. Red and green spots represent each sample in the low and high exposed groups, respectively.

Although seven features were extracted with two-fold difference in both mean and median between the low and high exposed group, no significant difference was found between their metabolites using t test (FDR < 0.10). Table 2.2.3 shows extracted features registered in the Kyoto Encyclopedia of Genes and Genomes (KEGG) (https://www.genome.jp/kegg/) with related pathways mentioned (two were excluded because of no information in KEGG.). Two (glycine and taurocholic acid) of the extracted features were related to bile acid biosynthesis. Furthermore, values for 3α-Hydroxy-7-oxo-5β-cholanic, another bile acid that is not listed in KEGG, were added in Table 2.2.3 (PubChem: https://pubchem.ncbi.nlm.nih.gov/). All of the extracted metabolites were lower in concentration in the exposed group.

3.2 Gene expression analysis in liver samples

Eleven gene expressions related to xenobiotic metabolism, lipid metabolism, and bile acid biosynthesis in rat liver samples were quantified using qPCR. I chose bile acid biosynthesis-related metabolic enzymes based on metabolome analysis results. The association between DDT concentration and gene expression is described in Table 2.2.4 along with other influencing factors. Significant sexual differences were not observed between male and female rats, with the lowest *p* value of 0.13 between sexes in *Cyp8b1*. Metabolic enzymes, such as CYP, share a lot of pathways and play multiple roles in mammals. In addition, it was difficult to identify the enzymes that were

typically categorized in bile acid biosynthesis. However, this study defined six enzymes (*Cyp7b1*, *Cyp8b1*, *Cyp27a1*, UDP-glucuronosyltransferase [*Ugt1a1*], and bile acid-CoA: amino acid N-acyltransferase [*BAAT*]) as important enzymes of bile acid considering previous studies (Ferdinandusse and Houten, 2006; Russell, 2003). DDT had a small influence on many of the bile acid-related genes such as *Baat* and *Cyp27a1* (Table 2.2.4). *Ugt1a1*, which is involved in bilirubin metabolism in mice (Wagner et al., 2005), was found to have a significant association with $p<0.01$. DDT concentration also significantly associated with *Cyp8b1*, with $p=0.08$.

3.3 Gene expression analysis in testis

Four genes (*Cyp7b1*, *Cyp11a1*, *Cyp19a1*, and hydroxysteroid 17-beta dehydrogenase 1 [*Hsd17b1*]), which have an important role in steroidogenesis, were selected for quantitative PCR in testis. The correlation coefficients using Spearman's rank test between DDT concentration and gene expression were 0.26, -0.26, 0.18, and -0.14 for *Cyp7b1*, *Cyp11a1*, *Cyp19a1*, and *Hsd17b1*, respectively. No strong correlation between DDT concentration and gene expression was found in testis samples.

4. Discussion

In this study, 114 metabolomes extracted from rat plasma showed no significant differences between the groups exposed to high and low DDT concentrations. PCA did not characterize the current sample dataset by DDT concentration. The group exposed to a higher concentration had lower mean concentrations in five metabolites compared with the group exposed to lower DDT concentrations. Three (Taurocholic acid, Glycine, 3.alpha.-Hydroxy-7-oxo-5.beta.-cholanic acid) out of five metabolites were related to bile acid biosynthesis. The downregulation of glycine due to 24 hr DDT exposure was reported in cultivated rat hepatocytes (same study suggested 6 hr DDT exposure showed upregulation of glycine) (Jellali et al., 2018). A few studies have examined the relationship between bile acid biosynthesis and DDTs. Thus, I analyzed the expression of the enzymes related to bile acid biosynthesis using quantitative PCR. I must emphasize that the small sample size of rats was limitation of this study during the gene analysis of rats exposed to DDT. In experimental rats, a strong naturally sexual difference in CYP is

reported (Asaoka et al., 2010). However, in this study, no significant difference in *cyp* gene expression was observed between the sexes. The expression level of some CYP is also age dependent (Asaoka et al., 2010), but multiple linear regression did not show strong association of age in many of gene expressions of metabolic enzyme. Gene analysis results revealed that *Cyp2b1* gene expression could be affected by DDT concentration. The relationship between DDT and constitutive androstane receptor (CAR) in animals has been investigated in previous studies (Harada et al., 2016; Kazantseva et al., 2013). Two years of DDT exposure upregulated isozyme contents of *CYP2B1*, a CAR target gene, and pentoxyresorufin O-dealkylase activity in rats (Harada et al., 2016). In addition, DDT induced cell cycle and apoptosis genes via CAR in mice using quantitative PCR are also reported (Kazantseva et al., 2013). UGT and sulfotransferase (SULT) are considered to be regulated by several nuclear receptors, including CAR (Buckley and Klaassen, 2009; Yanagiba et al., 2009; Yi et al., 2020). This study observed relationships between DDT concentration and *Ugt2b1* and *Sult1e1*. These results possibly were derived from CAR activity mediated by DDT in South Africa.

CYP7B1 and CYP27A1 are related to several reactions in the primary bile acid biosynthesis pathway (Russell, 2003). In this study, BAAT was involved with both glycine and taurocholic acid in primary bile acid biosynthesis pathway (Pellicoro et al., 2007). However, no significance in DDT concentration and *Cyp7b1*, *BAAT*, or *Cyp27a1* was observed in this study. Additionally, a significant association between DDT concentration and *Ugt1a1* and *Cyp8b1* was observed. CYP8B1 decides whether cholesterol becomes cholic acid or muricholic acid in primary bile acid biosynthesis pathway (Ferdinandusse and Houten, 2006). Finding a biomarker supported by a change in gene expression is desirable. The metabolome in the downstream of genes such as CYP8B1, which are responsible for particular reactions to decide the fate of cholesterol in primary bile acid synthesis, can be a good biomarker candidate reflecting the effects of target chemicals. This study comprehensively conducted untargeted metabolites and focused on bile acid biosynthesis using field samples. One study reported that DDT exposure induced the bile acid synthesis enzyme and altered hepatic bile acid in experimental mice (Lcmerrill et al., 2014). However, the relationship between bile acid biosynthesis and DDT has not been well investigated, even in *in vivo* studies. Further studies need to be conducted to reveal the effect of DDT on bile acid synthesis.

I also investigated steroid hormone biosynthesis pathways in the testis. Statistical analysis was not performed owing to the small sample size. Analyses using ovaries are likely important as well; however, the sample size was not sufficient to ignore the variations in the sexual cycle of females considering steroidogenesis. Thus, I did not analyze the ovary for gene expression changes. The target genes in present study play an important role in the testicular steroidogenesis (Pikuleva and Waterman, 2013; Sanderson, 2006). DDT caused apoptosis in the testis, which was probably because of testicular oxidative stress (Marouani et al., 2017). The testosterone level in rats decreased after DDT exposure (Krause, 1977; Lee et al., 2003). Bovine placenta showed the significant upregulation of *Cyp11a1* and *3β-hydroxysteroid dehydrogenase* (*3βHSD*) mRNA expression level because of DDT exposure (Wojciechowska et al., 2017). A significant increase in *Cyp19a1* mRNA expression level due to DDT exposure has previously been reported (Williams and Darbre, 2019). However, information obtained in a previous study suggested that testis-derived cells did not show a significant effect of less cytotoxic concentrations of DDTs on aromatase activity (CYP19A1 activity) (Sanderson, 2006). These results, which did not show a strong correlation between DDT concentration and target genes in testis, may be reasonable; however, further research with additional data, including steroid hormone concentration in plasma would help elucidate the effects of DDT on steroidogenesis. And this study targeted only testes, but gene profile in ovaries must be examined in DDT-sprayed areas to reveal the difference derived from DDTs exposure between males and females on steroidogenesis.

Recently, metabolome technique are being used for DDT sensitive animals, such as green mussel and frog (Song et al., 2016; Wolmarans et al., 2022). The *in vivo* study using African clawed frogs showed several pathways, including unsaturated fatty acid and galactose metabolism, which significantly changed due to DDT exposure (Wolmarans et al., 2022). Metabolome analyses using field-collected samples can be an important factor in determining the ecological toxicity of environmental hormones in chemically polluted areas. However, this study could not find any effective biomarker but bile acids as a candidate that reflected DDT exposure in wildlife in this study. In this study, all samples were contaminated with DDT to varying extents; therefore, they could not be separated into two groups, such as control and high exposed groups. This is a limitation of the present study. However, all samples were divided into four groups, and the first and

fourth quantiles were used as low and high exposed groups, respectively, for metabolome analysis. This may have prevented the extraction of effective biomarkers. Metabolomics has also been used to assess the *o,p'*-DDT's estrogenic ability (D. Wang et al., 2017). Further studies are needed for a better understanding of the relationship between DDT and metabolomic changes.

5. Conclusion

Metabolome analysis in this study identified bile acid as a candidate biomarker in rats exposed to DDT in sprayed areas, although the utility of these candidates has not fully been demonstrated. Rats' metabolic profiles can be changed over time, depending on their age and nutritional status (Mellert et al., 2011; Zhang et al., 2021). Thus, to assess the DDT effect more accurately, the present study should examine sex and age separately. The small sample size did not allow the proper statistical analyses, and this is limitation of this study. In addition to metabolome analysis, several metabolic gene expressions were examined. This study found that some metabolic enzymes, such as *Cyp2b1* in the liver of wild rat samples were associated with DDT accumulation. Disturbance of the xenobiotic enzymes in rats is of concern in DDT-sprayed areas, and continuous surveys are needed. The metabolites related to genes found in this study were also potential candidates that can be used to find new biomarkers. Metabolome and gene expression analyses targeting wild rats in DDT-polluted areas are rare. Field-based approaches can help reveal the effect of DDT in sprayed areas. These results provide new insights for future research in mammals living in DDT-polluted areas.

Figures and Tables

Table 2.2.1. Details for HPLC analysis

HPLC	
Solvent A	20 mM ammonium hydroxide/20 mM ammonium acetate (pH = 9.0) in ultrapure water:acetonitrile (95:5)
Solvent B	Acetonitrile
Flow rate	400 µl/min
Sample injection volume	5 µl
Column temperature	40 ℃
QTOF/MS	
Start - stop mass	50–1000
ion spray voltage (positive)	5500 V
ion spray voltage (negative)	-4500 V
Ion source temperature	500 ℃

Table 2.2.2. Primer and amplicon information of target and reference genes for quantitative polymerase chain reaction (qPCR)

Gene name	Product size (bp)	Forward primer (5'-3')	Reverse primer (5'-3')
Actb	169	GGTCCACACCCGCCACCAGTT	ACCCATACCCACCATCACACCCTG
Baat	89	ATGACCTGCCCTCTCGACT	GCCCAGGACCTTAGGATG
Cyp2b1	109	GCTCAAGTACCCCCATGTCG	ATCAGTGTATGGCATTTTACTGCGG
Cyp2c11	115	CGCACGGAGCTGTTTTTGTT	GCAAATGGCCAAATCCACTG
Cyp3a1	91	GATTCTGTGCAGAAGCATCGA	ATAGGGCTGTATGAGATTCTT
Cyp4a1	120	TCCACCCGCTTCACGGGCAGC	AGCCTTGAGTAGCCATTGCC
Cyp7b1	138	GAAGTCCTGCGTGACGAAAT	CCTCAGAACCTCAAGAATAGCG
Cyp8b1	80	GGCTGGCTTCCTGAGCTTGTT	ACTTCCTGAACAGCTCATCGG
Cyp11a1	102	GTATCTCCTCTACCAACAGTCC	GTGTGCCGTTCTCCCTCAG
Cyp19a1	102	TCCAGATTCGGCAGCAAGC	GAAAGGGCGGACCGTTCTC
Cyp27a1	93	TCTGGCTACCTGCACTTCCT	GTCTACCCCAGCCAAGATCA
Ugt1a1	152	ACACAGATCGCATGAACTTCC	AGGACTCAGAAGGTCCTTGAC
Ugt2b1	143	CAACCATTTAAAGAGAAGTCCTG	GGTAAGAATGGGTGTGGAAA
Sult1e1	142	GATGAAGAACAATCCATGCACC	CTCCTCAAATCTCTCCCTCAGG
Hsd17b10	81	ATCATTAACACTGCCAGTGTGGC	CACTATGCCCCCTTTGGATG

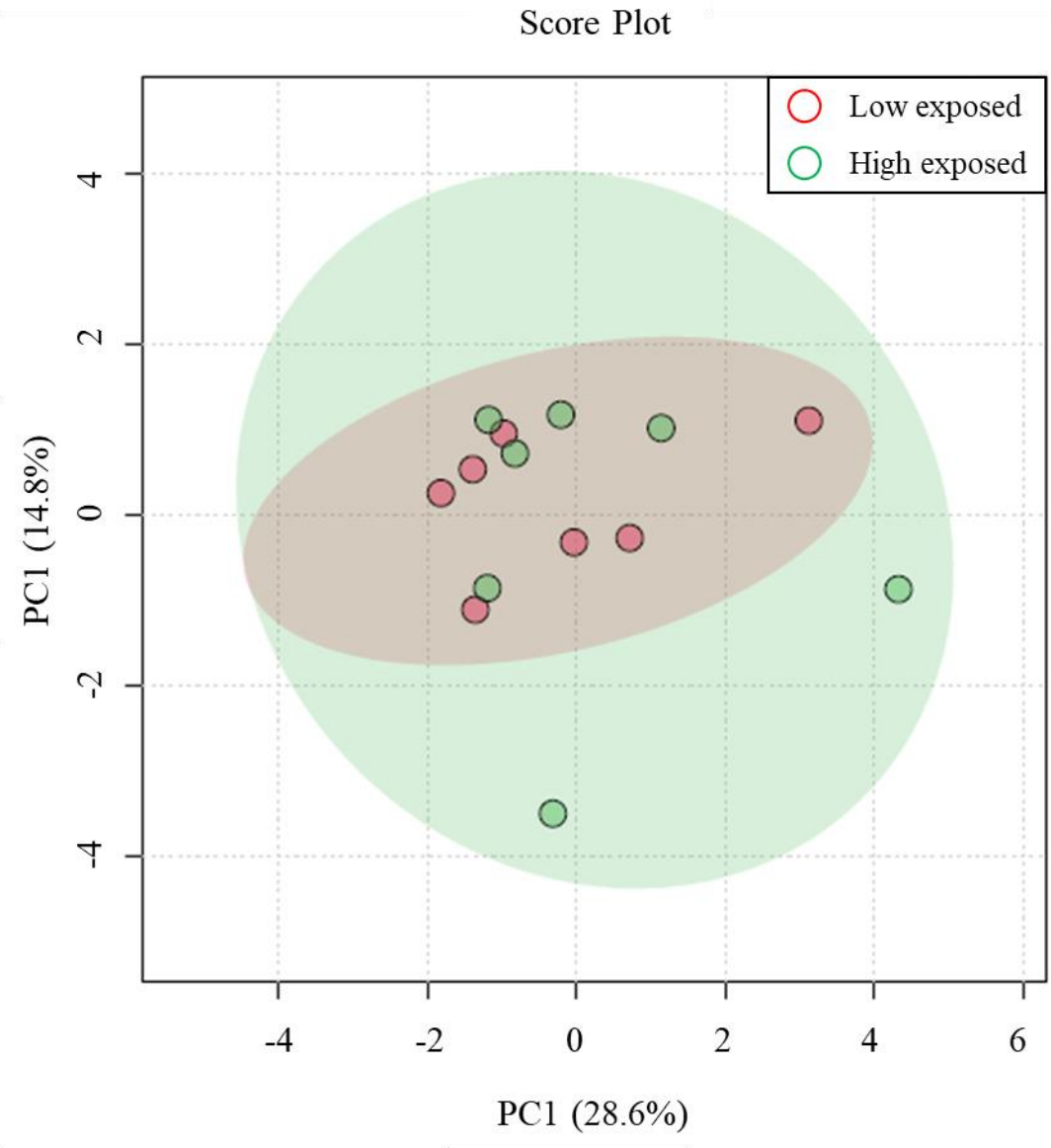

Figure 2.2.1. PCA using low and high exposed group. Totally 14 rats from low and high exposed group were analyzed depending on metabolome feature. Red and green circle expresses each rat for low and high exposed group respectively.

Table 2.2.3. Extracted metabolomes from fold change analysis.

Name	Fold Change	Database	Pathway listed in KEGG
Quinoline	0.21	KEGG	
Phosphoric acid	0.22	KEGG	map00190 Oxidative phosphorylation map00195 Photosynthesis map02010 ABC transporters map02020 Two-component system map02024 Quorum sensing map04111 Cell cycle – yeast and many other pathways for phosphoric acid
Taurocholic acid	0.37	KEGG	map00120 Primary bile acid biosynthesis map00121 Secondary bile acid biosynthesis map00430 Taurine and hypotaurine metabolism map01100 Metabolic pathways map04976 Bile secretion map04979 Cholesterol metabolism
Glycine	0.39	KEGG	map00120 Primary bile acid biosynthesis map00230 Purine metabolism map00260 Glycine, serine and threonine metabolism map00310 Lysine degradation map00440 Phosphonate and phosphinate metabolism map00460 Cyanoamino acid metabolism and many other pathways for glycine
3.alpha.-Hydroxy-7-oxo-5.beta.-cholanic acid	0.44	PubChem	

Five features having Kyoto Encyclopedia of Genes and Genomes (KEGG) ID were extracted with more than two-fold difference of mean and median between the low and high exposed group. 3α-Hydroxy-7-oxo-5β-cholanic acid was added from PubChem. The table also shows fold change, referred database, and pathway listed in KEGG.

Table 2.2.4. Multiple linear regression parameters for the association of DDT with gene expression in rat liver samples.

		Estimated parameters			
BAAT	**Variables**	**Estimated *β***	**Standard Error**	**t value**	***p* value**
	Age	0.01	0.19	0.03	0.97
	Sex (Female)	0.06	0.21	0.27	0.79
	DDTs	0.18	0.19	0.94	0.36
Cyp27a1	**Variables**	**Estimated *β***	**Standard Error**	**t value**	***p* value**
	Age	-0.12	0.18	-0.65	0.52
	Sex (Female)	-0.13	0.20	-0.63	0.53
	DDTs	0.29	0.18	1.60	0.12
Cyp2b1	**Variables**	**Estimated *β***	**Standard Error**	**t value**	***p* value**
	Age	-0.07	0.17	-0.39	0.70
	Sex (Female)	0.03	0.19	0.16	0.88
	DDTs	0.46	0.17	2.64	0.01
Cyp2c11	**Variables**	**Estimated *β***	**Standard Error**	**t value**	***p* value**
	Age	0.31	0.18	1.75	0.09
	Sex (Female)	-0.07	0.20	-0.32	0.75
	DDTs	0.32	0.18	1.77	0.09
Cyp3a1	**Variables**	**Estimated *β***	**Standard Error**	**t value**	***p* value**
	Age	-0.14	0.18	-0.75	0.46
	Sex (Female)	0.10	0.20	0.51	0.62
	DDTs	0.31	0.18	1.68	0.10
Cyp4a1	**Variables**	**Estimated *β***	**Standard Error**	**t value**	***p* value**
	Age	-0.21	0.17	-1.18	0.25
	Sex (Female)	-0.13	0.19	-0.66	0.52
	DDTs	0.39	0.17	2.27	0.03

Cyp7b1	**Variables**	**Estimated *β***	**Standard Error**	**t value**	***p* value**
	Age	-0.22	0.19	-1.18	0.25
	Sex (Female)	-0.13	0.21	-0.65	0.52
	DDTs	0.05	0.19	0.26	0.79

Cyp8b1	**Variables**	**Estimated *β***	**Standard Error**	**t value**	***p* value**
	Age	-0.22	0.17	-1.27	0.22
	Sex (Female)	0.31	0.19	1.62	0.12
	DDTs	0.32	0.18	1.80	0.08

Sult1e1	**Variables**	**Estimated *β***	**Standard Error**	**t value**	***p* value**
	Age	0.11	0.17	0.66	0.51
	Sex (Female)	0.29	0.18	1.57	0.13
	DDTs	0.45	0.17	2.72	0.01

Ugt1a1	**Variables**	**Estimated *β***	**Standard Error**	**t value**	***p* value**
	Age	-0.10	0.15	-0.62	0.54
	Sex (Female)	0.24	0.17	1.43	0.16
	DDTs	0.57	0.15	3.66	0.00

Ugt2b1	**Variables**	**Estimated *β***	**Standard Error**	**t value**	***p* value**
	Age	-0.06	0.16	-0.38	0.71
	Sex (Female)	0.17	0.18	0.96	0.35
	DDTs	0.53	0.16	3.20	0.00

Section bridge

Section 2 demonstrates possible ecological effects of DDT in a sprayed area. However, indicated in Section 2.2, wild rats can be exposed to DDT as well as various environmental pollutants. Thus, it is impossible to exactly evaluate the sole effect of DDT. To better understand the effects of DDT on mammals, a toxicity test reflecting the conditions of the DDT-sprayed area was necessary.

The following sections present a new approach to evaluate the toxicity of DDT using an *in vivo* animal model. Phenobarbital is a potent constitutive androstane receptor (CAR) activator in rats. DDT is known to have effects similar to phenobarbital on the liver. For example, both chemicals induce *Cyp2b1* gene expression and hepatomegaly. Thus, Section 3 interprets the utility of a new methodology using computed tomography (CT) and multiomics analysis with phenobarbital as the model chemical. Section 4 then evaluated DDT toxicity in rats applying the approach developed in section 3.

Chapter 3:

Comparison of micro-computed tomography (micro-CT), multiomic analysis, and classical methods for evaluating hepatomegaly induced by phenobarbital

Comparison of micro-computed tomography (micro-CT), multiomic analysis, and classical methods for evaluating hepatomegaly induced by phenobarbital

Highlights

- Micro-CT accurately evaluated hepatomegaly induced by phenobarbital in live rats.
- Various approaches (histopathology, quantitative PCR, clinical plasma biomarker, metabolome, and lipid analyses) were conducted and combined for the multiomics analysis.
- MB-PLS analysis extracted possible biomarkers that could help elucidate the mechanism of hepatomegaly.
- A combined imaging and multiomics approach could be used to conduct toxicity testing throughout an animal's lifetime

Abstract

Imaging technologies such as computed tomography (CT) are now used globally to evaluate chemical effects in animals. Compared to previous methods that required postmortem analysis, CT is beneficial as it can be used to evaluate toxicity throughout an animal's lifetime. This study aimed to demonstrate that CT could be utilized for toxicity tests. However, since the sole use of CT limits the understanding of molecular processes in the body, I identified multiomics as an effective method for covering the disadvantage of CT. In this study, both male and female rats were exposed to phenobarbital, which is a typical activator of the constitutive androstane receptor (CAR) known to induce hepatomegaly. Phenobarbital-induced hepatomegaly was evaluated using micro-CT, metabolomics, lipidomics, and various classical toxicity tests such as histopathology and quantitative PCR. The liver volume calculated using micro-CT was significantly correlated to liver volume. *Cyp2b1,* which is the most typical CAR target gene, was noticeably induced by phenobarbital in both sexes, but the expression of other genes and histopathology mainly showed that male rats had high sensitivity against phenobarbital when compared with females in this study. Multiomics analysis showed unique changes in the lipid profiles of exposed males and extracted possible biomarkers which could be utilized to estimate the biological processes involved in inducing hepatomegaly and sexual difference against chemical exposure. This research demonstrated the efficiency of micro-CT to evaluate hepatomegaly, and multiomics will thus help reveal the molecular processes throughout a lifetime. The combination of imaging and multiomics should be suitable for conducting toxicity tests using the same animals throughout their lifetime.

Key words

computed tomography, constitutive androstane receptor, evaluation hepatomegaly, lifetime

1. Introduction

Computed tomography (CT) is a non-invasive method for imaging human and animal bodies using x-rays and detectors. CT can produce 3D reconstructions, and its utility allows it to be clinically used in both human and veterinary medicine (Hathcock and Stickle, 1993; Kalender, 2006). Currently, the technique used for micro-CT has been applied in research fields. Its fundamental principles are shared with the CT methods used in human medicine, but micro-CT has a higher resolution and can target small animals such as rodents (Ritman, 2004). CT can be used to identify conditions such as cancer, circulatory system diseases, abnormal spinal conditions, inflammatory diseases, and injuries to the skeletal systems (National Cancer Institute, https://www.cancer.gov/). Several studies have used micro-CT in rodent (mice or rats) research to assess the bone (Bouxsein et al., 2010), lung (Xin et al., 2015), and gastrointestinal tract (Fredin et al., 2008), and has also been used to evaluate liver lesions in rodents. Liver steatosis, fibrosis, and tumors are all detectable using micro-CT, and a great deal of research has led to the development of this methodology (Cao et al., 2019; Fouillet et al., 1995; Schwenzer et al., 2009; Xuan et al., 2015). The use of micro-CT is technical, but a report to provide guidance for liver evaluations when using CT is in the process of being published (Fiebig et al., 2012). Micro-CT should enable more effective detection of internal changes in experimental animals and be utilized by more researchers in the future. However, the use of micro-CT to evaluate chemical compounds in small animals is still rare. Assessments using micro-CT to evaluate chemical toxicity on bone have been widely discussed (Campbell and Sophocleous, 2014; Wise et al., 2013). Micro-CT was considered a reliable method for the detection of fetal skeletal abnormalities (Winkelmann and Wise, 2009). In CT studies targeting bone, non-rodent species were also examined to detect chemical toxicities. For example, the relationship between bone length, mineral density, and dichlorodiphenyltrichloroethane (DDT) or its metabolites was examined using CT in a frog and bird (Lundberg et al., 2007; Steyn et al., 2018). CT detected a decreased cortical bone mineral density with a particular dichlorodiphenyldichloroethylene (DDE, metabolite of DDT) level in frogs (Lundberg et al., 2007). In soft tissues, micro-CT was able to detect lung damage and decreased lung volume induced by bleomycin exposure in mice (Cavanaugh et al., 2006; de Langhe et al., 2012). The use of micro-CT is spreading to several fields, but this technique has still not been generalized in the field of toxicology

to evaluate chemical compounds. Therefore, this study aimed to evaluate the use of the micro-CT method to test for toxic chemicals, using phenobarbital as the model chemical.

Phenobarbital is used as a sedative and antiseizure drug (https://pubchem.ncbi.nlm.nih.gov/). In the toxicology field, phenobarbital is known as a typical activator of the constitutive androstane receptor (CAR) and inducer of various xenobiotic metabolic enzymes representing the Cytochrome P450 family 2, subfamily b (CYP2B) (Waxman, 1999). Moreover, CAR works to maintain homeostasis and regulate hormone levels, such as steroid hormones (You, 2004). However, the carcinogenicity of phenobarbital on mammals was reported and was listed in Group 2B (possibly carcinogenic to humans) by the International Agency for Research on Cancer (IARC) (https://www.iarc.who.int/). Phenobarbital can increase liver weight in only a few days during continuous exposure, and its biological responses in the liver have been well investigated (la Vecchia and Negri, 2014; Thomas S. Argyris, 1968). Hepatocellular hyperplasia and hepatocellular hypertrophy were reported as the mechanism by which to increase the liver weight caused by phenobarbital in rodents (Ozawa shogo et al., 2011; Phillips et al., 1997; Ross et al., 2010; Shizu et al., 2013). Hepatic hypertrophy was mainly derived from the increased hepatocyte volume, which results from the proliferation of the smooth endoplasmic reticulum, and is related to phase 1 and 2 metabolic enzymes, oxidative status, and fatty metabolism. Hepatic hyperplasia is hepatocellular proliferation caused by an active replicative DNA synthesis (Hall et al., 2012; Ross et al., 2010). Phenobarbital induced hepatomegaly was considered to occur via CAR as CAR knockout mice did not show significant differences in their liver size after phenobarbital injection, which induced hepatomegaly in normal mice (Ross et al., 2010). Oxidative stress may be one of the pathways that leads to a heavier liver. However, null mice of CYP2B1, the most typical target gene, showed partially declining phenobarbital effects on hepatomegaly; thus, the other CAR target genes were suspected in this hepatic reaction (Li et al., 2017). The possible responsible pathways were genes related to cell cycle transition and cell growth regulation, such as cyclin (Ozawa shogo et al., 2011; Shizu et al., 2013). Analysis using amplified fragment length polymorphisms (AFLPs) identified the expression of 12 genes associated with cell cycle, growth regulation, and apoptosis that were upregulated in rats exposed to phenobarbital for 13 weeks (Elrick et al., 2005). These pathways will be considered as the cause of hepatomegaly induced by

phenobarbital. Many chemicals that had interactions with CAR, and then phenobarbital was widely used as typical CAR activators in the evaluation of toxic chemicals (Lake, 2018; Moore et al., 2006). In this study, phenobarbital was chosen as a model chemical to evaluate CT methods for toxicity tests due to the large amount of previous research using phenobarbital and its short-term dramatic effects on hepatomegaly.

Recently, another new technique dealing with big data, such as metabolomics and lipidomics, has also been utilized for toxicity tests. The metabolomic analysis helps us achieve a better understanding of the mode-of-action and identify the possible biomarkers related to chemical exposure (Ramirez et al., 2013). Plasma or serum is well-used for metabolomics and lipidomics, and small volumes (<100 uL) can be utilized to elucidate the metabolome and lipid profiles in animals (Tsugawa et al., 2020). Thus, these analyses can be conducted throughout an animal's lifetime. The results would explain the physiological status or changes related to chemical exposure, and the utilization of this data in regulatory and risk assessments is desirable (Ramirez et al., 2013). The effects of chemicals associated with CAR were also investigated using metabolomic (Hu et al., 2020; Zhang et al., 2019) and lipid analysis (Chen et al., 2019; Nguyen et al., 2017; Salihovic et al., 2016; Skoda et al., 2022). For example, metabolomics revealed that 4-bis[2-(3,5-dichloropyridyloxy)]benzene (TCPOBOP) which is a well-known CAR activator, altered the lipid profile in mice, and the energy metabolism associated with CAR such as fatty acid metabolism and lipid homeostasis was investigated (Chen et al., 2019). Multiomics which utilizes several "omics" is utilized to help improve our understanding of diseases and medicines (Hasin et al., 2017; Huang et al., 2017). This research also used metabolomics and lipidomics analyses combined with histopathology, clinical biomarkers, and quantitative PCR. In addition to the approach using micro-CT, the multiomics approach may help to reveal the mechanisms for chemical biological effects and help monitor toxicity in animals more accurately using plasma.

Toxicity tests using experimental animals are essential when evaluating new chemicals or new medicines. Toxicity tests from two different species (rodent and non-rodent) are recommended (Pharmaceuticals and Medical Devices Agency, PMDA, https://www.pmda.go.jp/english/index.html). Rodents have been widely used for assessments such as morphological, pathological, and biochemical analyses (Parasuraman, 2011). While most current tests assess toxicity after the animals have been

sacrificed, CT and metabolomics analysis could be used to evaluate animals throughout their lifetime and monitor the chronological changes that occur after the injection of the target chemicals. This study assessed the effects of phenobarbital on rats using both conventional (physical property, histopathology, gene expression, blood biochemical test) and new methods (CT, plasma metabolome, and lipids analyses). The liver is an especially susceptible organ where the toxicity of various drugs can be detected (Hardisty and Brix, 2005). Thus, the current study targeted the liver, especially hepatomegaly, in phenobarbital exposed rats to show the effectiveness of CT and plasma metabolome analysis as toxicity tests.

2. Materials and Methods

2.1 Animal experiments

All animal experiments, including chemical exposure and CT scanning, were conducted under ethical conditions approved by Hokkaido University (approval number: 21-0083 for animal husbandry and chemical exposure, 21-0019 for CT scanning). Wistar rats (n = 12 and 10 for males and females, respectively) that were approximately 7 weeks old, were imported to the experimental animal facility at the School of Veterinary Medicine, Hokkaido University from Japan SLC, Inc. (Shizuoka, Japan). The rats were kept in an exclusive cage with a plastic inner cage (2–3 rats per cage). The rats had *ad libitum* access to food (CLEA Rodent Diet CE-2, CLEA Japan, inc., Tokyo, Japan) and distilled fresh water. Each cage included two shepherd tubes (Shepherd Specialty Papers, Watertown, TN, USA) and wooden toys for biting (Japan SLC, Inc., Shizuoka, Japan). The rats were kept in 12 h light/dark conditions for the entire experimental period. The body weight and health of each rat were assessed by the veterinarian every two days during the acclimatization period and every day during the injection period. The Laboratory Animal Care and Use Committee of Hokkaido University guidelines were followed for all procedures related to animal experiments.

The rats were exposed to normal saline (6 males and 5 females) or phenobarbital sodium in normal saline (80 mg/ rat kg, injection volume was approximately 300–400 μL; 6 males and 5 females) after approximately one week of acclimatization. Phenobarbital sodium or normal saline were injected on day 1, 2, and 4 during the daytime (Figure 3.1). Approximately 24 h after the final injection, the rats were transferred to the

Central Institute of Isotope Science, Hokkaido University, and scanned using the whole-body Micro CT (Inveon, Siemens Medical Solutions USA Inc., Knoxville, TN, USA). The rats expectedly fell asleep approximately 0.5–1 h after being injected with phenobarbital due to its hypnogenesis, but all rats recovered by the following morning. There were no unexpected symptoms identified in the exposed rats. Rats were positioned in ventral recumbency on the CT bedding. During the CT procedure, the rats were first anesthetized with 4% and then 2.5%–3.5% sevoflurane to maintain them via spontaneous air ventilation. CT images were obtained in a step-and-shoot mode. Acquisition parameters were as follows: tube potential 80 kV, tube current 500 μA, exposure 200 μAs, angular sampling 1°per projection for a full 360°scan, and effective pixel size 107.02 μm. Images were reconstructed using a Feldkamp algorithm (Feldkamp et al., 1984). After CT scanning, the rats were immediately euthanized using much volume of sevoflurane and following cervical dislocation. Blood was then immediately collected maximumly from the caudal vena cava and centrifuged with 4000 × g for 10 min. The supernatant was frozen using liquid nitrogen and kept in –80℃ until further analysis. Their livers were weighed using a scale and put into measuring cylinders filled with normal saline to quantify their volume. The histopathological and RNA samples were then collected separately from the left lateral lobe.

2.2 Analysis of the CT images

The liver size was evaluated throughout the lifetime of the rats using CT. CT can be utilized to measure organ volume directly; however, the liver could not be separated from the other proximal organs, such as the stomach and spleen. Consequently, I have developed a method to estimate the liver size using the liver length and the following analyses. In these analyses, all the images were evaluated and reviewed by veterinary radiology specialist. OsiriX DICOM Viewer (https://www.osirix-viewer.com/) (Pixmeo SARL, Switzerland) was used for the image analyses, and liver length was measured using two different methods.

The first and second methods used the two- and three-dimensional diameters of liver length, respectively. The first method measured the two-dimensional diameter (Figure 3.2a-1) between the cranial tip (Figure 3.2a-2) and caudal tip (Figure 3.2a-3) on the x axis (major axis of bed, Figure 3.2a-1) of the liver. However, although this method

only focused on the distance of the x axis, the cranial and caudal tips of the liver usually did not share the same sagittal image. Because the length could not be shown by a single sagittal image, I depicted an illustration for easy understanding how the measuring was done in Figure 2a-1. The second method measured the three-dimensional diameter of the length between the point of the caudal vena cava attached to the liver on the diaphragm (Pointα) and the caudal edge of the liver (Figure 3.2b). After Pointα was fixed, this method searched the hepatic caudal point for the longest distance from Pointα, ignoring the sagittal direction. The first analysis method showed a better correlation with the absolute liver volume measured using the measuring cylinder (the data is not shown.), thus, this study used the first method with the following conditions: WL 300, WW 1500. The thoracic cavity was measured using perpendicular transverse images from the cranial dorsal tip of the 9^{th} thoracic vertebrae to the ground (Figure 3.2c-1). The identification of the cranial dorsal tip of the 9^{th} thoracic vertebrae was conducted using the following condition: WL 300, WW 1500. While the area of the thoracic cavity (Figure 3.2c-2) was measured using the following conditions: WL 40, WW 400. The liver volume (cm^3) was calculated as liver length (cm) × thoracic cavity (cm^2) (the image was described in Figure 3.2d).

The normalization of the liver size against the entire body was usually done using the 11^{th} thoracic vertebrae (T11) in dogs in the veterinary field (An et al., 2019; Kim et al., 2018). However, the area of the 11^{th} thoracic vertebrae did not represent the entire body size of the rats in the current study (data is not shown). Total bone volume was selected to normalize the liver size, and this was analyzed using SYNAPSE VINCENT (FUJIFILM, Tokyo, Japan). Volumes with CT values > 900 were extracted and measured as the bone volume.

2.3 Histopathology

The middle of the left lateral lobe was cut into < 5 mm-thick sections for histopathology and kept in deodorized 10% formalin neutral buffer solution (FUJIFILM Wako Pure Chemical Corporation, Osaka, Japan) until further analysis. The preparation of the histopathological specimen sections and the following analysis was conducted by Sapporo General Pathology Laboratory, Hokkaido, Japan, the company managing the histopathological study. Hematoxylin and eosin staining (HE stain) were then conducted.

All rats from the control and exposed groups were analyzed by the pathologist from Sapporo General Pathology Laboratory.

2.4 Plasma clinical biochemistry analysis

Seven parameters (GOT: aspartate aminotransferase, GPT: alanine transaminase, TCHO: total cholesterol, TG: triglyceride and HDLC: high-density lipoprotein cholesterol, DBIL: direct bilirubin and TBIL: total bilirubin) were quantified in rat plasma using FUJI DRI-CHEM 7000V with the slides of each parameter (FUJIFILM corporation, Tokyo, Japan). FUJI DRI-CHEM is a commercially available instrument for clinical biochemical analysis, and specifically designed slides were prepared for each chemical. Then, 10 µL of plasma was used to analyze each parameter. Quality assurance (QA) and quality control (QC) were conducted using QC cards attached to each slide and two standard solutions (high and low control) supplied by the same company. All procedures were conducted according to the manufacturer's protocols.

2.5 Gene expression analysis

The edge of the left lateral lobe was cut into small pieces and preserved in RNA stabilization and storage reagent (RNA later, Sigma-Aldrich, Saint Louis, MO, USA) and kept at −30°C. A piece of the liver was digested using 800 µL of TRI reagent (Sigma-Aldrich, MO, USA). Extracted nucleotides were mixed with 200 µL of chloroform and then homogenized well. The mixture was centrifuged at 12000 × g for 25 min, and the supernatant was collected. Supernatant was applied into the desalted silica membrane of the Nucleospin RNA kit (Macherey-Nagel Düren, Germany), following the manufacturer’s protocol. The quality and quantity of the RNA were checked using gel electrophoresis and Nanodrop-1000A spectrophotometer (Delaware, USA). The ReverTra Ace qPCR RT Kit (Toyobo, Osaka, Japan) was used to obtain the first-strand cDNA, according to the manufacturer’s protocol. Quantitative real-time PCR was performed on a QuantStudio 12K Flex real-time PCR system (Applied Biosystems, CA, USA) using cDNA and a Fast SYBR Green master mix (Applied Biosystems, CA, USA). The primers used in this study are summarized in Table 3.1 and some of the primers were used in previous studies (Hamid et al., 2017; Hemmati et al., 2019; Kataba et al., 2021; Kawase et al., 2008; Liaset et al., 2009; Liu et al., 2011; Michihara et al., 2011; Miksys

et al., 2000; Miura et al., 2011; L. Wang et al., 2017; Zhang et al., 2015; Zhu et al., 2020, 2013). The PCR protocol followed the default setting of the instrument. Briefly, initially 95℃ for 20 s, followed by 40 cycles of 95℃ for 1 s and 60℃ (for all the genes) for 20 s using 10 µL of mixture containing 5 µL of Fast SYBR Green master mix, 300 nM forward and reverse primers, and 6.7 ng of synthesized cDNA and sterile purified water (Milli-Q IQ 7000, Merck, Germany). Primer specificity was checked using BLAST (https://blast.ncbi.nlm.nih.gov/Blast.cgi) in advance and single peaks for the melting curve analysis after running on the machine. The gene expression in each rat was normalized using the housekeeping gene, *beta-actin*, and the relative expression of the exposed group compared with the control was used to calculate sex dependently using the comparative CT method (ΔΔCT method). The average gene expression in the male and female control rats was defined as one and was used for the calculation. For the three target genes, the results for a few rats (one rat for *Ccnb1*, two for *Cyp2b1*and three for *Ccnb2*) were out of the range of assured primer efficiency, but the lowest sample concentration was slightly lower than the lowest point for the primer efficiency level (the difference of the threshold cycle value was within 1.0). Thus, this research did not correct the value and included them in the analyses.

2.6 Plasma metabolome analysis (GC/MS analysis)

2.6.1 Extraction

First, 50 µl of plasma was mixed well with 250 µl of a mixture of a methanol, ultra-pure water, and chloroform (5:2:2). Then, 10 µl of internal standard (4 µg/mL ribitol in methanol) was added and incubated at 37℃ for 30 min at 1200 rpm. The mixture was centrifuged at 15000 × g for 5 min at 4℃. The supernatant was then transferred to a new 1.5 ml tube and 200 µl of ultra-pure water was added. The aliquot was centrifuged again at 15000 × g for 5 min at 4℃. Next, 250 µl of the supernatant was transferred into a new 1.5 mL tube with a hole on the cover. Methanol was removed from the extract using a vacuum evaporator (CVE-2100, Tokyo Rikakikai, Tokyo, Japan) for two hours at room temperature; the samples were then kept at -80℃ for more than 30 min. Frozen extracts were dried using a freeze dryer (DC401, Yamato Scientific, Tokyo, Japan) overnight.

Two derivatizations were conducted for the following GC-MS/MS analysis. The pierced cover of 1.5 mL tube was replaced with a new unpierced cover. The 1st and 2nd

derivatizations were conducted using 80 µl of 20 mg/mL methoxy amine-HCL in pyridine (GL Sciences Inc., Tokyo, Japan) and 40 µl of N-methyl-N-trimethylsilyl-trifluoroacetamide (Thermo Fisher Scientific, Waltham, MA, USA), respectively. After adding each derivatization reagent, the mixture was mixed well and kept at 30℃ for 90 min in the 1st reaction and at 37℃ for 30 min in the 2nd reaction with gently shaking at 1200 rpm. The derivatized extracts were centrifuged at 15000 × g for 5 min at 4℃; the supernatant was then used for gas chromatography (Nexis GC-2030, Shimadzu, Kyoto, Japan) in tandem with mass spectrometry analysis (TQ8050 NX, Shimadzu, Kyoto, Japan) (GC-MS/MS).

2.6.2 Quantification

All samples were quantified using GC-MS/MS with a standard polysiloxane GC column (DB-5, Agilent, CA, USA) with an inner diameter of 0.25 mm and film thickness of 1.0 µm. Metabolome quantification and identification were conducted using the Smart Metabolites Database Ver.2 (Shimadzu, Shimadzu, Kyoto, Japan). The parameters for GC and MS/MS in this analysis were applied as per the manufacturer's instruction and the details are described in Table 3.2. Peak identification was conducted using the product ion, target ion/reference ion ratio, and retention time normalized using n-alkane in advance. In total 149 chemicals were registered as animal blood derived metabolites in the database. The time program (totally 37 min) started at 100℃ for 4 min, heated up to 320℃ (rate 10%) with holding at 320℃ for 11 min. The description of quality assurance (QA) and quality control (QC) for GC/MS/MS is combined with subsection 2.7 Plasma untargeted metabolome analysis (HPLC-qToF/MS) and is presented in 2.7.3.

2.7 Plasma untargeted metabolome analysis (HPLC-qToF/MS)

The metabolome and lipid analyses were carried out at the Center for Preventive Medical Science, Chiba University using high performance liquid chromatography (HPLC) along with time-of-flight mass spectrometry (HPLC-qToF/MS). Organic solvents for the mobile phase (qToFMS grade of acetonitrile and methanol) were purchased from Wako Pure Chemical Industries (Osaka, Japan); ammonium hydroxide, formic acid, and ammonium bicarbonate were purchased from Sigma-Aldrich (Saint Louis, MO, USA). Ethylenediamine-N,N,N',N'-tetraacetic acid, disodium salt, dihydrate

(EDTA $2NH_4$) was purchased from Dojindo Laboratories (Kumamoto, Japan); and ammonium acetate was purchased from Wako Pure Chemical Industries (Osaka, Japan).

2.7.1 Extraction

For extraction 100 μL of plasma was mixed with methanol containing 100 μM N,N-diethyl-2-phenylacetamide and d-camphor-10-sulfonic acid (Wako Pure Chemical Industries, Osaka, Japan) as an internal standard. The mixture was then centrifuged at 14000 × g for 5 min at 4℃. The supernatant was applied to a cartridge (AMICON ULTRA 0.5 mL, Merck, Darmstadt, Germany) conditioned with ultra-pure water (RFD280NC, ADVANTEC, Tokyo, Japan) and then centrifuged at 14000 × g for 60 min at 4℃. The eluted liquid was transferred to a vial for quantification using the ExionLC™ AD system (SCIEX, Tokyo, Japan) with qToF/MS (SCIEX, Tokyo, Japan) and electrospray ionization (ESI). Lipid analysis was performed as reported previously, with slight modification (Tsugawa et al., 2020). Briefly, 20 μL of plasma was mixed with 200 μL of Methanol containing 2 μg/mL internal standard mix (EquiSPLASH LIPIDOMIX Quantitative Mass Spec Internal Standard, Avanti Polar Lipids, Birmingham, England). The mixture was kept at -80℃ for approximately two hours and then transferred to a glass tube. Next, 100 μL of chloroform was added and mixed vigorously; the mixture was again kept at -80℃ overnight. The glass tubes were centrifuged at 3000 × g for 10 min at 4℃. The supernatant was transferred into HPLC vials and then used for lipid analysis.

2.7.2 Quantification

All samples were quantified using HPLC-ToF/MS using SeQuant ZIC-HILIC (3.5 μm, 100 × 2.1 mm) (Merck, Darmstadt, Germany) and SeQuant ZIC-pHILIC (5 μm, 100 × 2.1 mm) (Merck, Darmstadt, Germany) for the positive and negative ion modes for metabolome analysis respectively, and using an ACQUITY UPLC Peptide BEH C18 Column (1.7 uM, 2.1 mm×50 mm) (Waters, Milford, MA, USA) for both positive and negative ion modes for lipid analysis. The LC and qToF/MS conditions for metabolome and lipid analyses were modified from previous reports (Okahashi et al., 2021; Saigusa et al., 2016; Zhang et al., 2012). For both ion modes of metabolome analysis, the gradient program was as follows: 95% solvent B, then at t = 6 min: 40% B, t = 9 min: 5% B, t = 9.01–11 min: 90% B, t = 11.01–18 min: 95% B. The detailed information for the other

parameters of metabolome analysis is presented in Table 3.3. The LC and qToF/MS conditions for the lipid analysis are shown in Table 3.4. For both ion modes of lipid analysis, the gradient program started at 0% solvent B for 1 min, then, at t = 5 min: 40% B, t = 7.5 min: 64% B, t = 7.5–12: 64% B, t = 12.5: 82.5% B, t = 19: 85% B, t = 20: 95% B and then immediately returned to the initial conditions for 5 min.

The metabolome and lipids were analyzed using Mass Spectrometry – Data Independent AnaLysis (MS-DIAL) software version 4.9.0 (Tsugawa et al., 2020, 2015) and R statistical environment Ver 4.1.2 (https://www.r-project.org/). The following libraries were used for peak selection and annotation of metabolome analysis: HPLC-qToF/MS: RIKEN (Tsugawa et al., 2015), Massbank of North America (https://mona.fiehnlab.ucdavis.edu/), human metabolome database (Wishart et al., 2018), and National Institute of Standards and Technology (2020) tandem mass spectrometry library. The specimen with the highest calculated MS/MS spectrum similarity score (at least more than 80) was used for the analyses.

2.7.3 QA/QC and data preprocessing

Blank samples were prepared to check contamination in the extraction phase and overflow during GC-MS/MS and LC-qToF/MS quantification. Blank samples comprised the same volume of ultra-pure water as the samples used in each analysis instead of plasma, along with the internal standard; the other procedures of extraction were the same as those used for the plasma sample. Pooled plasma using all the samples was prepared for QC. Extraction of QC samples was conducted using the same method as that used for the samples. In total, seven QC samples were analyzed regularly during GC-MS/MS and LC-qToF/MS quantification of 22 samples. All peaks were normalized using each internal standard, locally weighted least-square regression (locally estimated smoothing function, LOESS), and cubic spline with the QC samples. The metabolomes were discarded from dataset if they showed the following characteristics: 1) the ratio of blank average/QC average was more than 10%, 2) relative CV was more than 0.3, 3) no detection rate was more than 30% in the entire sample, 4) the concentration exceeded the maximum levels of GC-MS/MS, and 5) the annotation level was less than two as proposed in a previous report (Schymanski et al., 2014) for LC-qToF/MS analysis. In some metabolomes quantified using GC-MS/MS, identification of the peak was not reliable because of a close

peak with the same target and reference ion. As I did not have the standard solution for each metabolome to check the exact retention time, these undetermined peaks were also excluded from the GC-MS/MS analysis.

The identifier of the extracted metabolome from GC/MS/MS and LCqToF/MS was unified into KEGG (Kyoto Encyclopedia of Genes and Genomes, https://www.genome.jp/kegg/) using the PubChem Identifier Exchange Service from NCBI (National Library of Medicine, https://www.ncbi.nlm.nih.gov/). The non-registered metabolome in KEGG was excluded from the sample data set. When the same chemical compounds were analyzed in both GC/MS/MS and HPLCqToF/MS, the data from GC/MS/MS were adopted. In total, 78 metabolites from GC/MS/MS, 20 metabolites from LC-qToF/MS (1 and 19 from positive and negative ion mode respectively) and 223 lipids (72 and 151 from positive and negative ion mode respectively) passed these conditions and were included in the dataset for subsequent analysis.

2.8 Statistical analysis

2.8.1 General statistical analysis

JMP 16 (SAS Institute, NC, USA) software was used for general statistical analysis. The Welch t-test was used to compare the clinical biochemistry analysis between the control and exposed samples. The correlation between physical characteristics and liver sizes and between normalized liver sizes in different methods were calculated using the Pearson correlation coefficient. The results of the histopathology were converted into numerals to compare with the other results and scored from 0−0.8 in steps of 0.2 for each grade.

Because of the sample size, the normal distribution was not investigated, and consequently, both parametric and non-parametric methods were utilized for gene comparisons between the control and exposed groups. The comparison of gene expression between the control and exposed groups was investigated using both the Welch t-test and Wilcoxon test, and significant differences were defined when both statistical tests showed significant results (p value < 0.05).

2.8.2 Statistical analysis for metabolome and lipid analysis

The correlation between male liver volume (liver volume MC/bone volume) and metabolomes from GC/MS was investigated using Spearman's rank correlation coefficient, and the significantly correlated metabolites (p value < 0.05) were used for pathway analysis using MetaboAnalyst 5.0 (https://www.metaboanalyst.ca/) (hypergeometric test and relative-betweeness centrality as enrichment and topology analysis respectively). Pathway enrichment analysis was evaluated using p value and the false discovery rate (FDR) was calculated using MetaboAnalyst. The results of the lipid analysis were assessed and visualized using BioPAN, LIPID MAPS (https://lipidmaps.org/) (Lopez-Clavijo et al., 2021). In LIPID MAPS, the Z-score, for which each weighted reaction was calculated (the higher score means the reaction is more activated.) and activated and suppressed reactions in the exposed group were compared with the control and classified when the changes were significant (p< 0.05). Detailed information on the statistical analysis of LIPID MAPS was described in a previous report (Lopez-Clavijo et al., 2021; Nguyen et al., 2017).

2.8.3 Statistical analysis for multiomics analysis

For multiomics analysis, the features with coefficients of variation (CV) < 0.3 among the samples (all male and female rats) were discarded. The remaining results from the gene, metabolome, and lipid analyses were used for multiomics analysis. For the gene expression analysis, this study has discussed the results for sex-separately; however, the data for the female rats was renormalized using the male control for the classification of the four groups in the multiomics analysis to evaluate sex differentiation.

DIABLO model to classify four groups

Data Integration Analysis for Biomarker discovery using Latent variable approaches for Omics studies (DIABLO) (Singh et al., 2019) was conducted using a mixOmics package (Rohart et al., 2017) to classify the four groups (male control, male exposed, female control, and female exposed) based on the gene, metabolome, and lipid profiles. The classification performance, the number of components, and variable selections in the DIABLO model were determined using 100 times repeated three-fold

cross-validation. The model which showed the lowest balanced error rate was selected. Selected variables were put in networks connected with each other when highly correlated (correlation coefficient > 0.75).

MB-PLS model to find the possible biomarker

Multiblock partial least squares regression (MB-PLS) was also conducted for males using a mixOmics package (Rohart et al., 2017) to explore the genes, metabolomes, and lipidomes associated with increased liver volume. The correlations of all the variables to the normalized liver volume were tested using Spearman's rank correlation coefficient. The variables with p values > 0.05 (Spearman's rank correlation test) were discarded. I targeted only male rats because the variance in the female liver volumes was low, and most variables were dismissed. The selected variables were analyzed again using sparse partial least squares regression (sPLS) (versus normalized liver volume), and the improper variables were excluded from the dataset so that the mean absolute error would become the minimum. Selected variables were included into the network using a mixOmics package.

3. Results

3.1 Micro-CT

The physical characteristics and liver sizes for both sexes are described in Table 3.5 (summary in each group) and Table 3.6 (correlation of each parameter) for the classical methods (liver weight and liver volume) and CT scanning (bone volume, liver length, and liver volume) analyses. Body weights in both sexes were similar for the control and exposed groups; 199.6 g and 200.0 g for the male control and exposed groups, respectively, and 150.4 g and 150.6 g for the female control and exposed groups, respectively. The weight and volume of the livers, however, were significantly larger in the exposed group than the control group for the male rats ($p < 0.05$), however, the same tendency was not seen in the female rats. All the pairs among the parameters were significantly correlated ($p < 0.001$) (Table 3.6a), and the liver size, liver weight (weight scale), and liver volume (measuring cylinder) were strongly correlated (correlation coefficient 0.99). This study targeted the liver size and thus, the following sections use liver volume (measuring cylinder) as the representative of liver size based on the classical methods. When comparing the classical method and CT method, liver length (without area of thoracic cavity, Figure 3.2a-1) (CT) was well correlated (correlation coefficient 0.87), but liver volume was calculated using the area of the thoracic cavity (CT) as it had a better correlation coefficient (Table 3.6a). In addition, Figure 3.3 shows a regression analysis to evaluate the CT methodology. Normalized liver sizes using the entire body size were also evaluated and summarized in Table 3.7. Normalization was done using body weight and bone volume. Most pairs of normalized liver sizes significantly correlated ($p < 0.05$). The combination of the classical method (liver volume from measuring cylinder/body weight) and the CT method (liver volume from CT/bone volume) were also well correlated (correlation coefficient 0.74). Exposed male rats had higher liver volumes (CT) when normalized by the bone volumes (normalized liver volume) than the control male rat, as shown by the liver weight/body weight comparisons in Figure 3.4. The comparisons between the control and exposed male rats showed that there were larger livers in the exposed group regardless of the normalization method for rat size (Table 3.5). However, female rats did not show any significant differences between groups.

3.2 Classical evaluation method for chemical toxicity

Hepatocellular mitotic figures and enlarged Kupffer cells were detected in exposed rats using a histopathological analysis. The levels were scored from 0−4, which indicates no abnormality to intensity. All the abnormality detected in the current study was level 1 and 2 (slight change). Over 50% of the male rats expressed hepatocellular mitotic figures and enlarged Kupffer cells and only one female showed hepatocellular mitotic figures, however, there were no other abnormalities in the histopathological analysis. The results are summarized in Table 3.8, and the photos of representative areas from each group are shown in Figure 3.5.

The results of the clinical biochemical analysis (ALP, GOT, GPT, TCHO, TG, HDLC) are shown in Table 3.9. For DBIL and TBIL, many samples recorded concentrations at the detection limit (0.1 mg/dL); thus, these data were excluded from the table. No significant changes were seen in the females between the control and exposed groups. In the male, TCHO and HDLC levels in the exposed group were significantly higher than in the control group as the TCHO and HDLC levels were 44.3 and 32.8 in the control and 61.5 and 43.5 in the exposed groups, respectively. No significant changes were observed in ALP, GOT, GPT, and TG.

The results of the quantitative PCR are summarized in Table 3.10. The relative gene expression levels of various cytochrome P450s, bile acid related genes, cyclins, and oxidative stress or apoptosis pathway related genes in the male and female exposed groups compared with their controls are shown in Table 3.10a-d. The expression of *Cyp2b1*, which is a typical target of phenobarbital, was dramatically induced in both sexes (628.2 ± 164.27 and 2891.1 ± 1017.38-fold in males and females, respectively). In male rats, various cytochrome P450 gene expressions were significantly induced, with *Cyp3a1* and *Cyp27a1* induced by 11.03 and 1.87-fold, respectively, in the exposed group. However, except for *Cyp2b1* and *Cyp3a1*, female rats did not show any strong differences in cytochrome P450 expression between groups. *Cyp8b1* was downregulated in both sexes, especially in exposed males (0.64 ± 0.26, p value < 0.05). There were significant differences in *Ugt1a1*and *Baat* in the males, but no consistent degree of significance was observed between sexes for any target gene (Table 3.10b). *Cyclin* gene expression levels were highly induced in both sexes (Table 3.10c). The induction level for *Cyclin* was greater in male rats but was only considered significant in females. When focusing on

gene expression levels related to the pathways for oxidative and apoptosis, *Sod1* in males and *Bax* in male and female exposed groups were significantly upregulated (Table 3.10d).

3.3 Metabolome and lipid analyses

The metabolites, which were significantly correlated to liver volume, were extracted, and the details are in Table 3.11. The metabolites were used for pathway enrichment analysis, but a relevant pathway was not identified (Table 3.12).

Forty-eight lipids were used for lipid analysis (most of the detected lipids were unprocessed in LIPID MAPS) and listed in Table 3.13. The results of the lipid analysis are shown in Figure 3.6 (lipid class), Figure 3.7 (lipid species and fatty acid), and Table 3.14 (related genes). In males, several significant reactions were observed between the control and exposed groups; for example, the reactions between phosphatidylcholine (PC) and phosphatidylethanolamine (PE) and between PC and diacylglycerols (DG) (Figure 3.6). Overall, the concentration of DG seemed to increase, and PE seemed to decrease as the reactions from PC to DG and PE to PC were activated, but the reaction from DG to PC, PE and phosphatidic acid (PA) were relatively suppressed. However, the results for the lipids in females did not show any significant reaction among lipid class.

I mentioned the results and discussion regarding multiomics analysis separately in section 5 (5. Results and discussion of multiomics analysis).

4. Discussion

To avoid any misunderstandings, I would like to first clarify for the readers an issue related to this study. Adaptive hypertrophy caused in the liver was mostly defined as a non-adverse effect depending on factors such as the mechanisms and dose (Hall et al., 2012). Especially with phenobarbital, a pause in exposure resulted in the rat liver recovering to the same size as that of the control rats (13 weeks exposure then 4 weeks withdrawal) (Ozawa shogo et al., 2011). This report considered hepatomegaly as the toxic effect induced by phenobarbital in this research. However, the current study did not detect enough phenobarbital toxicity in the exposed rats using the above methods. The current research could thus not conclude if the detected liver changes were toxic for the rats. The predictive models to evaluate carcinogenic hypertrophy were discussed (Liu et al., 2017).

However, further discussion is required to define the toxicity of phenobarbital.

The classical method (measuring cylinder) was used to determine the true absolute volumes of the rat livers. The CT method was thus compared with the results from the classical method to evaluate its accuracy. The liver volumes determined using the measuring cylinder and CT were found to be well correlated (Pearson correlation coefficient, ρ = 0.96; Table 3.6). The liver length was also strongly correlated with the liver volume (measuring cylinder; ρ = 0.87), however, using the area of the thoracic cavity can result in more accurate estimations of the volume. The inclusion of the thoracic cavity in the estimation of liver size was previously applied for radiographic analysis in veterinary medicine (Kim et al., 2018). This research has demonstrated that the calculation using both liver length and the thoracic area should be effective even in rats. Numerous previous reports have evaluated the liver or tumor using contrast enhanced CT (Fiebig et al., 2012; Fouillet et al., 1995). The images in this study did not enable differentiation of the liver from the spleen and stomach, a limitation which might have been overcome by the use of a contrast medium. However, the exclusion of a contrast medium ensured the accurate evaluation of the toxic chemical, phenobarbital, without exposing the rats to other chemicals for the duration of the experiment. The liver size should be normalized against the entire body size to assess several different stages of growth. As mentioned above, in veterinary medicine T11 has been widely used for normalization in dogs and cats. However, the use of T11 failed in the current study (data was not shown.). Consequently, two indicators for body size (body weight and bone volume) were used. I consider that bone volume (mL) can be normalized more easily than body weight (g), as it uses the same units for calculation, which as the liver (mL) (we do not have any evidence in this point). The body weight of rats can change within a day, which is in contrast to the relatively steady volume maintained by bone. This study utilized a special software (SYNAPSE VINCENT) to measure only the bone volume. For easier access using CT, body weight could be an alternative as the correlation between liver volume/ body weight and liver volume/ bone volume was significantly and highly correlated with correlation coefficient of 0.81 in females and 0.99 in males (Table 3.7).

Cyp2b1 was shown to be induced 628.2 and 2891.1 folds in the male and female phenobarbital exposed groups, respectively (Table 3.10). These results suggest that the activation of CAR by phenobarbital was successful. When comparing the liver sizes

between the control and exposed groups, hepatomegaly induced by phenobarbital was identified in the exposed male rats (Table 3.5; all the normalization methods showed the same level of significance.). The evaluation of the liver size based on the liver volume/bone volume showed the same results and significance as that of the liver weight/ body weight when compared between the male control and exposed groups (Figure 3.4). From these results, I concluded that the present CT method could detect hepatomegaly throughout the lifetime of the rats exposed to phenobarbital. The usefulness of two-dimensional analysis using x ray radiographic examination was investigated in dogs and compared with normal liver, microhepatia and hepatomegaly (Semi et al., 2019). Even using two-dimensional method, this research showed effective estimation of the liver size in rats. This research used only one development stage (7-8 weeks rats). Further study needs several growth stages of rats and several toxic chemicals to evaluate and ensure the method itself. The current estimation methodology does not directly demonstrate the exact volume of livers, which is a limitation of the present study. However, the Pearson correlation coefficient between measurements of liver volume using measuring cylinder and CT analysis showed a high correlation as stated above. Further analysis using regression analysis (Figure 3.3) gives an equation: [liver volume (MC) = 0.69 x liver volume (CT) – 0.2] to estimate the volume of liver using CT.

Blood biochemical analyses were conducted. Once the liver was injured, biochemical liver markers were dramatically increased. For example, chronic phenobarbital injection induced more than twice the levels of ALP and ALT in dogs (Müller et al., 2000). The combination of these markers has been used in human medicine to diagnose liver disease (Lin, 2009). Unfortunately, in this study, blood biochemical analyses, such as ALP and GOT, did not show strong differences between the control and exposed groups in both sexes. Furthermore, the histopathological test did not show significant damage to the hepatocytes of the exposed group. From these results, it is considered that the destruction of the hepatocytes did not occur in the rats when these biochemical parameters did not significantly change. While blood collection was done after euthanasia in this research, the rat blood can be collected throughout their lifetime from tails, which strengthen the power of chemical toxicity detection using micro-CT throughout a lifetime.

Postmortem analysis (histopathology and gene expression in liver) was also conducted in this study. Notably, hepatocellular mitotic figures were seen in some individuals in the exposed group. This suggests that the upregulated gene expression of cyclin B in the exposed group could be one of mechanisms of induced cell proliferation.

Moreover, the relationship between cyclin and CAR has previously been investigated; phenobarbital and TCPOBOP exposure induce cyclins in rodent livers (Bhushan et al., 2021; Blanco-Bose et al., 2008; Shizu et al., 2013). The results of this study support previous studies that had upregulated cyclin levels showed that phenobarbital induces hepatocellular hyperplasia in the rat liver (Ross et al., 2010; Shizu et al., 2013). The Yes-Associated Protein (YAP) knockout mice had a notable Cyp2b induction but significantly lower expression of Cyclin B1 when compared with wild rats after TCPOBOP exposure. Thus, the YAP was associated with CAR induced hepatomegaly, independently of CAR induced metabolic enzymes (Bhushan et al., 2021).

The gene expression levels for several antioxidative enzymes are shown in Table 3.10. SOD, CAT, and GPx are well-known endogenous antioxidative enzymes that can decrease the superoxide radical anion (SOD) and H_2O_2 (CAT and GPx) (Pisoschi and Pop, 2015). Some metals and chemicals, such as lead and DDT, can decrease the ability of these enzymes and cause oxidative stress or apoptosis (Liu et al., 2010; Marouani et al., 2017). In male rat livers, most of the enzymes were slightly induced (Table 3.10c). Acute toxicity when using microcystins in rats has been reported, and enzymes dramatically alter their up and down-regulation within 24 h (Xiong et al., 2010). Thus, this research cannot reveal whether phenobarbital-CAR directly affected the expression of these genes or if the antioxidative gene was induced by reacting to oxidative stress. The CYP superfamily which induced by phenobarbital can be a cause of active oxygen species (Imaoka et al., 2004). Nuclear factor erythroid 2-related factor 2 (Nrf2) was a transcription factor related to antioxidative responses. For example, *Hmox1* and *Txnrd1* in Table 3.10c were regulated by Nrf2 (https://www.kegg.jp/kegg/). One study reported that Nrf2 activation was tightly associated with CAR activation (Rooney et al., 2019). These pathways possibly induced mRNA expression of antioxidative enzymes in the current study. However, the levels of upregulation were not noticeable, and histopathological analysis did not detect significant differences, which would indicate oxidative stress between the control and exposed groups. Phenobarbital induced

hepatomegaly was found to be induced by both hepatocellular hypertrophy and hyperplasia in rodents (Ross et al., 2010), but the current study could not find enough evidence of hepatocellular hypertrophy from both histopathology and gene analysis. Another possible mechanism behind the cause of hepatomegaly by the CAR activator is its antiapoptotic effect. The suppression of apoptosis against ultraviolet (UV) light was seen in rat hepatocytes exposed to phenobarbital in a dose-dependent manner (Gährs and Schrenk, 2021). In another report, phenobarbital induced the release of tumor necrosis factor-alpha in mesenchymal cells in the liver and worked antiapoptotic. Interestingly, that research also showed that the number of transcriptomes that were affected by phenobarbital was greater in mesenchymal cells than hepatocytes (Riegler et al., 2015). Antiapoptotic effects regulated in mesenchymal cells could be a possible mechanism of phenobarbital induced hepatomegaly.

5. Results and discussion for the multiomics analysis

5.1 Comparison among the four groups using the DIABLO model

The DIABLO classification error rate was 6.0% when 100 times of three-fold cross-validation was repeated. The DIABLO model extracted variables (17 genes, 10 metabolites, and 45 lipids) for the determination of component 1 and variables (3 genes, 5 metabolites, and 10 lipids) for component 2. The variables were ranked depending on their level of contribution to the determination of components 1 and 2 (Figure 3.8 and 3.9). For example, *Gpx1*, *Cyp4a1*, and *Bax* were identified as highly contributing genes for component 1, while *Baat*, *Cyp2b1*, and *Ugt1a1* were identified as major contributors for component 2. In total, 15 metabolomes were identified, but there were no significantly enriched pathways (FDR < 0.1) found in the pathway enrichment analysis (data not shown). Several lipid classes, such as PC and PE hexosylceramides (HexCer) were proposed (Figure 3.8 and 3.9). The score plots from the DIABLO analysis show that sex differences were clearly separated by component 1 in relation to the genes, metabolome, and lipids (Figure 3.10). Components 1 and 2 helped to differentiate between control and exposed in both sexes. The network among the selected variables is shown in Figure 3.11. Two networks were described, and included the genes *Cyp2b1*, *Cyp3a18*, *Ugt1a1*, and *Baat*, as well as three metabolites and eight lipids (Figure 3.11-a). Another network (Figure 3.11-b) included only two genes (*Bax* and *Gpx1*), six metabolites, and more than

30 lipids. The lipid profiles were different as the network 11-a included only PC and PE while that on the 11-b had PC and PE as well as others such as fatty acids (FA), phosphatidylethanol (PEtOH), phosphatidylinositol (PI), and HexCer.

Color map showed cluster analysis, and I defined five cluster from variables (Figure 3.12). The DIABLO model clearly separated the male control and exposed groups using the selected variables (at columns) in the cluster analysis. However, the model was not effective at identifying the differences between the female control and exposed groups. Cluster A showed similar results between the males and females, as the level of both exposed groups was higher than that of the control. In this cluster, well-known CAR associated genes such as *Cyp2b1* and *Cyp3a1* were listed, and noticeable inductions of these enzymes were already reported in both sexes (Table 3.10). The variables such as galacturonic acid and glycerol 2-phosphate in this cluster could help to understand the biological changes commonly preserved in both sexes against phenobarbital exposure. The network 11-a shown in Figure 3.11 mainly contributed to component 2 and some of them were listed in cluster A. Statistics demonstrated that both galacturonic acid and glycerol 2-phosphate are related to *Baat* and *Ugt1a1*, which play important roles in bile acid biosynthesis (Ferdinandusse and Houten, 2006; Wagner et al., 2005) and could thus be used to estimate gene expression induction using plasma. Contrary to cluster A, cluster E included only lipids, and the controls for both sexes had higher levels than the respective exposed groups. Cluster D clearly separated the male and female groups regardless of phenobarbital exposure. Some variables in this cluster were consistent with those that highly contributed to component 1 in Figure 3.8. Interestingly, Figure 3.12 showed the male-unique lipid profile between control and exposed in cluster C. PC and PE are the most abundant lipids in mammalian cells, and both are involved in several biological processes such as very-low-density lipoprotein (VLDL) secretion (van der Veen et al., 2017). Cluster C predominately consisted of PC and PE, and the profile of the exposed male was more similar to females than the male control, and no noticeable change was found in females between the control and exposed. This cluster reflected male specific changes of the lipid profile shown in Figure 3.6. Significant differences of the normalized liver weight are only seen in the male, although noticeable inductions of *Cyp2b1* were found in both sexes. The lipid profile (mainly PE such as PE 34:2 and PE 40:5) shown in cluster C may be associated with pathways connected to hepatomegaly in

males. However, there were two reports to investigate the relationship between lipids and CAR, and the PE did not show significant differences in the TCPOBOP-exposed mice (Chen et al., 2019; Skoda et al., 2022). The PC and PE can be synthesized using individual pathways from the choline and ethanolamine respectively, but around 20%−30% of the PC was produced by trimethylation of the PE in the liver (Calzada et al., 2016; van der Veen et al., 2017). The conversion from PE to PC which is mediated by N-methyltransferase (PEMT) (Table 3.14) could be activated in this study (Figure 3.6). Pemt is regulated by estrogen (Resseguie et al., 2007), but one report showed that TCPOBOP exposure did not induce Pemt in mice (Chen et al., 2019). In the same report, the expression of several genes related to fatty acid metabolism, such as fatty acid synthase (Fasn), sterol regulatory element binding protein-1 (Srebp1), and carnitine palmitoyltransferase 1A (Cpt1a) were significantly changed in TCPOBOP exposed mice (Chen et al., 2019). Further gene analysis targeting the enzyme and its regulator related to the PE-PC reaction would provide further evidence that PE is a biomarker.

There are at least three possibilities that could explain the relationship between lipids and hepatomegaly, as shown in Figure 3.13. The first is that lipids contributed directly to phenobarbital induced hepatomegaly (a). The second is that lipid profiles were changed as a result of biological processes through hepatomegaly (b), and the last is that genes induced by phenobarbital altered lipid profiles independently of hepatomegaly (c). For example, dietary fatty acids such as omega-3 (n-3) and omega-6 (n-6) are reported to have various functions in mammalian bodies. Both are related to cell proliferation and inflammation as precursors of lipid mediators (Larsson et al., 2004; Wall et al., 2010). The metabolomics report indicated that n-3 polyunsaturated fatty acids had anti-inflammatory effects on purine metabolism, fatty acid metabolism, and oxidative stress response pathways (Peng et al., 2019). Thus, lipids could be the molecules responsible for inducing hepatomegaly (Figure 3.13 a). Biomarkers that are directly related to hepatomegaly are desirable (Figure 3.13 a and b), but I am not sure of the biological relationship between hepatomegaly and detected lipids (PE 34:2 and PE 40:5). Further investigations are required to reveal the biological meaning of the change in the lipid profile following phenobarbital exposure. Furthermore, this research has only targeted 21 genes, and thus global gene profiles such as microarray analyses could provide more accurate associations between the genes and lipids that induce hepatomegaly.

5.2 Discovering of biomarker related to increased liver volume using the MB-PLS model

The DIABLO model separated four groups including both sexes. When focusing on hepatomegaly, the females did not show significant change, and the variance of their normalized liver volumes was small. To identify more suitable biomarkers with which to evaluate hepatomegaly, MB-PLS was used to identify variables that reflect an increased liver volume in males. In total 13 genes, 4 metabolomes, and 47 lipids were used for in the following analyses. The correlation among components 1 and 2 was proposed for each block (gene, metabolite, and lipid), and the normalized liver volume was depicted in Figure 3.14. When focusing on component 1, all the blocks and liver volumes were well correlated, for example, the gene and liver volumes were correlated with a correlation coefficient of 0.929. Sample distribution is shown in Figure 3.15. The loading plot ranked contribution score of each variable was used to determine components 1 and 2 (Figure 3.16 and 3.17). For component 1, *Baat*, *Cyp3a1,* and *Cyp2b1* were found to be high contributors among the genes, while for component 2, *Cyp4a1* and *Gpx1* were identified. Ether-linked phosphatidyl-ethanolamine (PE-O) was listed as a high contributor for the determination of component 1, such as PE O-34:0|PE O-18:0_16:0 and PE O-40:5|PE O-20:1_20:4. PE O-40:5 is highly unsaturated, and these PE-Os contains arachidonic acid in its structure. Eicosanoids, which are signaling molecules related to inflammation, are synthesized from arachidonic acid, but the association between the changes in PE-O and eicosanoids activity was unclear (Graessler et al., 2009; Harizi et al., 2008). Component 1 was mostly contributed by PE-Os with negative contribution scores, while ceramides (Cer) such as Cer 42:2;2O|Cer 18:1;2O/24:1 and Cer 44:2;2O|Cer 18:1;2O/26:1 were contributed positively to the model. Correlated variables were connected in network analysis (Figure 3.18). Unfortunately, all the metabolome data were excluded in the network, but many genes and lipids were confirmed to be related to each other. Briefly, the network may be separated left, which had CYPs or right, which included genes related to oxidative stress and apoptosis. Most lipids were positively correlated to Sod1 and Gpx1 but were negatively correlated with CYP. Interestingly, oxidative stress related genes had unique interactions with lipids. These genes had connections with various classes of lipids, including FA, cardiolipin (CL), HexCer, and PMeOH, when compared with most of the other genes that had connections with mainly PE and PE-O. Component 1 was more likely

to explain the liver volume (Figure 3.14). Many PE-O species such as PE O-34:0 (PE O-18:0_16:0) and PE O-40:5 (PE O-20:1_20:4) were listed as highly contributing variables for component 1 (Figure 3.16), and these lipids had numerous interactions with gene expression, including *Cyp2b1* and *Cyp3a1*. Thus, these lipids may be candidate biomarkers for CAR activation or CAR-mediated gene induction. However, one report investigated the relationship between lipid profiles (in plasma and liver) and acetaminophen (APAP) exposure in mice (Ming et al., 2017). It was previously reported that CAR plays an important role in APAP toxicity in animals (Mendell et al., 2002). The single APAP exposure dramatically changed the PC and PE profiles in mice at 3−6 hours after injection and returned them to relatively normal levels after 24 h in plasma (the most species of PE increased after APAP exposure) (Ming et al., 2017). PE-O could be a sensitive biomarker with which to detect liver damage, but even within 24 hours, its profile would dramatically change. This study also investigated the acute toxicity of phenobarbital. In the future, PE-O should be investigated in a time-dependent manner after exposure to evaluate the efficiency of PE-O as a biomarker.

In contrast to PC and PE, FA, CL, and Cer were mainly associated with genes related to oxidative stress (*Gpx1*, *Sod1* and *Bax*) in the range of current target genes; for example, Cer 42:2;2O and Cer 44:2;2O, which contributed most to the determination of component 1 with positive coeffient values, could be utilized as specific biomarkers. Cer is a second messenger regulating apoptosis and proliferation and associated with oxidative stress. Its signal interfered with current target genes such as GPx (Andrieu-Abadie et al., 2001). The association with oxidative stress and inflammation in hepatic steatosis was also previously reported (Seo et al., 2016). The effectiveness of Cer as a biomarker for oxidative stress was investigated previously (Gaggini et al., 2020). The results of this investigation follow on this previous study and indicated that Cer could be utilized as a biomarker to estimate antioxidative status with accountable mechanism. In particular, this study has identified two species (Cer 42:2;2O and Cer 44:2;2O) and further investigations should aim to elucidate the utility of these Cers using other chemicals which induce hepatomegaly. A previous report also identified the association of oxidative stress with CL (Paradies et al., 2014) and HexCer (Apostolopoulou et al., 2018), but the knowledge of lipidomics is still expanding, and a standard oxidative stress marker in rats has not yet been revealed.

5.3 Summary of multiomics analysis

The correlation among liver volume, histopathology results, gene expression, and candidate biomarker lipids with which to clearly visualizing the results of the MB-PLS are shown in Figure 3.19. PE-Os, such as 34:0 and 40:5, seem to clearly explain the *Cyp2b1*, *Cyp3a1*, and *Ugt1a1* expression levels in highly expressing individuals (Figure 3.19, orange). However, ceramides such as 42:2;2O and 44:2;2O relate to the expression of *Gpx1* and *Sod1* (Figure 3.19, grey). This relationship can be explained based on Cer molecular function. These lipids may be effective indicators to explain biological process changes in the liver due to phenobarbital exposure. Unfortunately, because of the low variance among all samples, TCHO and HDLC were excluded from the multiomics analysis. These biomarkers were only significantly induced in exposed males. The male unique lipid profile seen in cluster C in Figure 3.12 may result in these parameters. However, at some points, the results of this research were not consistent with the results of a previous study that targeted CAR (Chen et al., 2019; Skoda et al., 2022) as mentioned above. Thus, I must examine this approach using several chemicals to further assess and demonstrate the utility of extracted biomarkers.

6. Conclusion

Toxicity tests using animal experiments are required to ensure the safe use of both chemicals and medicines. CT can be used to visualize the effects of chemicals throughout a lifetime and continuously monitor individual animals. This research revealed that CT could be used to detect hepatomegaly induced by phenobarbital. In the molecular analysis, the reactivity of *Cyp2b1* was higher in females than in males (Table 3.10a), and for most other genes and the liver volume, there was a significant difference only between the control and exposed males. The Cyp2b independent pathways for CAR may cause these sex polymorphisms, as it was previously reported that *Cyp2b* null mice showed significant liver enlargement and upregulation of Nrf2-regulated genes (Li et al., 2017; Rooney et al., 2019). The lipid profile clearly showed that there were unique changes in clustered PE such as PE 34:0 and PE 40:5 in exposed males. These lipids may reflect male specific gene expression and increased liver volume. The MB-PLS model extracted several lipids as possible biomarkers to explain hepatomegaly in male. These lipids were correlated with various genes such as *Cyp2b1*, *Baat*, and *Bax*. Lipid analyses can be

conducted throughout a lifetime and provide useful means to estimate biological processes for which humans previously needed postmortem analysis such as gene expression in liver.

Phenobarbital induced hepatomegaly was also associated with the pregnane X receptor (PXR). PXR is also known as the receptor for xenobiotic chemicals and induces various metabolic enzymes. One of the typical target genes of PXR is *CYP3A* (Yoshinari, 2019). The gene expression of various metabolic enzymes was regulated by several nuclear receptors, and *CYP3A* was also mediated by both CAR and PXR (Ueda et al., 2002). The unique effects of PXR on hepatomegaly were considered as pregnenolone 16α-carbonitrile (PCN) (typical PXR activator) significantly exacerbated the phenobarbital induced hepatomegaly; even single exposures to PCN did not result in strong differences in liver size (Shizu et al., 2013). The peroxisome proliferator-activated receptor (PPAR) regulates fat and carbohydrate in the animal body (Olefsky, 2001). The PPAR agonist induced hepatomegaly dose-dependently and was involved in lipidomic changes in rats (Ament et al., 2016). This research targeted the CAR activator, but the other receptors and other transcription factors, such as PXR, PPAR and YAP, should be investigated in future studies.

This is a pioneering study to advocate a new evaluation method for toxic chemicals which combines micro-CT, metabolomics, and several classical methods such as histopathological analysis. The use of CT was rare for assessments of liver size when exposed to chemicals, and lipidomics will help reveal the molecular processes and the relevant mechanisms throughout a lifetime. I should apply this method to other toxic chemicals to further evaluate the method itself. I trust that this report will lead to further studies to develop this new toxicity test for the evaluation of chemicals throughout an animals' lifetime.

Figures and Tables

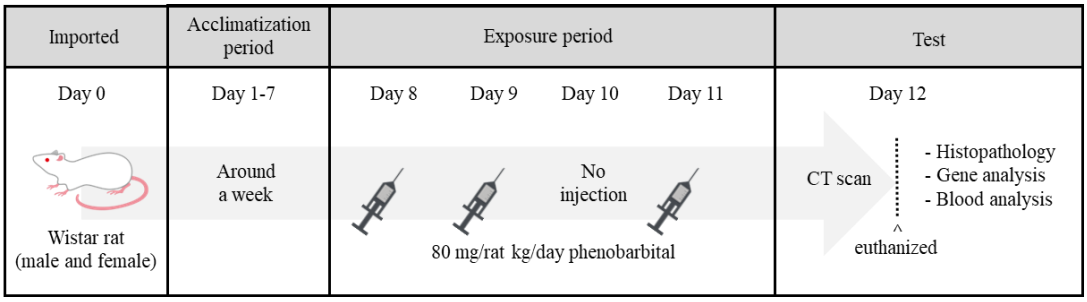

Figure 3.1. Experimental design.

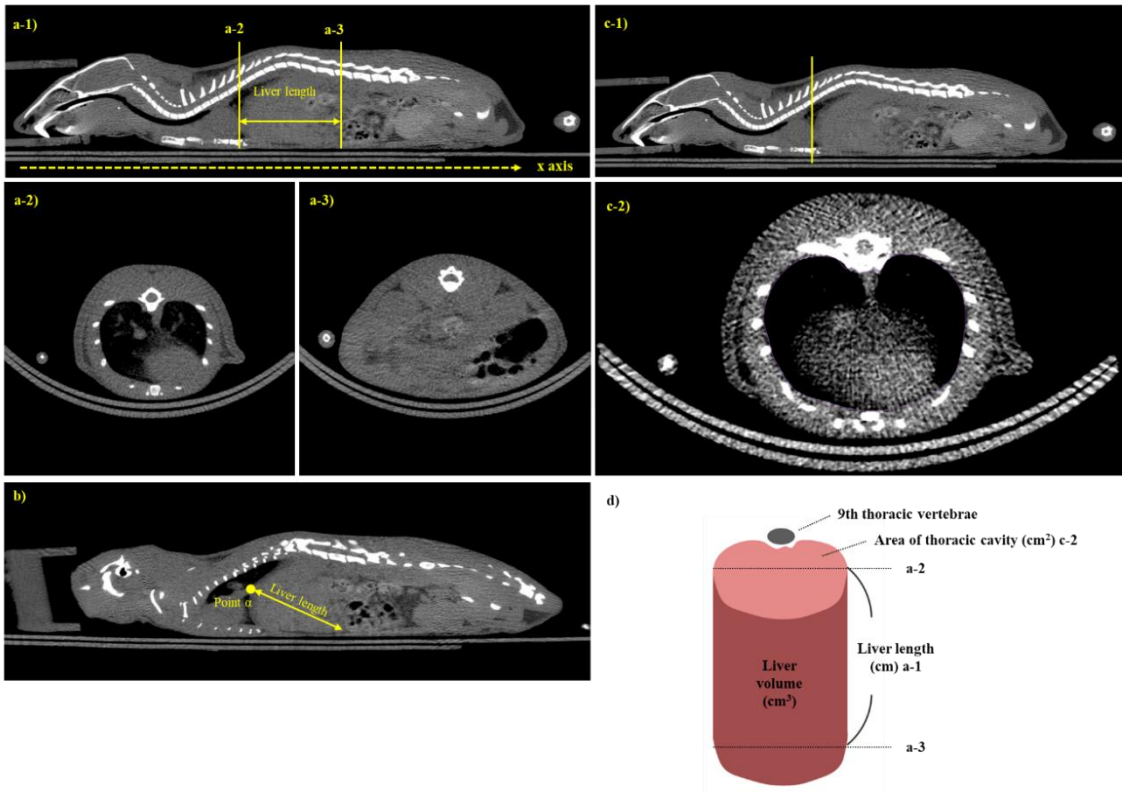

Figure 3.2. Methods for evaluating liver size. Liver size was calculated using liver length (**2a-1**) and thoracic cavity (**2c-2**). (**2a)** Liver length was defined as the x axis difference between the cranial and caudal tips of the liver (two-dimensional distance). a-1: conceptual scheme of the liver length; a-2: transverse image of the cranial liver tip; a-3: transverse image of the caudal liver tip. **(2b)** Liver length was defined as the difference between the point of the caudal vena cava attached to the liver on the diaphragm (Pointα) and the caudal edge of the liver (three-dimensional distance). **(2c)** The thoracic cavity area was measured using transverse images at the dorsal and cranial tips of the 9th thoracic vertebrae (2c-1, -2). **(2d)** Formalized simple three-dimensional figure of the liver with the area of the thoracic cavity as its base. Liver volume was calculated using the area of the thoracic cavity and liver length as follows: Liver volume (cm^3) = Liver length (cm) × Thoracic cavity (cm^2).

Table 3.1. Primer information

Gene name	Product size (bp)	Forward primer (5'-3')	Reverse primer (5'-3')
Abcb11	131	CGTGCTTGTGGAAGAAGTTG	GGGAGTAGATGGGTGTGACTG
Abcc2	145	CCATTATCCGTGCCTTTGAG	ACGACCAAGTTTCCAACCAG
Actb	97	GTCCACCCGCGAGTACAAC	GACGACGAGCGCAGCGATA
Baat	89	ATGACCTGCCCTCTCGACT	GCCCAGGACCTTAGGATG
Bax	166	AGGACGCATCCACCAAGAAG	CAGTTGAAGTTGCCGTCTGC
Cat	126	GCCCTCTTGCCTCACGTTCT	ACATCGGGTTTCTGAGGGGC
Ccnb1	110	ACAACGGTGAATGGACACCA	GCCACGGTTCACCATGACTA
Ccnb2	198	GTGCTGGGCCAAGGAAAATG	GGAGTTCAGCTGAGGGATCG
Cyp2b1	109	GCTCAAGTACCCCCATGTCG	ATCAGTGTATGGCATTTTACTGCGG
Cyp3a1	91	GATTCTGTGCAGAAGCATCGA	ATAGGGCTGTATGAGATTCTT
Cyp3a18	74	AAGCACCTCCATTTCCTTCATA	TCTCATTCTGGAGTTTCTTTTG
Cyp4a1	120	TCCACCCGCTTCACGGGCAGC	AGCCTTGAGTAGCCATTGCC
Cyp7b1	138	GAAGTCCTGCGTGACGAAAT	CCTCAGAACCTCAAGAATAGCG
Cyp8b1	80	GGCTGGCTTCCTGAGCTTGTT	ACTTCCTGAACAGCTCATCGG
Cyp27a1	93	TCTGGCTACCTGCACTTCCT	GTCTACCCCAGCCAAGATCA
Gpx1	155	TCCCGTGCAATCAGTTCGGA	GGTAAAGAGCGGGTGAGCCT

Hmox1	108	ACACGGGTGACAGAAGAGGCTAA	CTGTGAGGGACTCTGGTCTTTG
Rela	79	CATACGCTGACCCTAGCCTG	TCACTGAGCTCCCGATCAGA
Sod1	120	CTGAAGGCGAGCATGGGTTC	TCTCTTCATCCGCTGGACCG
Tgfb1	168	AGGGCTACCATGCCAACTTC	CCACGTAGTAGACGATGGGC
Txnrd1	150	GTCACACCAACTCCTCTCGG	TGTGTCCTCGAGTTTCCAGC
Ugt1a1	152	ACACAGATCGCATGAACTTCC	AGGACTCAGAAGGTCCTTGAC

This table shows the gene names, product size, and forward and reverse primer.

ATP binding cassette subfamily B member 11 (Abcb), ATP binding cassette subfamily C member 2 (Abcc2), beta actin (Actb), bile acid CoA:amino acid N-acyltransferase (Baat), BCL2 associated X (Bax), catalase (Cat), cyclin B1 (Ccnb1), cyclin B2 (Ccnb2), cytochrome P450 (Cyp), glutathione peroxidase 1 (Gpx1), heme oxygenase 1 (Hmox1), RELA proto-oncogene, NF-kB subunit (Rela), superoxide dismutase 1 (Sod1), transforming growth factor, beta 1 (Tgfb1), thioredoxin reductase 1 (Txnrd1), UDP glucuronosyltransferase (Ugt)

Table 3.2. GC and MS conditions for the metabolome analysis.

<Injector>	
Temperature	280℃
Injection Mode	Splitless
<Carrier Gas>	
Pressure	81.5 kPa
Total Flow	17.1 mL/min
Column Flow	1.1 mL/min
Linear Velocity	39 cm/s
<MS setting>	
Ion Source Temperature	200℃
Interface Temperature	280℃
Solvent Cut Time	3.5 min
Detector Voltage	0.5 kV

Table 3.3. LC and qToF/MS conditions for the metabolome analysis.

HPLC (positive ion mode)	
Solvent A	0.1% formic acid in water
Solvent B	0.1% formic acid in acetonitrile
Flow rate	200 µl/min
Sample injection volume	2 µl
Column temperature	40°C

HPLC (negative ion mode)	
Solvent A	20 mmol/L ammonium bicarbonate in water *
Solvent B	Acetonitrile
Flow rate	200 µl/min
Sample injection volume	2 µl
Column temperature	40°C

QTOF/MS	
Start - stop mass (MS2 mode)	50–800
ion spray voltage (positive)	5500 V
ion spray voltage (negative)	-4500 V
Ion source temperature	350°C

* Approximately 1.5 g of ammonium bicarbonate and 1 mL of 28% ammonium hydroxide were mixed in 1 L of ultrapure water for solvent A.

Table 3.4. LC and qToF/MS conditions for the lipid analysis.

HPLC (both positive and negative ion mode)	
Solvent A	5 mM ammonium acetate and 10 nM EDTA 2NH4 in acetonitrile:methanol:ultrapure water (1:1:3)
Solvent B	5 mM ammonium acetate and 10 nM EDTA $2NH_4$ in 2-propanol
Flow rate	300 µl/min
Sample injection volume	1 µl
Column temperature	45℃
QTOF/MS (positive ion mode)	
Start - stop mass	70–1250
ion spray voltage (positive)	5500 V
Ion source temperature	250℃
QTOF/MS (negative ion mode)	
Start - stop mass	70–1250
ion spray voltage (negative)	-4500 V
Ion source temperature	300℃

Table 3.5. Physical characteristics and liver sizes (absolute and estimated) in control and phenobarbital exposed rats.

		Body weight (g)	Liver weight (g)	Liver volume (MC, mL)	Bone volume (CT, cm^3)	Liver length (CT, cm)	Liver volume (CT, cm^3)
Male	Control	199.60 (±9.76)	9.30 (±0.65)	8.92 (±0.67)	7.24 (±0.33)	3.28 (±0.12)	12.94 (±0.71)
	Exposed	199.99 (±9.70)	10.36* (±0.83)	10.08* (±0.79)	7.32 (±0.28)	3.40 (±0.20)	14.78* (±1.53)
Female	Control	150.42 (±10.12)	6.51 (±0.72)	6.45 (±0.70)	6.72 (±0.14)	2.82 (±0.30)	9.71 (±1.22)
	Exposed	150.61 (±10.81)	6.97 (±0.72)	6.85 (±0.68)	6.41 (±0.36)	2.81 (±0.19)	10.28 (±0.96)

		Liver weight /Body weight (%)	Liver volume (MC) /Body weight (%)	Liver volume (MC) /Bone volume	Liver volume (CT) /Body weight (%)	Liver volume (CT) /Bone volume
Male	Control	4.66 (±0.12)	4.46 (±0.13)	1.23 (±0.04)	6.48 (±0.22)	1.79 (±0.04)
	Exposed	5.18* (±0.30)	5.04* (±0.24)	1.38* (±0.08)	7.37* (±0.45)	2.01* (±0.15)
Female	Control	4.32 (±0.20)	4.28 (±0.20)	0.96 (±0.10)	6.43 (±0.44)	1.44 (±0.17)
	Exposed	4.62 (±0.21)	4.54 (±0.20)	1.07 (±0.08)	6.82 (±0.31)	1.60 (±0.09)

Body and liver weight and bone and liver volume were described in Table 2. Liver volume was measured using both a measuring cylinder (MC) and computed tomography (CT). * indicates a significant difference between the control and exposed groups with both the Welch t test and Wilcoxon test ($p < 0.05$). Brackets contain the standard deviation (SD) for each group.

Table 3.6. Correlation among parameters (body and liver weight, liver and bone volume).

a) Both Sexes	Body weight	Bone volume	Liver weight	Liver volume*[1]	Liver length	Liver volume*[2]
Body weight	***1.00***	***0.88***	***0.95***	***0.94***	***0.89***	***0.92***
Bone volume		***1.00***	***0.83***	***0.83***	***0.74***	***0.84***
Liver weight			***1.00***	***0.99***	***0.87***	***0.96***
Liver volume*[1]				***1.00***	***0.87***	***0.96***
Liver length					***1.00***	***0.89***
Liver volume*[2]						***1.00***

b) Male	Body weight	Bone volume	Liver weight	Liver volume*[1]	Liver length	Liver volume*[2]
Body weight	***1.00***	***0.94***	***0.69***	***0.71***	***0.59***	***0.63***
Bone volume		***1.00***	***0.74***	***0.71***	0.50	***0.70***
Liver weight			***1.00***	***0.97***	***0.64***	***0.87***
Liver volume*[1]				***1.00***	***0.67***	***0.89***
Liver length					***1.00***	***0.71***
Liver volume*[2]						***1.0***

c) Female	Body weight	Bone volume	Liver weight	Liver volume*1	Liver length	Liver volume*2
Body weight	***1.00***	***0.54***	***0.93***	***0.92***	***0.87***	***0.89***
Bone volume		***1.00***	0.34	0.34	0.28	0.39
Liver weight			***1.00***	***0.98***	***0.81***	***0.95***
Liver volume*1				***1.00***	***0.80***	***0.93***
Liver length					***1.00***	***0.85***
Liver volume*2						***1.00***

(a) both sexes, (b) males, (c) females. *1 and *2 indicate the liver volume determined by the measuring cylinder and CT respectively. Italics in bold indicate a significant correlation between pairs with $p \leq 0.001$ for (a) and $p < 0.05$ for (b and c).

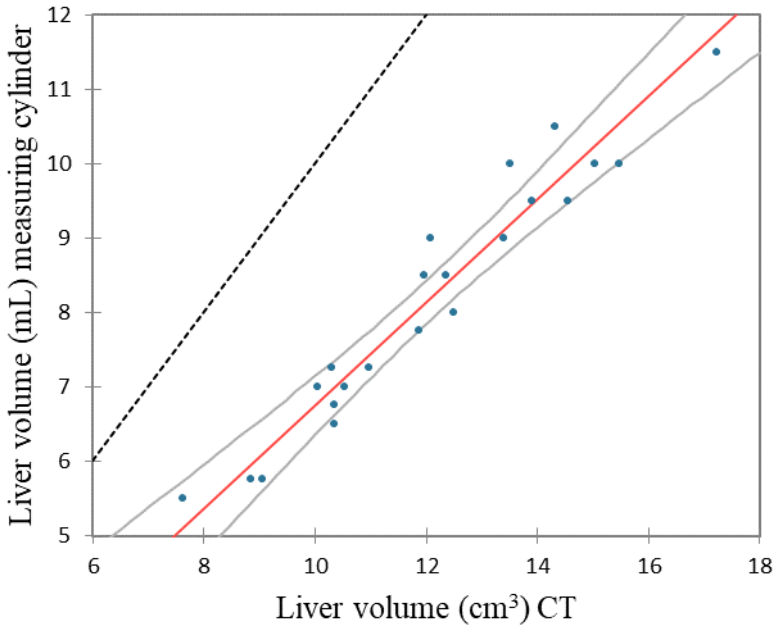

	Estimate	Lower CL (mean)	Upper CL (mean)
Intercept	-0.20	-1.18	0.78
Slope	0.69	0.61	0.78

Figure 3.3. Liver volumes determined by measuring cylinder vs from the CT. Liver volumes in all rats used in this study were plotted by measuring cylinder vs by the CT. The line was described using the Deming regression by XLSTAT (Addinsoft, Paris, France).

Table 3.7. Correlation among the normalized liver sizes.

a) Both sexes	Liver weight /Body weight	Liver volume (MC) /Body weight	Liver volume (MC) /Bone volume	Liver volume (CT) /Body weight	Liver volume (CT) /Bone volume
Liver weight /Body weight	1.00	0.95	0.87	0.66	0.81
Liver volume (MC) /Body weight		1.00	0.81	0.70	0.74
Liver volume (MC) /Bone volume			1.00	0.44	0.92
Liver volume (CT) /Body weight				1.00	0.67
Liver volume (CT) /Bone volume					1.0

b) Males	Liver weight /Body weight	Liver volume (MC) /Body weight	Liver volume (MC) /Bone volume	Liver volume (CT) /Body weight	Liver volume (CT) /Bone volume
Liver weight /Body weight	1.00	0.95	0.90	0.80	0.80
Liver volume (MC) /Body weight		1.00	0.98	0.81	0.84
Liver volume (MC) /Bone volume			1.00	0.74	0.80
Liver volume (CT) /Body weight				1.00	0.99
Liver volume (CT) /Bone volume					1.00

c) Females	Liver weight /Body weight	Liver volume (MC) /Body weight	Liver volume (MC) /Bone volume	Liver volume (CT) /Body weight	Liver volume (CT) /Bone volume
Liver weight /Body weight	1.00	0.93	0.86	0.75	0.84
Liver volume (MC) /Body weight		1.00	0.88	0.72	0.81
Liver volume (MC) /Bone volume			1.00	0.57	0.91
Liver volume (CT) /Body weight				1.00	0.81
Liver volume (CT) /Bone volume					1.00

All pairs among the normalized liver sizes by the body weight and bone volume were significantly correlated when using the Pearson correlation coefficient (p value ≤ 0.05) except the correlation between liver volume (MC)/bone volume and liver volume (CT)/body weight in female. (a) both sexes, (b) males, and (c) females.

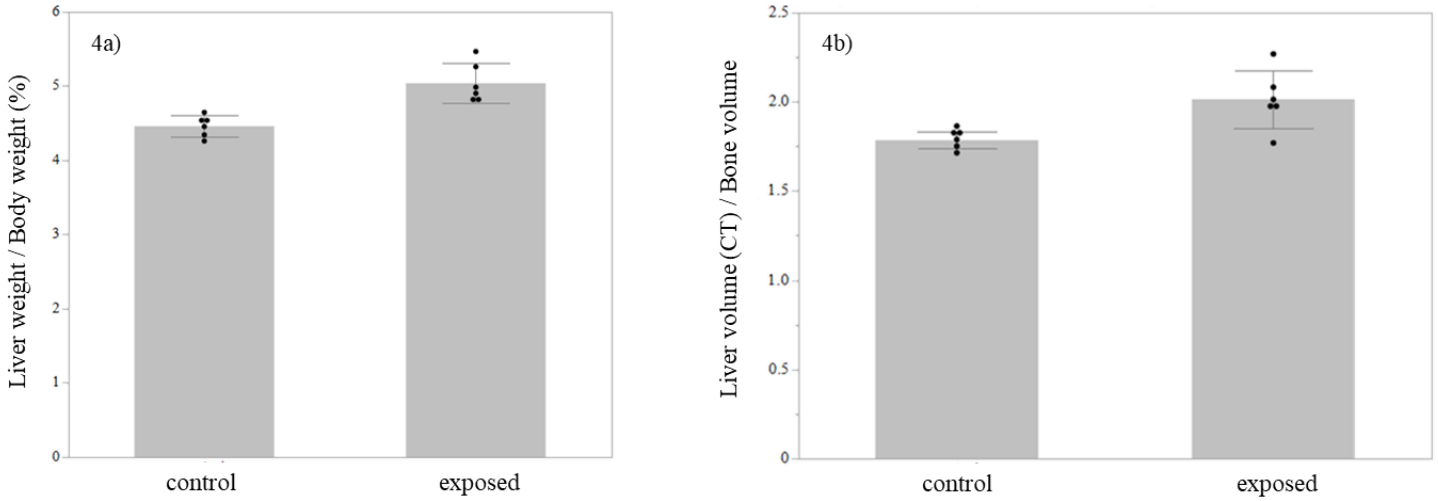

Figure 3.4. Comparison of liver sizes between the male control and exposed groups using the classical (4a) and CT (4b) methods. Error bars indicate standard deviation (SD) in each sample (six control and exposed male rats) and individual sizes were depicted by dots.

Table 3.8. Histopathological analysis summary for the control and exposed rats.

	Male		Female	
	Control	Exposed	Control	Exposed
Hepatocellular mitotic figure	-	1 (n:3), 2 (n:1)	-	1 (n:1)
Enlarged Kupffer cell	-	1 (n:4)	-	-

Hepatocellular mitotic figures and enlarged Kupffer cells were found in the exposed group. The levels were scored from 0–4 (no abnormality to intensity). The table shows the score with the n number in brackets. Score 0 was not reported in the table.

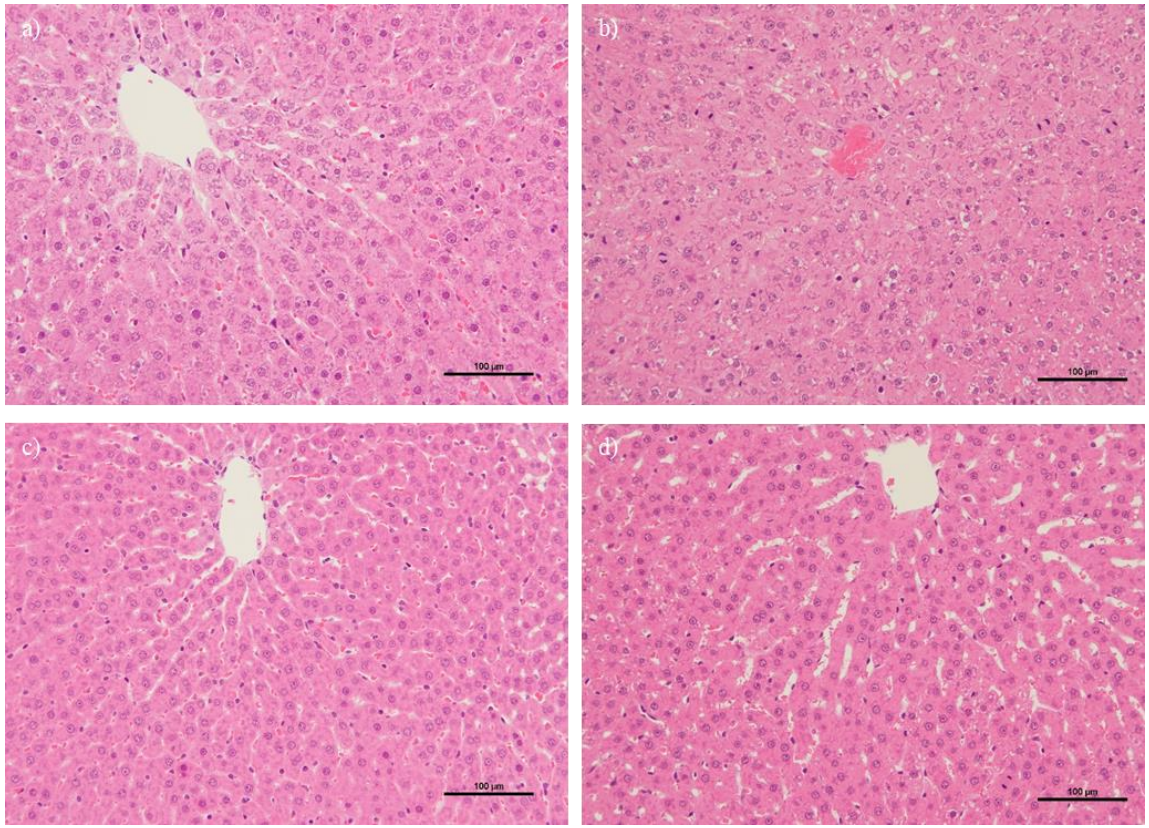

Figure 3.5. Histopathological analysis. Results of the histopathological tests for the **(a)** male control, **(b)** male exposed, **(c)** female control, and **(d)** female exposed.

Table 3.9. Plasma biochemical analysis of the control and phenobarbital exposed rats.

	Male		Female	
	Control	Exposed	Control	Exposed
ALP (U/L)	531.5 (±76.7)	561.3 (±36.0)	348.0 (±97.3)	420.0 (±128.4)
GOT (U/L)	51.5 (±5.1)	56.3 (±11.9)	50.4 (±10.1)	52.2 (±6.2)
GPT (U/L)	26.8 (±1.8)	31.7 (±5.8)	22.4 (±2.7)	27.6 (±5.7)
TCHO (mg/dL)	44.3 (±4.0)	61.5* (±9.5)	64.4 (±7.2)	63.6 (±10.0)
TG (mg/dL)	104.0 (±28.8)	121.0 (±32.3)	91.6 (±22.9)	86.2 (±25.3)
HDLC (mg/dL)	32.8 (±4.3)	43.5* (±8.3)	52.8 (±1.9)	51.8 (±6.7)

Each value is the average for each group with the standard deviation (SD) in brackets.

Table 3.10. Gene expression profiles determined using qPCR in the phenobarbital exposed rats.

7 a)	*Cyp2b1*	*Cyp3a1*	*Cyp3a18*	*Cyp4a1*	*Cyp7b1*	*Cyp8b1*	*Cyp27a1*
Male Exposed	628.2* (±164.27)	11.03* (±2.21)	1.96 (±1.11)	1.45 (±0.29)	1.72* (±0.33)	0.64* (±0.26)	1.87* (±0.52)
Female Exposed	2891.1* (±1017.38)	8.57* (±2.37)	1.72 (±0.77)	0.71 (±0.21)	0.98 (±0.18)	0.60 (±0.29)	1.01 (±0.10)

7 b)	*Ugt1a1*	*Abcb11*	*Abcc2*	*BAAT*
Male Exposed	1.82* (±0.33)	1.88 (±0.47)	1.39 (±0.25)	1.81* (±0.29)
Female Exposed	1.34 (±0.11)	1.00 (±0.14)	0.88 (±0.26)	1.09 (±0.12)

7c)	*Ccnb1*	*Ccnb2*
Male Exposed	12.35 (±11.88)	6.52 (±5.08)
Female Exposed	3.71* (±1.94)	2.99* (±1.29)

7 d)	*Bax*	*Cat*	*Gpx1*	*Hmox1*	*Rela*	*Sod1*	*Tgfb1*	*Txnrd1*
Male Exposed	1.63* (±0.23)	1.35 (±0.16)	1.99 (±0.66)	1.76 (±1.01)	1.19 (±0.31)	1.91* (±0.43)	1.42 (±0.39)	1.34 (±0.39)
Female Exposed	1.32* (±0.17)	1.04 (±0.16)	0.93 (±0.17)	0.77 (±0.22)	0.90 (±0.12)	1.15 (±0.30)	1.23 (±0.30)	1.08 (±0.33)

Each value presented is the average for exposure group with the standard deviation (SD) in brackets after normalization using *beta actin* and then the expression of the control rats (male and female separately). (a) various cytochrome P450, (b) bile acid related gene, (c) cyclin, and (d) oxidative stress or apoptosis pathway related gene.

Table 3.11. Metabolites correlated with liver volume.

Name	KEGG
L-Methionine	C00073
Oxoglutaric acid	C00026
Hypotaurine	C00519
Ornithine	C00077
Cadaverine	C01672
D-Ribose	C00121
Homogentisic acid	C00544
Galacturonic acid	C08348
Pyridoxamine	C00534
Xanthosine	C01762

Metabolites correlated with the normalized liver volume are listed using their registered KEGG IDs.

Table 3.12. Pathway enrichment analysis of metabolites.

Pathway name	Match Status	*p* value	FDR
Arginine biosynthesis	2/14	< 0.01	0.23
Glutathione metabolism	2/28	0.01	0.46
D-Glutamine and D-glutamate metabolism	1/6	0.04	0.74
Taurine and hypotaurine metabolism	1/8	0.05	0.74
Ubiquinone and other terpenoid-quinone biosynthesis	1/9	0.05	0.74
Vitamin B6 metabolism	1/9	0.05	0.74
Butanoate metabolism	1/15	0.09	1
Citrate cycle (TCA cycle)	1/20	0.11	1
Pentose phosphate pathway	1/21	0.12	1
Alanine, aspartate and glutamate metabolism	1/28	0.16	1
Cysteine and methionine metabolism	1/33	0.18	1
Arginine and proline metabolism	1/38	0.21	1
Tyrosine metabolism	1/42	0.22	1
Aminoacyl-tRNA biosynthesis	1/48	0.25	1
Purine metabolism	1/66	0.33	1

Selected metabolites in Table 3.11 were analyzed using pathway enrichment analysis, and the extracted pathways are shown with their match status and FDR.

Table 3.13. Lipids used in the LIPID MAPS analyses.

FA(18:3)	PE(38:4)	PC(40:6)
FA(20:3)	PE(38:5)	PC(40:7)
FA(20:2)	PE(39:4)	PC(36:3)
FA(20:4)	PE(40:5)	PC(38:3)
FA(20:5)	PE(40:6)	PC(38:6)
FA(22:5)	PE(40:7)	PA(34:1)
DG(34:2)	PC(34:1)	PA(36:2)
DG(36:3)	PC(34:2)	PA(38:3)
PA(34:2)	PC(36:0)	PA(38:4)
PA(36:3)	PC(36:1)	PA(38:5)
PE(34:1)	PC(36:2)	PA(38:6)
PE(34:2)	PC(36:4)	PA(40:6)
PE(36:0)	PC(38:4)	DG(36:4)
PE(36:1)	PC(38:5)	PI(36:2)
PE(36:2)	PC(39:4)	PI(38:4)
PE(36:4)	PC(40:5)	PI(38:6)

fatty acids (FA), diacylglycerols (DG), phosphatidic acid (PA), phosphatidylethanolamine (PE), phosphatidylcholine (PC), phosphatidylinositol (PI)

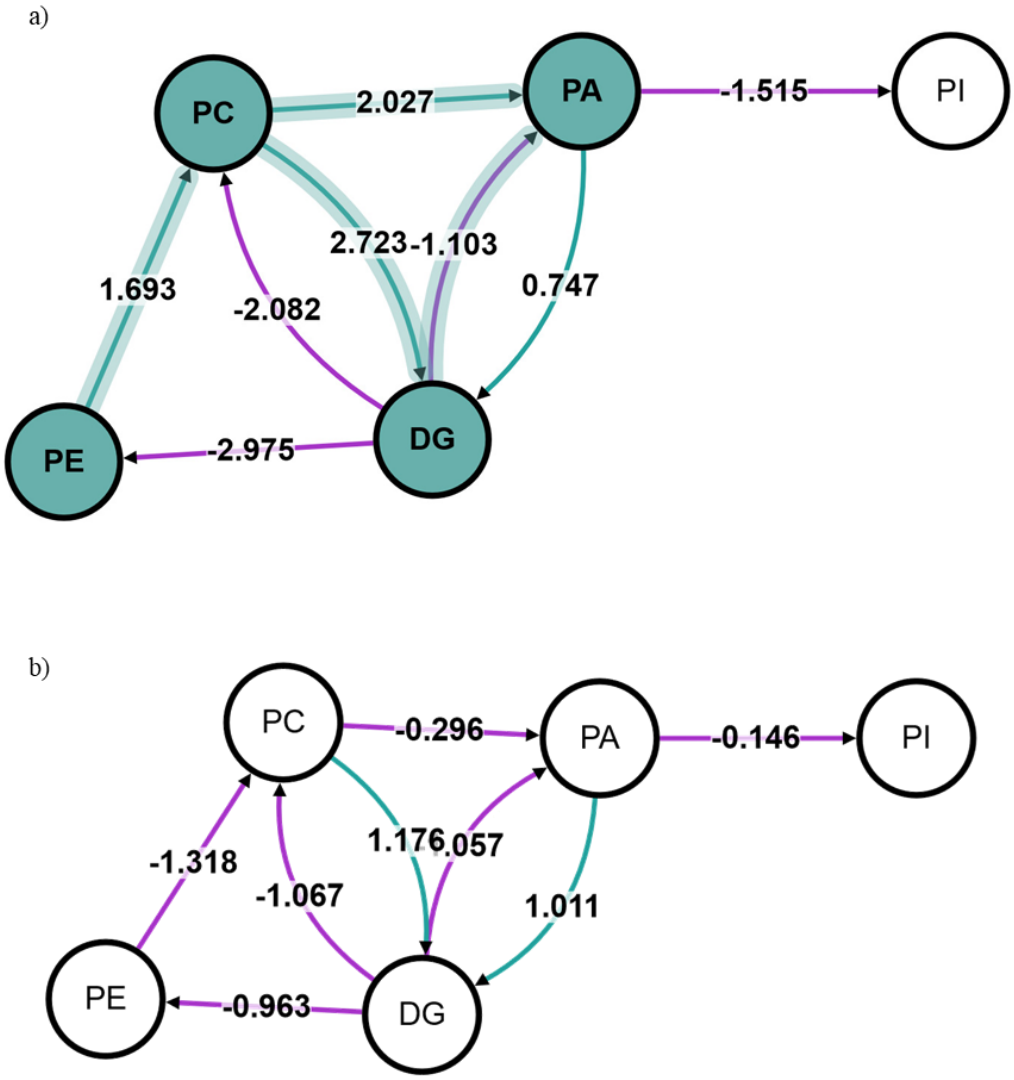

Figure 3.6. Reaction analysis among lipids. Reactions among the lipids of the exposed compared with the control. Reactions recognized by BioPAN software (https://lipidmaps.org/tool/biopan/doc/index.html) among glycerolipids and glycerophospholipids were connected to each other. Green and violet lines indicate positive and negative Z-scores, respectively. Arrows of active and suppressed reactions ($p < 0.05$) are highlighted using broader lines with green and violet arrow respectively. Reactions among lipids in **(a)** males and **(b)** females.

diacylglycerols (DG), phosphatidic acid (PA), phosphatidylethanolamine (PE), phosphatidylcholine (PC), phosphatidylinositol (PI)

a)

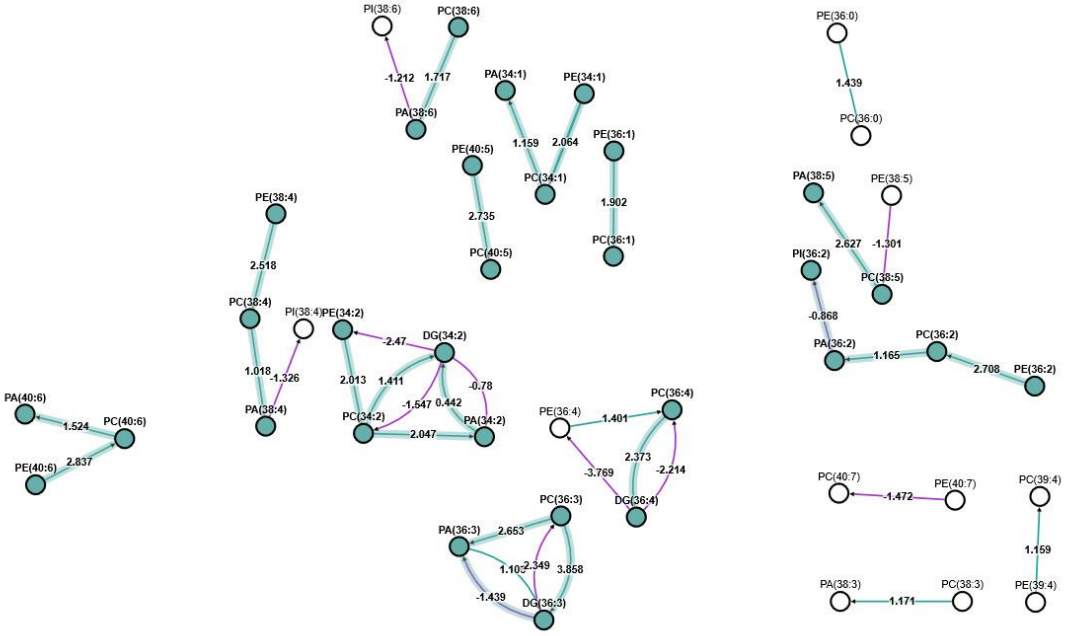
PI(38:6)
PC(38:6)
-1.212
1.717
PA(38:6)
PA(34:1)
PE(34:1)
1.159
2.064
PC(34:1)
PE(36:1)
1.902
PC(36:1)
PE(40:5)
2.735
PC(40:5)
PE(36:0)
1.439
PC(36:0)
PA(38:5)
PE(38:5)
2.627
-1.301
PI(36:2)
PC(38:5)
-0.868
PE(38:4)
2.518
PC(38:4)
PI(38:4)
PE(34:2)
-2.47
DG(34:2)
1.018
-1.326
2.013
1.411
-0.78
PA(38:4)
PC(34:2)
-1.547
0.442
PA(34:2)
2.047
PA(36:2)
PC(36:2)
1.165
2.708
PE(36:2)
PA(40:6)
1.524
PC(40:6)
PE(40:6)
2.837
PE(36:4)
1.401
PC(36:4)
2.373
-2.214
-3.769
DG(36:4)
PC(40:7)
-1.472
PE(40:7)
PC(39:4)
1.159
PC(36:3)
PA(36:3)
2.653
1.103
-2.349
3.858
-1.439
DG(36:3)
PA(38:3)
1.171
PC(38:3)
PE(39:4)

b)

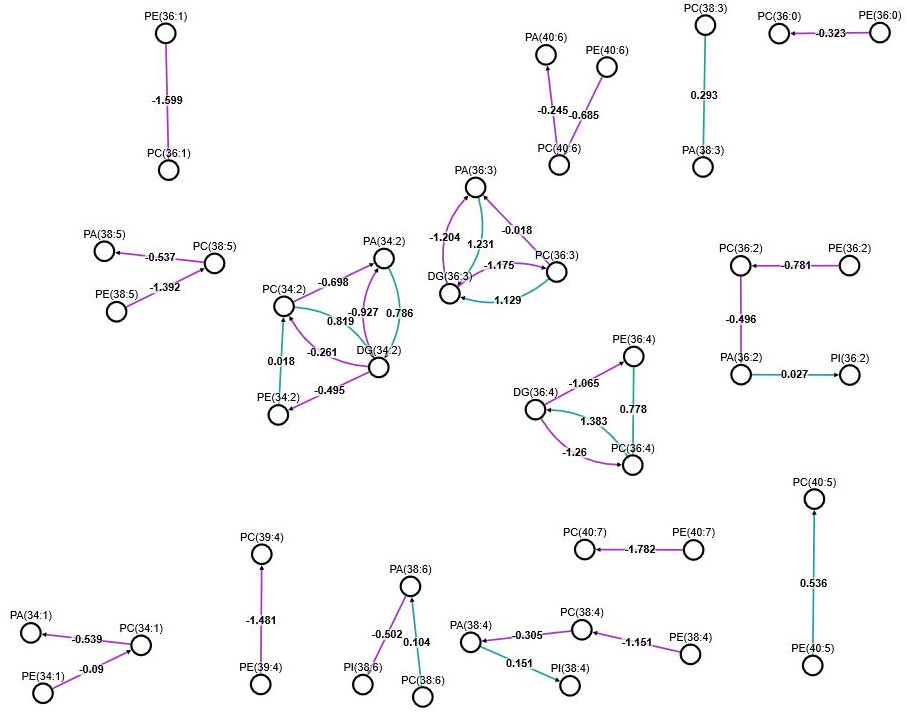
PE(36:1)
-1.599
PC(36:1)
PA(40:6)
PE(40:6)
-0.245
-0.685
PC(40:6)
PC(38:3)
0.293
PA(38:3)
PC(36:0)
-0.323
PE(36:0)
PA(36:3)
-1.204
1.231
-0.018
DG(36:3)
PC(36:3)
-1.175
1.129
PA(38:5)
-0.537
PC(38:5)
PE(38:5)
-1.392
PA(34:2)
PC(34:2)
-0.698
-0.927
0.786
0.819
-0.261
DG(34:2)
0.018
PE(34:2)
-0.495
PC(36:2)
-0.781
PE(36:2)
-0.496
PA(36:2)
0.027
PI(36:2)
PE(36:4)
DG(36:4)
-1.065
0.778
1.383
-1.26
PC(36:4)
PC(40:5)
0.536
PE(40:5)
PC(40:7)
-1.782
PE(40:7)
PC(39:4)
-1.481
PE(39:4)
PA(38:6)
-0.502
0.104
PI(38:6)
PC(38:6)
PA(38:4)
-0.305
PC(38:4)
-1.151
PE(38:4)
0.151
PI(38:4)
PA(34:1)
-0.539
PC(34:1)
PE(34:1)
-0.09

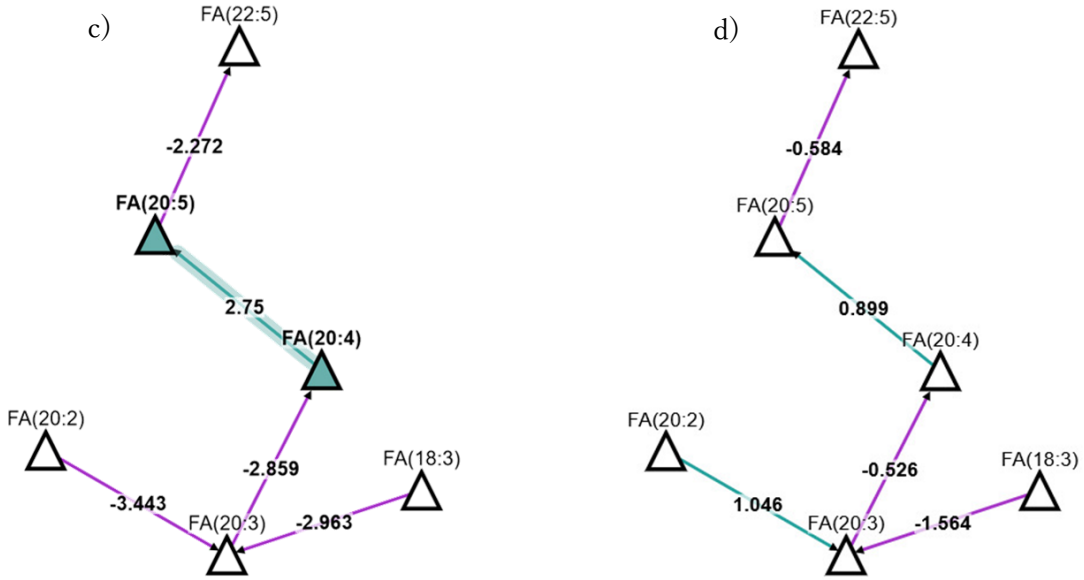

Figure 3.7. Reaction analysis among lipids. Visualized reactions among the lipids exposed when compared with the control. Reactions recognized by BioPAN software (https://lipidmaps.org/tool/biopan/doc/index.html) among circles (glycerolipids and glycerophospholipids) and triangles (fatty acids) were connected with each other. Green and violet lines indicate positive and negative Z-scores, respectively. The arrows of active and suppressed reactions (p value < 0.05) are highlighted using broader lines with green and violet arrows respectively.

a) Reaction among lipid species in male
b) Reaction among lipid species in female
c) Reaction among fatty acid in male
d) Reaction among fatty acid in female

Table 3.14. Genes in charge of lipids reaction changed in exposed male.

Reactions chains	Z-score	Predicted genes
PE(40:6) → PC(40:6) → PA(40:6)	3.084	*PEMT, PLD1, PLD2*
PE(40:5) → PC(40:5)	2.735	*PEMT*
PC(36:3) → PA(36:3)	2.653	*PLD1, PLD2*
PC(38:5) → PA(38:5)	2.627	*PLD1, PLD2*
PE(34:2) → PC(34:2) → PA(34:2) → DG(34:2)	2.599	*PEMT, PLD1, PLD2, PLPP1, PLPP2, PLPP3*
PE(38:4) → PC(38:4) → PA(38:4)	2.5	*PEMT, PLD1, PLD2*
PE(34:2) → PC(34:2) → DG(34:2)	2.421	*PEMT*
PC(36:4) → DG(36:4)	2.373	No genes have yet been identified
PE(34:1) → PC(34:1) → PA(34:1)	2.279	*PEMT, PLD1, PLD2*
PE(36:1) → PC(36:1)	1.902	*PEMT*
PC(34:2) → PA(34:2) → DG(34:2)	1.76	*PLD1, PLD2, PLPP1, PLPP2, PLPP3*
PE(36:2) → PC(36:2) → PA(36:2) → PI(36:2)	1.735	*PEMT, PLD1, PLD2, CDS1, CDS2, CDIPT*
PC(38:6) → PA(38:6)	1.717	*PLD1, PLD2*
PC(36:3) → DG(36:3) → PA(36:3)	1.71	*DGKA, DGKB, DGKD, DGKE, DGKG, DGKH, DGKI, DGKK, DGKQ, DGKZ*

Reactions and its Z-score which changed significantly in exposed in male compared with control are listed. Predicted genes in charge of its reaction are also shown from LIPID MAP analysis.

Abbreviation

Cdipt	CDP-diacylglycerol--inositol 3-phosphatidyltransferase
Cds	CDP-diacylglycerol synthase
Cept	choline/ethanolaminephosphotransferase
Chpt	choline phosphotransferase
Dgk	diacylglycerol kinase
Elovl	ELOVL fatty acid elongase
Fads	fatty acid desaturase
Pemt	phosphatidylethanolamine N-methyltransferase
Pld1	phospholipase D
Plpp	phospholipid Phosphatase

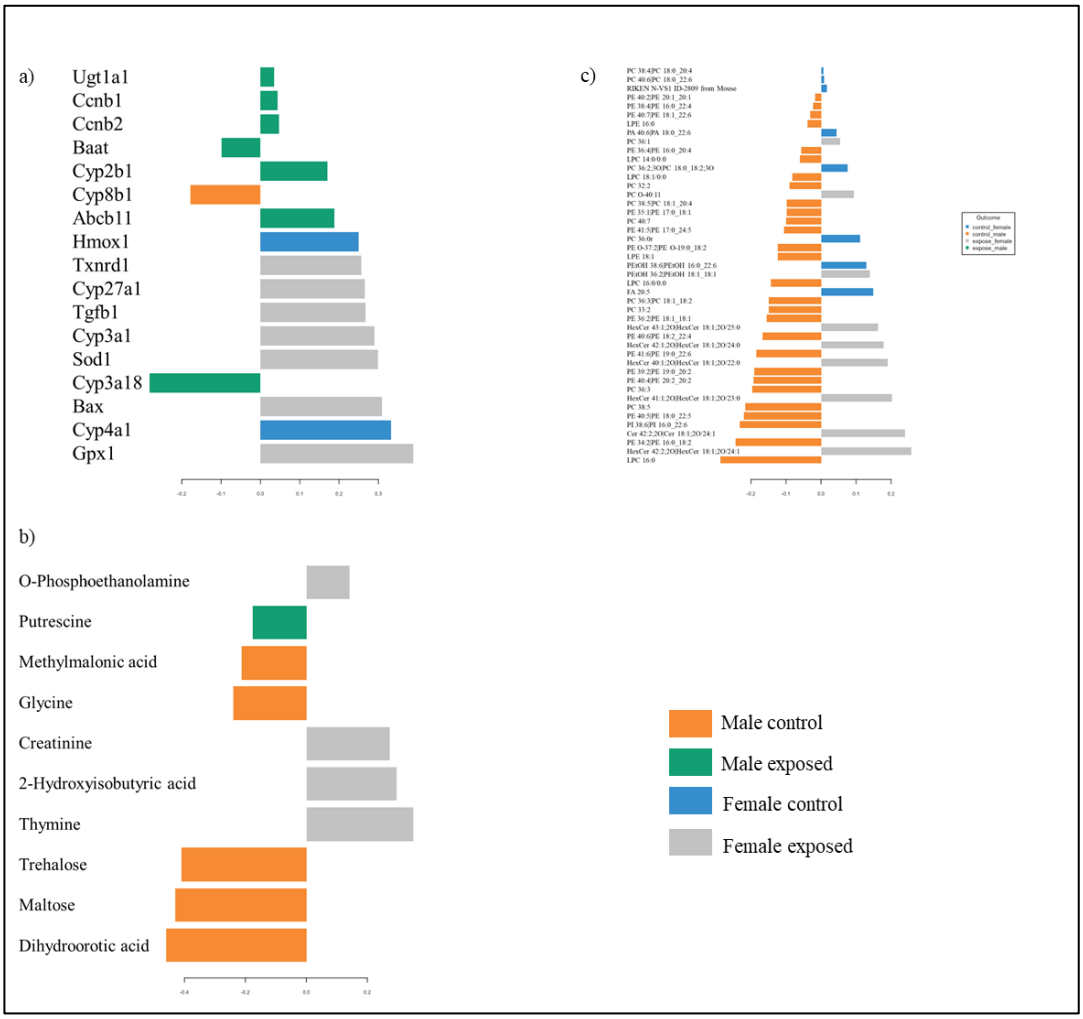

Figure 3.8. Contribution scores for component 1. Contribution scores of the selected variables for component 1 are shown using a bar plot. The bar length reflects the importance of each variable in this model, and its direction indicates a positive or negative coefficient for each variable. The bar color indicates the rat groups which has the highest mean of each variable.

a) Gene expression
b) Metabolites
c) Lipids

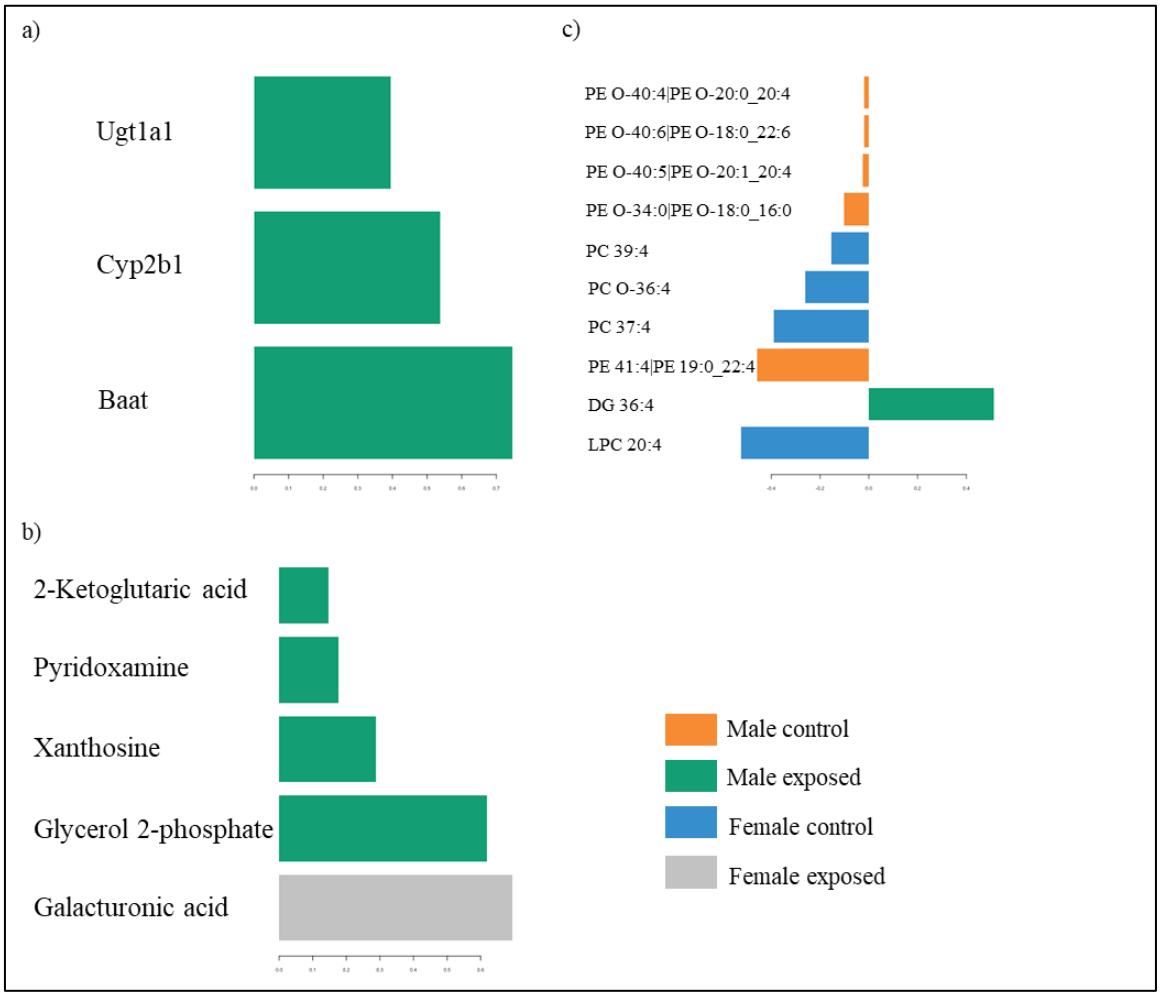

Figure 3.9. Contribution scores for component 2. Contribution scores of the selected variables for component 2 are shown using a bar plot. The bar length reflects the importance of each variable in this model, and its direction indicates a positive or negative coefficient for each variable. The bar color indicates the rat groups which has the highest mean of each variable.

a) Gene expression
b) Metabolites
c) Lipids

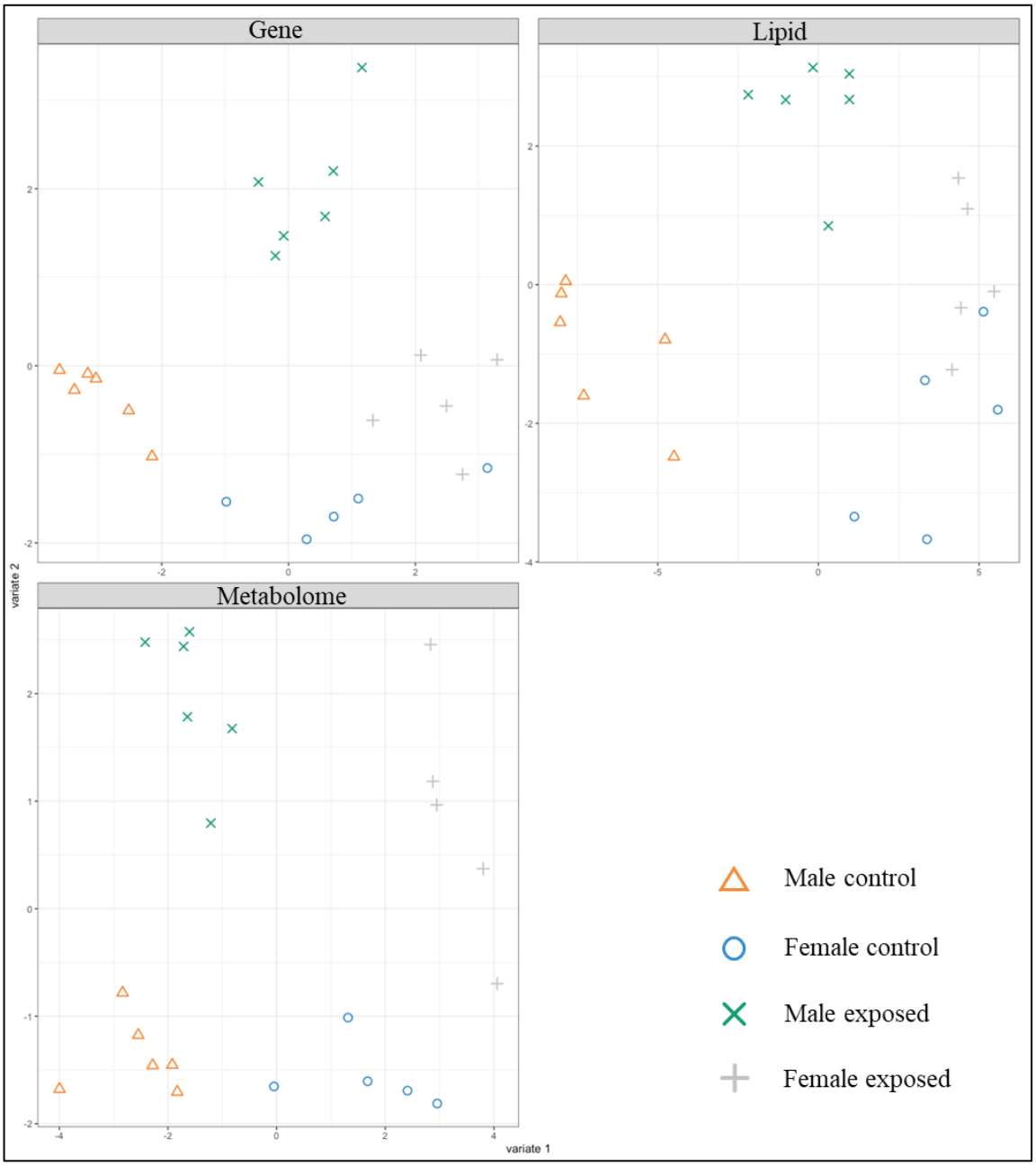

Figure 3.10. Score plots for the individual rats in the DIABLO model. Score plots for individual control and phenobarbital exposed rats in each gene, metabolome, and lipid block using components 1 and 2.

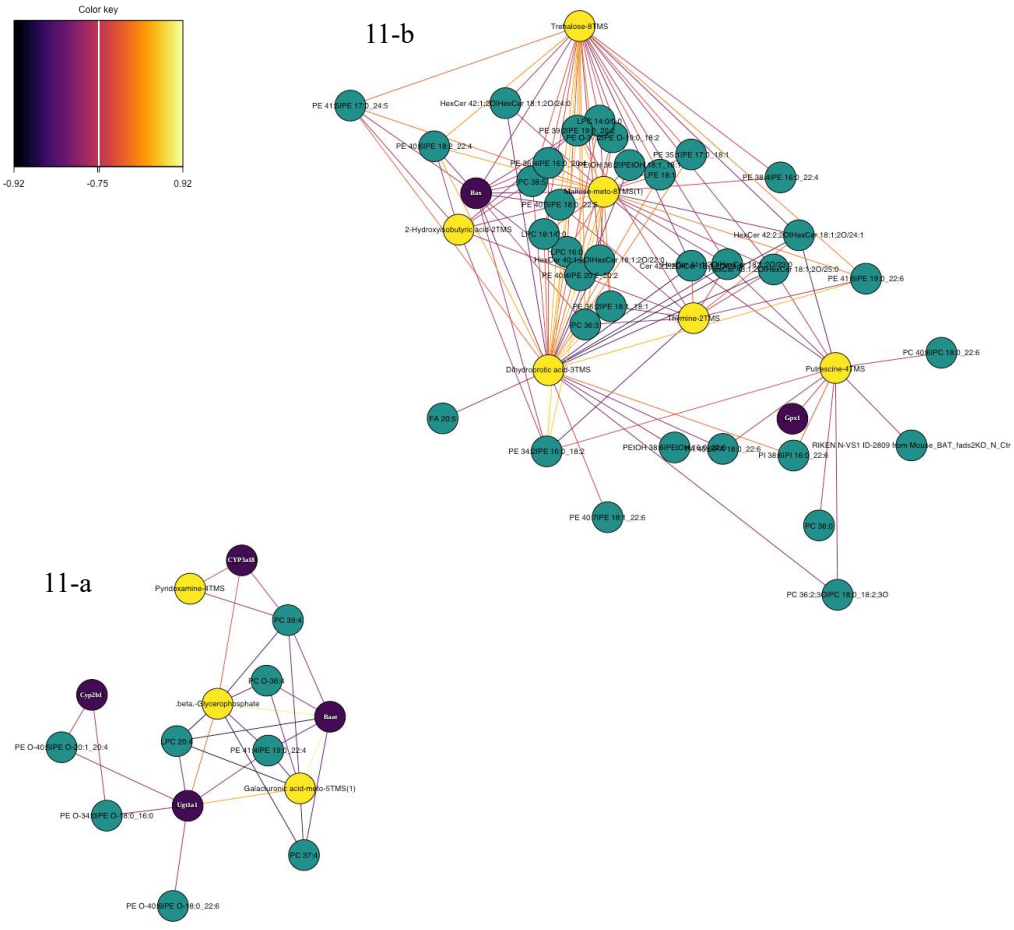

Figure 3.11. Network analysis for the Data Integration Analysis for Biomarker discovery using Latent variable approaches for Omics studies (DIABLO) model. Selected variables in the DIABLO model were connected to each other depending on their correlation. Two networks (a, left) and (b, right) were described. Violet, gene expression; yellow, metabolomes; and green, lipids. Positive and negative correlations are shown using yellow and violet lines, respectively. Lines indicate when a correlation was found between the variable blocks (gene, metabolites, and lipids).

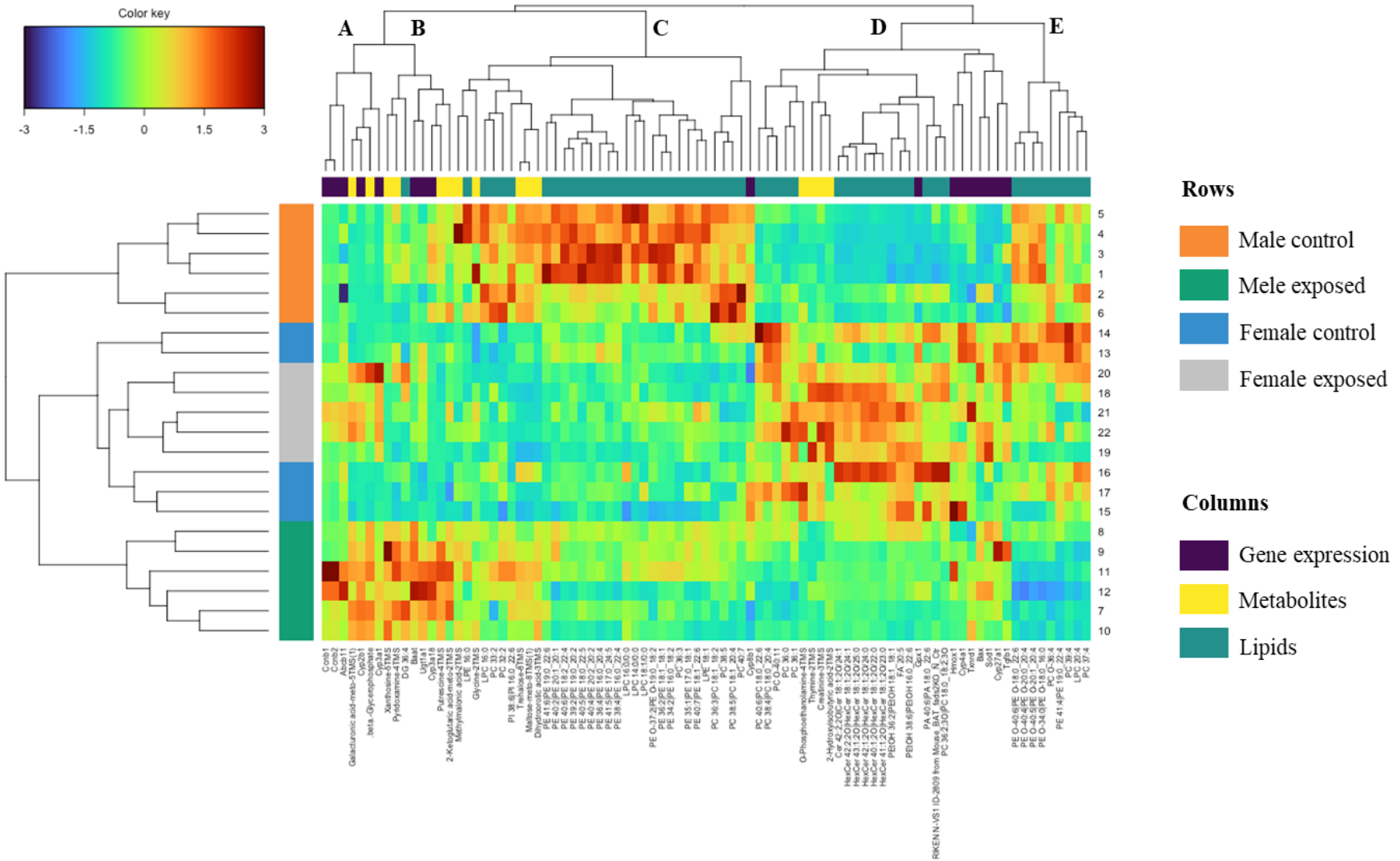
Color key
-3
-1.5
0
1.5
3
A
B
C
D
E
Rows
Male control
Mele exposed
Female control
Female exposed
Columns
Gene expression
Metabolites
Lipids

Figure 3.12. Cluster analysis. Selected variables in the DIABLO model were classified using cluster analysis. A color map showed cluster analysis of individual rats (at columns) and selected variables (at rows) using the normalized value of each variable, and five variable clusters (A–E) were defined. Colors indicate the rat groups as follows: orange, male controls; green, males exposed to phenobarbital; blue, female controls; and grey, females exposed. Gene expression, the metabolome, and lipids are shown in violet, yellow and green, respectively. Each color block shows the normalized level of each variable from the lowest (dark blue) to the highest (dark red).

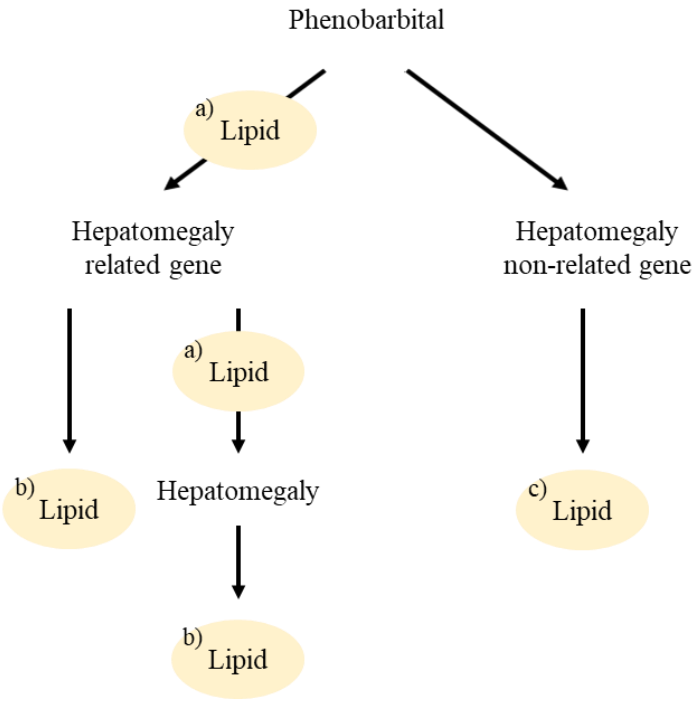

Figure 3.13. Possible relationship between lipids and hepatomegaly. Lipids can be separated, which contributed to phenobarbital induced hepatomegaly directly (a) and changed as the results of biological processes through hepatomegaly (b), changed by phenobarbital induced genes independent on hepatomegaly (c).

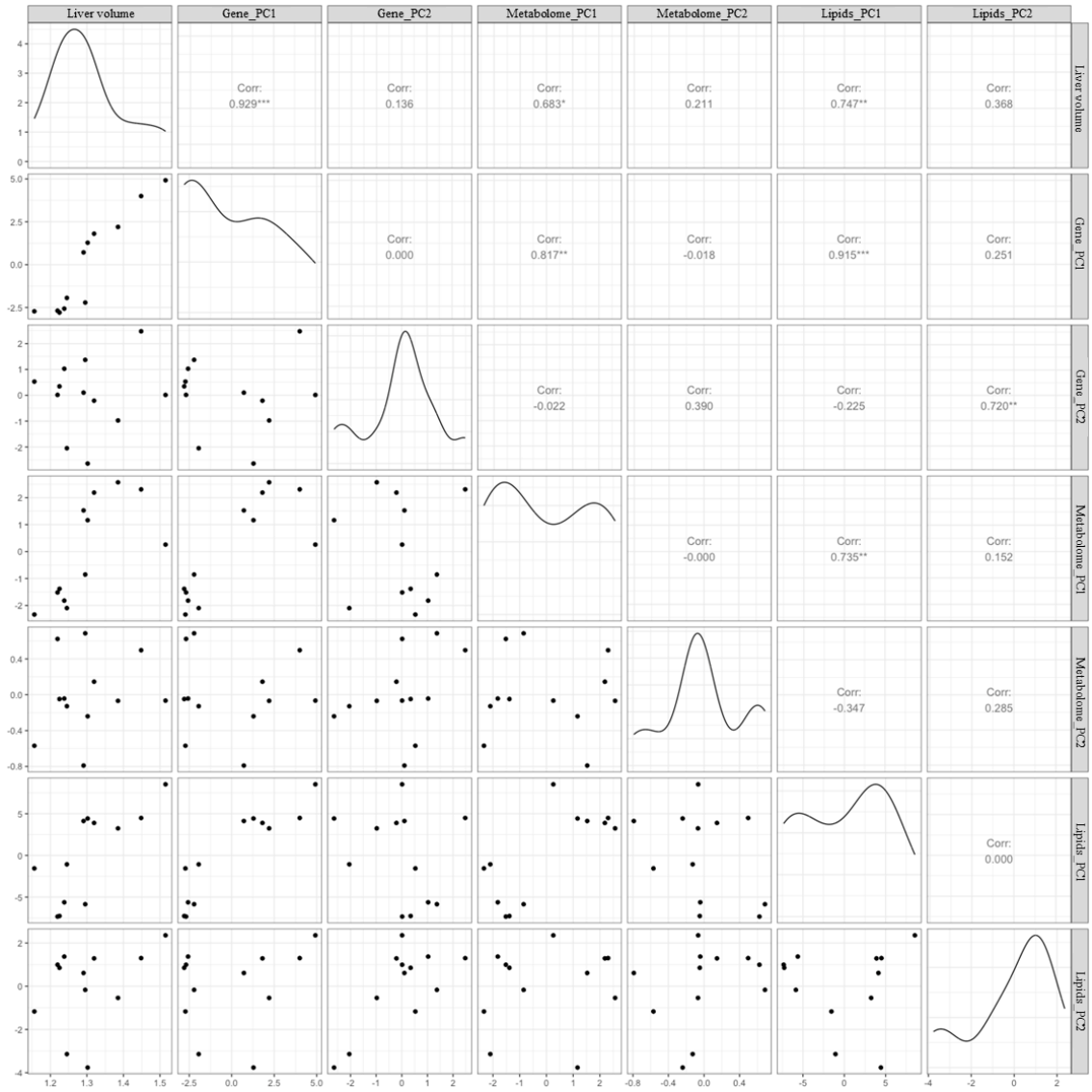

Figure 3.14. Correlation among each block and normalized liver volume. The proposed components for 1 and 2 from each block in the MB-PLS are visualized using the correlation values among them and the normalized liver volume.

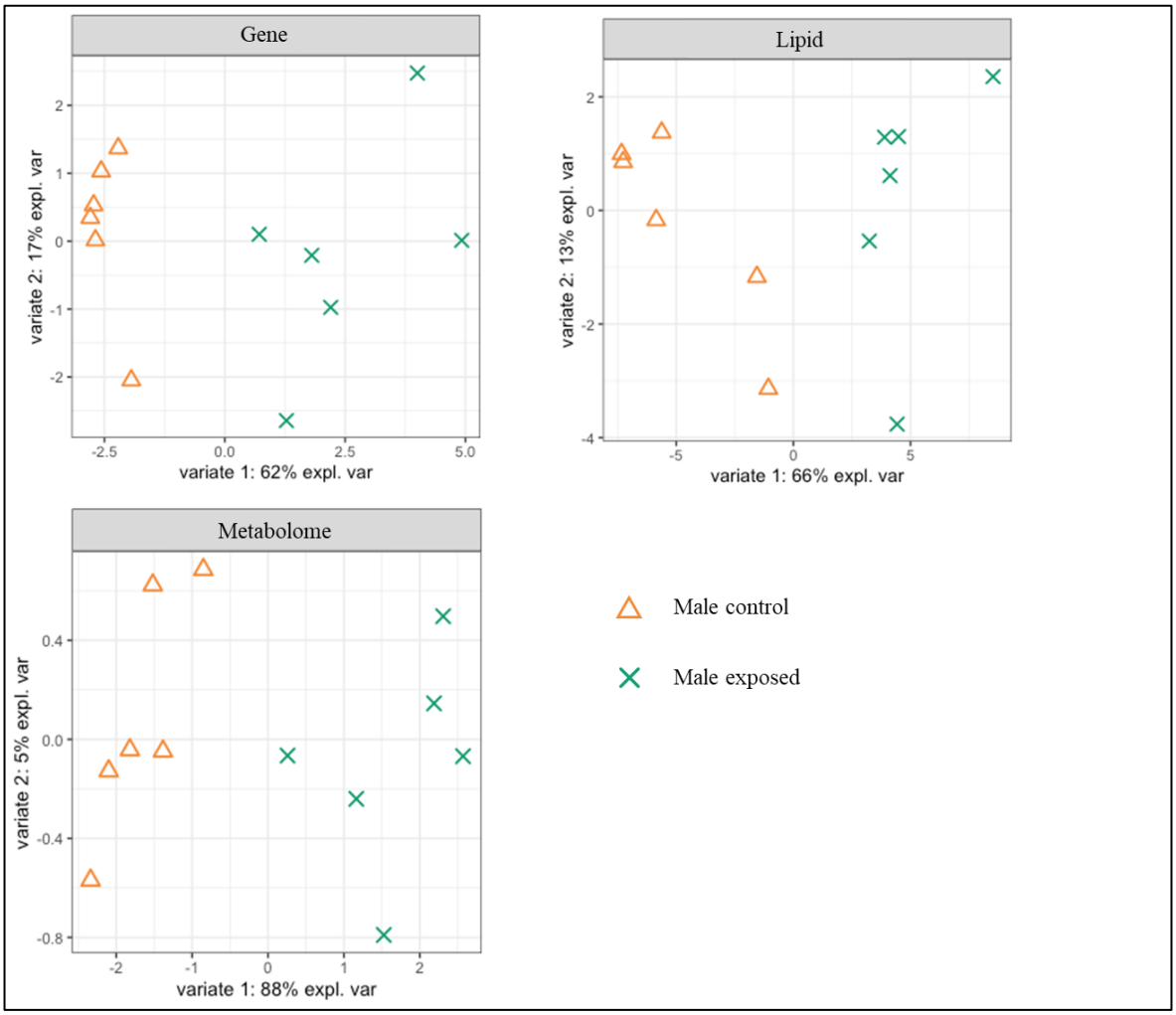

Figure 3.15. Score plots for the individual rats in the MB-PLS model. Score plots showed the individual rats in each gene, metabolome, and lipid block using components 1 and 2.

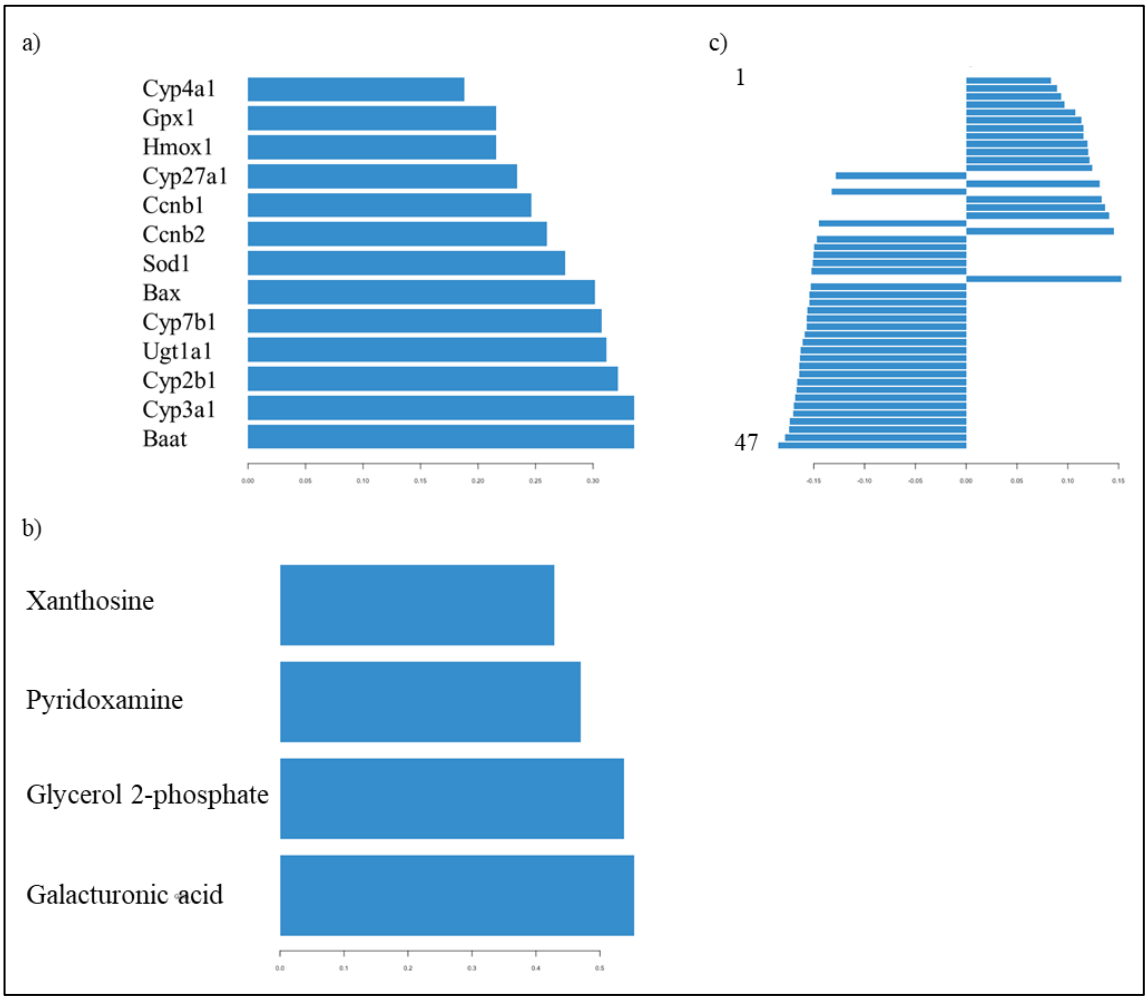

Figure 3.16. Contribution scores for component 1 in the MB-PLS. Contribution scores for all the selected variables to component 1 are shown using a bar plot. The bar length reflects the importance of each variable in this model, and its direction indicates a positive or negative coefficient for each variable. The lipid labels are defined in Table 3.16.

a) Gene expression
b) Metabolites
c) Lipids

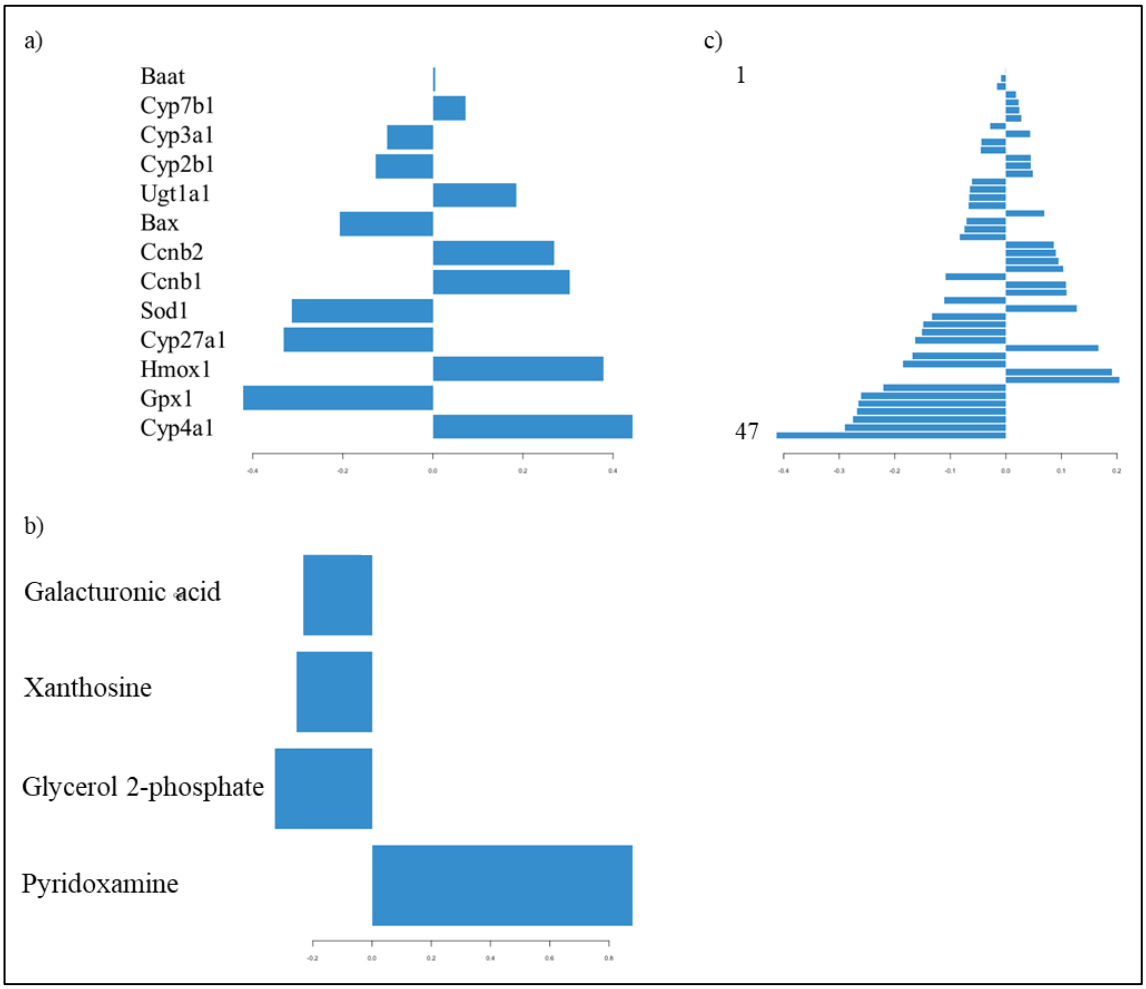

Figure 3.17. Contribution scores for component 2 in the MB-PLS. Contribution scores for all the selected variables to component 2 are shown using a bar plot. The bar length reflects the importance of each variable in this model, and its direction indicates a positive or negative coefficient for each variable. The lipid labels are defined in Table 3.17.

a) Gene expression
b) Metabolites
c) Lipids

Table 3.15. Lipid labels used in Figure 3.16.

Contribution score on component 1			
1	CL82:5|CL26:0_18:1_18:1_20:3	25	PE34:0|PE17:0_17:0
2	PC36:2;3O|PC18:0_18:2;3O	26	Cer42:2;2O|Cer18:1;2O/24:1
3	FA20:5	27	PE40:7|PE18:1_22:6
4	HexCer41:1;2O|HexCer18:1;2O/23:0	28	PE39:4|PE17:0_22:4
5	FA18:3	29	PE38:4|PE16:0_22:4
6	HexCer43:1;2O|HexCer18:1;2O/25:0	30	LPEO-18:1
7	PA36:2|PA18:1_18:1	31	PEO-40:4|PEO-18:0_22:4
8	PMeOH41:7|PMeOH19:1_22:6	32	PE40:4|PE20:2_20:2
9	PA40:6|PA18:0_22:6	33	LPC20:4
10	HexCer42:1;2O|HexCer18:1;2O/24:0	34	PEO-38:5|PEO-18:1_20:4
11	PEtOH38:5|PEtOH18:0_20:5	35	PCO-36:4
12	PC32:1;3O|PC16:1_16:0;3O	36	PE40:5|PE18:0_22:5
13	PE36:2|PE18:1_18:1	37	PE39:2|PE19:0_20:2
14	HexCer40:1;2O|HexCer18:1;2O/22:0	38	PE41:4|PE19:0_22:4
15	PE38:5|PE18:0_20:5	39	PC40:7
16	PA36:2|PA18:0_18:2	40	PEO-38:4|PEO-18:0_20:4
17	ST27:1;O;S	41	PEO-36:2|PEO-18:0_18:2
18	HexCer42:2;2O|HexCer18:1;2O/24:1	42	PC38:5
19	PE41:5|PE17:0_24:5	43	PEO-40:6|PEO-18:0_22:6
20	Cer44:2;2O|Cer18:1;2O/26:1	44	PEO-36:1|PEO-20:1_16:0
21	PC36:3|PC18:1_18:2	45	PEO-40:4|PEO-20:0_20:4
22	PC37:4	46	PEO-40:5|PEO-20:1_20:4
23	PC38:5|PC18:1_20:4	47	PEO-34:0|PEO-18:0_16:0
24	PE40:6|PE18:2_22:4		

cardiolipin (CL), phosphatidylcholine (PC), fatty acid (FA), hexosylceramides (HexCer), phosphatidic acid (PA), phosphatidylmethanol (PMeOH), phosphatidylethanol (PEtOH), phosphatidylethanolamine (PE), ceramide (Cer), ether-linked lyso-phosphatidylethanolamines (LPEO), ether-linked phosphatidylethanolamine (PEO), ether-linked phosphatidylcholines (PCO)

Table 3.16. Lipid labels used in Figure 3.17.

Contribution score on component 2			
1	PE O-38:4|PE O-18:0_20:4	25	PE 39:2|PE 19:0_20:2
2	FA 18:3	26	PE 41:5|PE 17:0_24:5
3	PE O-40:6|PE O-18:0_22:6	27	Cer 42:2;2O|Cer 18:1;2O/24:1
4	PE O-36:2|PE O-18:0_18:2	28	PEtOH 38:5|PEtOH 18:0_20:5
5	PE 40:5|PE 18:0_22:5	29	Cer 44:2;2O|Cer 18:1;2O/26:1
6	PE 38:4|PE 16:0_22:4	30	PMeOH 41:7|PMeOH 19:1_22:6
7	PE 40:7|PE 18:1_22:6	31	PA 36:2|PA 18:1_18:1
8	PC 36:3|PC 18:1_18:2	32	PC 38:5|PC 18:1_20:4
9	PE O-38:5|PE O-18:1_20:4	33	HexCer 42:2;2O|HexCer 18:1;2O/24:1
10	PE O-36:1|PE O-20:1_16:0	34	PE 38:5|PE 18:0_20:5
11	PC 38:5	35	PC 37:4
12	PE O-40:4|PE O-18:0_22:4	36	PE 36:2|PE 18:1_18:1
13	PE 39:4|PE 17:0_22:4	37	PC 40:7
14	PE 40:4|PE 20:2_20:2	38	HexCer 40:1;2O|HexCer 18:1;2O/22:0
15	PE O-40:4|PE O-20:0_20:4	39	PA 36:2|PA 18:0_18:2
16	LPC 20:4	40	ST 27:1;O;S
17	PE 41:4|PE 19:0_22:4	41	HexCer 41:1;2O|HexCer 18:1;2O/23:0
18	LPE O-18:1	42	PC 36:2;3O|PC 18:0_18:2;3O
19	PE 34:0|PE 17:0_17:0	43	FA 20:5
20	PE O-40:5|PE O-20:1_20:4	44	HexCer 42:1;2O|HexCer 18:1;2O/24:0
21	PA 40:6|PA 18:0_22:6	45	CL 82:5|CL 26:0_18:1_18:1_20:3
22	PE O-34:0|PE O-18:0_16:0	46	HexCer 43:1;2O|HexCer 18:1;2O/25:0
23	PE 40:6|PE 18:2_22:4	47	PC O-36:4
24	PC 32:1;3O|PC 16:1_16:0;3O		

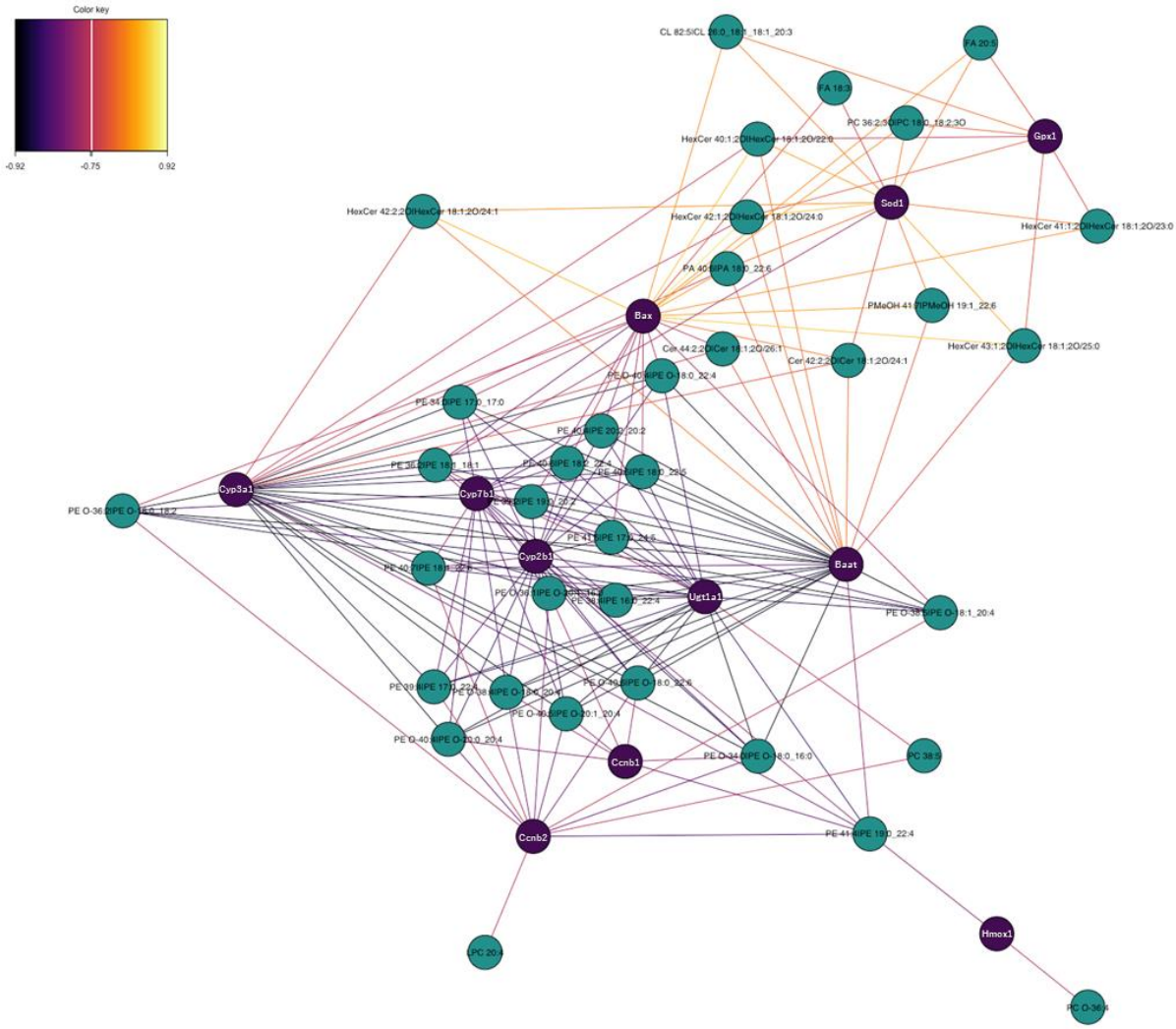

Figure 3.18. Network analysis for the multiblock partial least squares regression (MB-PLS model). Selected variables were connected to each other depending on their correlation. Violet: gene expression, green: lipids. Positive and negative correlations are shown using yellow and violet lines, respectively. Lines indicate when a correlation was found between the variables blocks (genes, metabolites, and lipids).

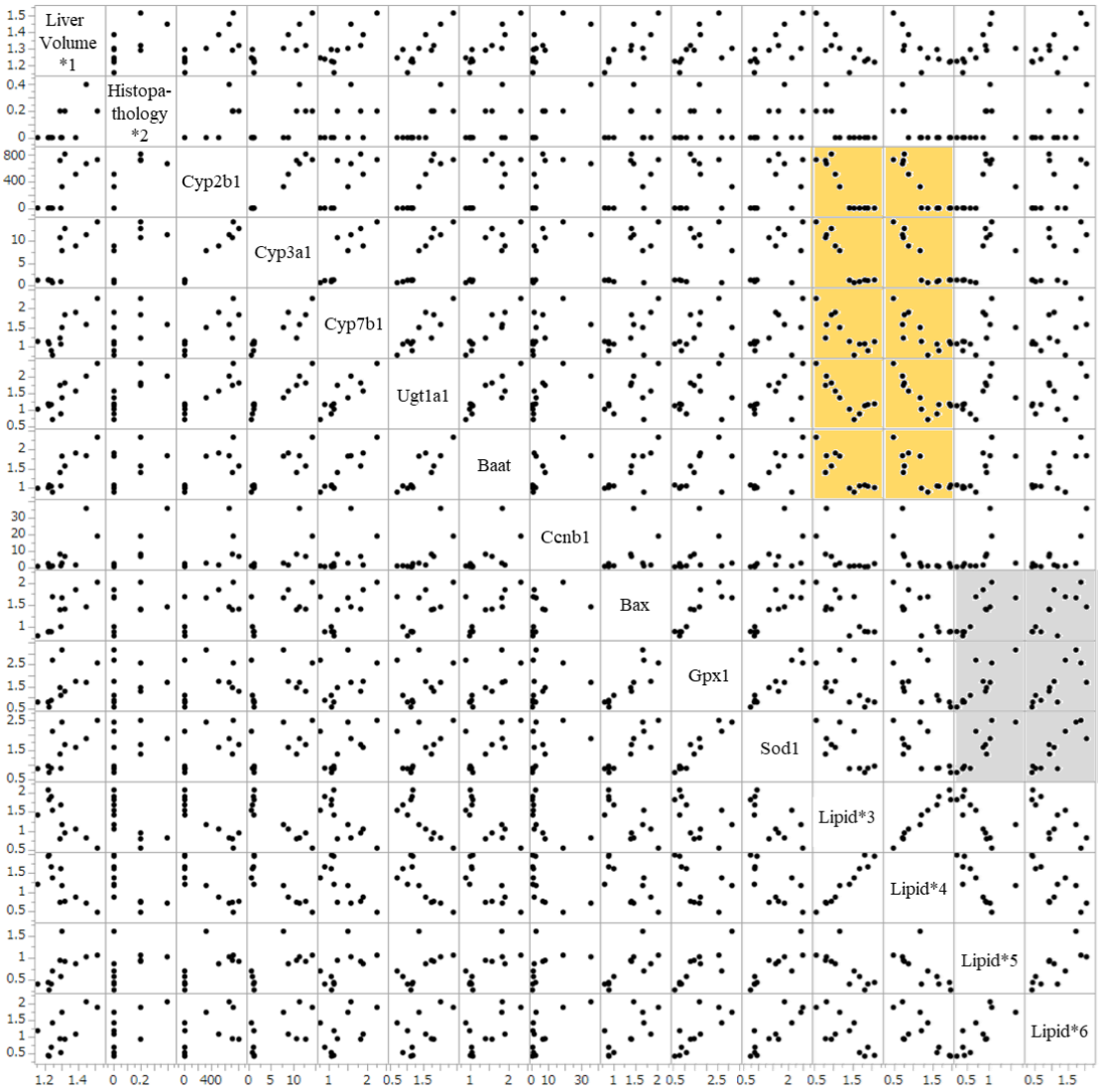

Figure 3.19. Correlation between gene expression and candidate biomarkers in the lipids. Correlations among normalized liver volume, histopathology results, some of the gene expression and candidate biomarkers in the lipids are shown. Colored background shows the well-correlated pairs between PE-O (orange), Cer (grey) and particular gene expressions.

*1-6 indicates below.

*1 Normalized liver volume

*2 Hepatocellular mitotic figure in histopathology

*3 PE O-34:0|PE O-18:0_16:0

*4 PE O-40:5|PE O-20:1_20:4

*5 Cer 42:2;2O|Cer 18:1;2O/24:1

*6 Cer 44:2;2O|Cer 18:1;2O/26:1

Chapter 4:

The evaluation of DDT's effect using rats of three generations based on DDT-sprayed areas

Evaluation of the effects of DDT using rats from three generations based on DDT-sprayed areas

Highlight

- Three generations Wistar rats were exposed to low concentrations of DDTs through food.
- Overall, no visible toxicity was observed in DDT-exposed rats of both sexes.
- The liver was significantly larger in DDTs-exposed females compared with that in control rats, but CT did not detect a significant difference.
- Further studies are necessary to understand the biological effects of low concentrations of DDTs, and these results should be applied to DDT-sprayed areas.

Abstract

Section 3 successfully demonstrated the utility of computed tomography (CT) to evaluate hepatomegaly. Dichlorodiphenyltrichloroethane (DDT) induces phenobarbital-like changes in the liver. Multigenerational toxicity of DDT has been investigated to reveal new toxicities in rats. Therefore, in this study, I used the CT approach with the method presented in Section 3 to examine three generations of rats exposed to DDT. To mimic the DDT-sprayed area, rats were exposed to a low concentration of DDT mixture (DDT and its metabolites) through food. Although the liver size was larger in DDT-exposed females compared with that in the control, the significance was inconsistent when the liver volume was determined using a measuring cylinder and CT. Further, histopathological analysis did not show any visible change in any of the rats. As the detection of such a small change is difficult even for CT, further studies are needed to complete the CT method in future. Overall, I did not detect any toxic effects of DDT in the rats exposed in this study; further, F2 analysis (third generation, for which DDT exposure was stopped) did not show any unique effects compared with those of F1 rats, which were directly exposed to DDT. However, this does not deny the risks of DDT in mammals. This research used a limited approach, and other molecular parameters need to be analyzed to accurately evaluate the toxicity of DDT in the liver.

Key words: DDT, computed tomography, hepatomegaly, multigeneration

1. Introduction

To date, animal experiments have revealed many toxicities of dichlorodiphenyltrichloroethane (DDT) and its metabolites in rodents. Well-known findings of DDT toxicities include carcinogenicity in the liver and endocrine disruption derived from its agonistic effect on the estrogen receptor (Beard, 2006). DDT has an effect similar to phenobarbital on the liver. For example, a two-year exposure study of DDT in rats revealed dose-dependent CYP2B1 induction and significant hepatomegaly compared with that in the control group in both sexes (Harada et al., 2016). These effects were also seen in phenobarbital-exposed rats (Section 3). The ability to induce CYP2B was found in DDT as well as its metabolites, dichlorodiphenyldichloroethylene (DDE) and dichlorodiphenyldichloroethane (DDD) (Nims et al., 1998). The two-year exposure study also demonstrated adenoma and carcinoma in the livers of rats exposed to DDT, in contrast to their absence in the control rats (Harada et al., 2016). One of the mechanisms revealed was the ability of DDT to activate constitutive androstane receptor (CAR) and to induce the cell cycle and anti-apoptotic protein expression (Kazantseva et al., 2013). A histopathological report showed abnormal mitoses in DDT-exposed rats accompanying cell necrosis, followed by DDT-induced hepatocellular hyperplasia (Yna Kostka et al., 2000). These histopathological changes can also be reflected in micro-computed tomography (CT) analyses.

DDT exposure was preserved in DDT-exposed rats transgenerationally as observed by sperm epimutation and diseases derived from epigenetic changes in the offspring. Pathological analysis showed a higher frequency of testis-related diseases in F3, which had only ancestral DDT exposure, than that in F1 (directly DDT-exposed). DDT affects various epigenetic processes such as DNA methylation and histone retention (King et al., 2019; Skinner et al., 2018). This transgenerational approach has also been used in examining several other chemicals such as vinclozolin (Nilsson et al., 2018) and glyphosate (Kubsad et al., 2019). These studies reported new findings of toxicity on offspring, which had indirect chemical exposure. Thus, toxicity tests using multiple generations experimental animals can reveal unknown toxicity of chemicals.

In DDT-sprayed area, wild rats are exposed to a mixture of DDT and its metabolites throughout their lifetime and across dozens of generations. Thus, to mimic

the DDT sprayed area and evaluate its effect in wild animals, I used a mixture of DDT, DDE, and DDD (DDTs), with a low concentration of DDTs compared to that in the previous DDT *in vivo* exposure test, in a three-generation test using Wistar rats. I developed a new methodology to evaluate chemical toxicity in the liver in Section 3. I then evaluated the effect of DDT using the approach used in the previous section for phenobarbital.

2. Materials and Methods

2.1 Animal experiment

All animal experiments, including chemical exposure and CT scanning, were conducted under ethical conditions approved by Hokkaido University (approval number: 20-0132 for animal husbandry and chemical exposure, 21-0019 for CT scanning). Briefly, I conducted DDTs exposure using DDT-containing food throughout three generations (F0, F1 and F2). DDT exposure started from the gestation period of F0. F1 was exposed to DDTs throughout their lifetime, F2 got DDT through transplacental exposure or mother's milk but did not get direct exposure of DDT. Control groups were prepared for F1 exposed group. I defined three groups for exposed status (control, exposed and F2), two for sexes (male and female) and two for experimental duration (eight and 14 weeks). Experimental design was summarized in Figure 4.1, and the number of rats provided in this research were listed in Table 4.1.

Six pregnant Wistar rats (approximately 11 weeks old, 2nd day of pregnancy) (F0) were imported to the experimental animal facility at the School of Veterinary Medicine, Hokkaido University from Japan SLC, Inc. (Shizuoka, Japan). Three of the six pregnant rats were handled as the exposed group and provided powder food (CLEA Rodent Diet CE-2, CLEA Japan, inc., Tokyo, Japan) containing a mixture of DDT and its metabolites (DDT: 2.5 mg/kg food, DDE and DDD 1.25 mg/kg food). Food for the exposed group was prepared by dripping the DDT mixture in organic solvents (hexane:acetone, 9:1) onto the powder food (12.5 ml organic solvents/kg food, approximately 0.2 ml × 60 drops). The powder food containing DDT was mixed well using a hand mixer for 10 min (to prepare a small amount) or a commercial stirrer overnight (for large amounts) (SKH-40, Misugi Co., Osaka, Japan). The mixed food was kept at room temperature for a couple of

days and mixed regularly to ensure complete evaporation of all the hexane and acetone. Each cage with an inner plastic cage included one pregnant rat with a shepherd shack (Shepherd Specialty Papers, Watertown, TN, USA), a food container with cover (Roden CAFÉ, Oriental Yeast Co., Tokyo, Japan), and wooden toys for biting (Japan SLC, Inc., Shizuoka, Japan). After parturition, the mothers in the exposed group were continuously exposed to the DDTs mixture and took care of the pups until weaning, for approximately four weeks. After weaning, the juveniles (F1) were separated from the mother, sexed, and assigned to new cages with three or four rats of the same sex. For juveniles, a shepherd tube (Shepherd Specialty Papers, Watertown, TN, USA) was used instead of a shepherd shack, along with food container with cover and wooden toys. Throughout the experiment, the rats were kept under 12 h light/dark conditions with *ad libitum* access to food and distilled fresh water. The control rats were housed under the same conditions as the exposed group except for the presence of the DDT mixture in food. Exposed rats continuously received DDT through food at the same concentration administered to their mother until eight and 14 weeks. Three exposed female rats (approximately 11 weeks age) were randomly selected and mated with exposed males. Just before parturition, the food for pregnant females was changed from DDT-containing to a normal diet. The new generation (F2) was then reared in the same manner as the F1 rats. For control rats, I did not perform examination using the F2 generation to reduce the number of animals used in this research. However, the F1 control was used for comparison with the F2 rats because F1 and F2 control rats need not be differentiated. Approximately half of the F1 and F2 rats were euthanized using carbon dioxide inhalation at eight weeks. The remaining half of the rats were transferred to the Central Institute of Isotope Science, Hokkaido University, and subjected to whole-body micro-CT scanning at 14 weeks of age (Inveon, Siemens Medical Solutions USA Inc., Knoxville, TN, USA). The CT settings and conditions were the same as those described in Section 3. After CT scanning, the rats were immediately euthanized using an excess of sevoflurane and subsequent cervical dislocation. Liver weights and volumes were measured using a scale and a measuring cylinder. The plasma and liver (for histopathological and quantitative PCR analyses) were collected using the same method as described in Section 3.

During the DDT exposure period, a veterinarian checked the rat health conditions every day, but no unexpected symptoms were identified in the exposed rats. Every 2–3

days, the consumed food was weighed, and every 6 days, all the food was renewed. During the entire period, The Laboratory Animal Care and Use Committee of Hokkaido University guidelines were followed for all procedures related to the animal experiments.

2.2 Classical tests

The methodology already described in Section 3 was used for histopathology (Section 3_2.3) and plasma clinical biochemistry analysis (Section 3_2.4) with slight modifications. Briefly, histopathological analysis was conducted at Sapporo General Pathology Laboratory using randomly selected rats from each group (control, exposed, and F2) at 14 weeks of age. Seven parameters (GOT: aspartate aminotransferase, GPT: alanine transaminase, TCHO: total cholesterol, TG: triglyceride, HDLC: high-density lipoprotein cholesterol, DBIL: direct bilirubin, and TBIL: total bilirubin) were used in Section 3 as clinical biomarkers; however, in this study, the rats were evaluated for GOT, GPT, TCHO, blood urea nitrogen (BUN), and creatinine (CRE) using FUJI DRI-CHEM 7000V.

For evaluating the *Cyp2b1* gene expression level, liver samples from eight-week-old control and exposed rats were used. RNA extraction, cDNA synthesis, and quantitative PCR were conducted using same method and primer set described in Section 3_2.5. The gene expression in each rat was normalized to that of the housekeeping gene, *beta-actin*. The gene expression level in each sex was determined based on the relative expression of exposed F1 and F2 rats compared with that of the control using the comparative CT method (ΔΔCT method). Samples outside the range that showed a good primer efficiency (around 100%) were included in the calculation by substituting the maximum cycle number with the range plus one cycle. The average gene expression in the male and female control rats was defined as one and was used for the calculation.

2.3 Statistical analysis

JMP 16 (SAS Institute, NC, USA) software was used for the statistical analyses. The control and exposed (F1 and F2) animals were compared using the Tukey-Kramer HSD or the Steel-Dwass test, depending on sample distribution, for evaluating differences in normalized liver size, clinical biochemical parameters, and *Cyp2b1* gene expression. Body weight and bone volume between groups were compared using the Tukey-Kramer HSD test. Correlation between liver sizes was evaluated using the Pearson correlation coefficient with robust estimation or Spearman's rank correlation coefficient, depending on sample distribution. Significant differences and correlations in all the tests were defined when the p value < 0.05.

3. Results

The results of the physical characteristics and liver sizes in rats at 14 weeks are shown in Table 4.2; the liver sizes normalized using body weight and bone volume are summarized in Table 4.3. Body weight and bone volume were significantly higher in F2 compared with those in the control males, but no significant difference was observed between the control and exposed F1 (F1) using the Tukey-Kramer HSD test at $p < 0.05$. Male rats showed significant differences between the control and F1 based on liver weight/body weight, but the significance was inconsistent among other parameters even in liver volume (MC)/body weight. No other significant difference was observed in males (Table 4.3). The normalized liver sizes of females were significantly heavier in F1 rats and larger in F1 and F2 exposed rats compared with that in the control ($p < 0.05$) when a weighing scale and measuring cylinder were applied. However, the significance shown in females disappeared when the liver size analyzed by CT was used. Table 4.4 shows the correlation between liver sizes (determined by weight scale, measuring cylinder, and CT) of all the rats in this study using the Pearson correlation or Spearman's rank correlation test. All the pairs were significantly correlated when the test was carried out on both sexes. However, although females still showed a significant correlation in all the pairs, CT did not evaluate liver size properly in males. Figure 4.2 showed a regression analysis of liver sizes using two measurements. The strength of the correlation between liver sizes measured using a measuring cylinder and CT was weaker than that observed in the phenobarbital study (Table 3.6 and 4.4). The comparison between the classical (liver weight/body weight) and CT (liver volume/bone volume) methods to evaluate the changes in liver sizes is shown visually in Figure 4.3.

In addition, the rat livers were evaluated using histopathology and clinical biochemical analyses. However, histopathological analysis did not show any visible difference between the control and exposure group (Figure 4.4). The results of clinical biochemical analysis are shown in Table 4.5. When focusing on liver parameters (GOT, TCHO, and GPT), both sexes showed no significant difference at 8 weeks, and only F1 females at 14 weeks showed significantly higher blood liver parameters compared with that in the control group. Kidney markers (BUN and CRE) showed significant differences in some pairs between the control and F2 groups, for example females at 8 weeks had 0.23 mg/dL of CRE in control and 0.36 mg/dL in F2.

Quantitative PCR showed dramatical induction of *Cyp2b1* as follows: male rats, 93.3-fold (sd: ± 35.7) and 3.9-fold (sd: ± 1.2) in F1 and F2 exposed rats compared with that in the control; female rats, 304.3-fold (sd: ± 170.0) and 6.0-fold (sd ±5.7) at eight weeks age. All the pairs between the control, and the exposed F1 and F2 groups showed a significant difference with $p < 0.05$.

4. Discussion

Section 3 shows that CT could accurately estimate the liver size (Table 3.6 and Figure 3.3) throughout the lifetime of an animal. However, this study does not show an adequate correlation, with several outliers; the significant difference found by using a measuring cylinder could not be detected in the CT analysis (Table 4.3 and 4.4). Although phenobarbital-exposed rats were well-positioned on the CT bedding, some of the rats in this study were positioned in ventral recumbency with their spines off the midline; this was a technical problem. However, it did not seem to be the main reason for the lower correlation in this study. Section 3 showed the effective dose of administrated phenobarbital at which the rats slept after injection. However, this study used a low concentration of DDT and no symptom induced by DDTs was observed in the animal behavior throughout the experiment. As shown in Table 4.6, the phenobarbital study shows a higher variance of liver sizes among rats than that in the present study. Such a small variance in the present DDT study hindered the detection of changes in the liver using CT analysis. This might be a limitation of using CT and the current estimation methodology to evaluate hepatomegaly. In this study, no histopathological change was observed. The biological changes caused by DDTs exposure in the liver would thus be limited in this study, and such a small biological reaction without pathological changes would be difficult to detect even with CT analysis. However, when focusing on females, which showed a significant difference in liver size, the tendency between the liver volume (MC)/Bone volume and liver volume (CT)/Bone volume was similar (Table 4.3). The significant difference detected in liver size using a measuring cylinder should not be defined as DDT toxicity. This result might indicate the possibility of using CT to detect a previously undetectable biological process in the lifetime of an animal. Again, this is a pioneering study demonstrating the use of CT for assessing liver toxicity induced by chemical exposure. This study estimated liver volume based on liver length and thoracic

area, but various further approaches should be discussed on evaluating liver size using CT analysis. Further, techniques such as positioning the rats appropriately on the bedding must be well-guided for applying CT analysis to evaluating the liver. *Cyp2b1* expression was dramatically induced in exposed rats of both sexes at 8 weeks of age. This induction may be seen at 14 weeks (time point of CT analysis). Therefore, the mechanisms of hepatomegaly shown in the females in this study could be also due to the biological response via CAR which was demonstrated in Section 3. However, to access the adverse outcome pathway (AOP) of hepatomegaly, further molecular analyses such as those presented in Section 3 are necessary.

The clinical biochemistry analysis evaluated various liver (GOT, TCHO, GPT) and kidney (BUN, CRE) markers. This study showed a significantly higher concentration of CRE in F2 than in the control. The animal supplier company (Japan SLC, Inc.) has reported the reference values of these parameters, for example, 0.25 ± 0.02 mg/dL of CRE in 10-week-old females (http://jslc.co.jp/english/). The current result in F2 (0.36 mg/dL in female at 8 weeks) showed a slightly higher concentration than that in this reference. However, the chemical-induced kidney injury showed a dramatic increase of these parameters in rats; their nonspecific induction, not only in kidney damage is well known (Diwan et al., 2013; Griffin et al., 2019; Palipoch and Punsawad, 2013). The induction detected in this study is not sufficient to indicate the toxicity of DDT on the kidney. BUN and CRE were the most used biomarkers of kidney disease, particularly acute kidney injury. However, its low sensitivity and specificity are commonly issued in the clinical field and new biomarkers have been developed (Griffin et al., 2019). This study mainly targeted the liver in DDT-exposed rats. However, the relationship between kidney disease and ancestral DDT exposure has been discussed previously in rats (King et al., 2019). An epidemiological study has also indicated the association of DDT with chronic kidney disease in humans (Lv et al., 2022). This study used BUN and CRE for a brief check of the kidney condition because of their easy access and low cost (same methodology as liver parameters). Further analysis of the kidney is needed using newly developed biomarkers. The liver parameters did not show a noticeable difference between groups (Table 4.5), but exposed F1 females at 14 weeks had significantly higher GOT, TCHO, and GPT than those of controls. These parameters were reported to change in an age-dependent manner in rats (Matsuzawa et al., 1993); older rats have higher levels and

greater variance among individuals. While female Wistar rats at 10 weeks showed 85.4 ± 8.3 of GOT and 39.6 ± 7.0 of GPT, 175.8 ± 84.9 of GOT and 86.6 ± 41.0 of GPT were reported for females at 20 weeks (Japan SLC, Inc.). The elevations observed in this study can be masked by such a large variance among individuals. As discussed in Section 3, hepatic injuries cause a dramatic increase in these parameters. In addition, a histopathological study in the present study did not support the presence of liver damage. Hence, although significant changes would indicate the biological response in the liver to DDTs exposure, the biological significance of these parameter elevations is unclear in this study.

The liver size was significantly larger in the females of the F2 exposure group compared with that in the control females. F2 could show the effect of DDT through two pathways: epigenetic changes caused by ancestral exposure, and indirect exposure through the placenta or through milk. This study did not differentiate these pathways; however, DDT intake through milk in this study should not be ignored as several reports have shown that breast milk can transmit DDT to human infants (Azeredo et al., 2008; Bouwman et al., 2012). DDTs exposure was stopped upon the birth of F2 rats, but these results might indicate that the effects of such a low concentration of DDTs last until 14 weeks age in F2 as observed by the change in liver size. However, these effects cannot be defined as toxic effects, as indicated by the histopathological analysis (Figure 4.4).

As introduced above, two-year DDT exposure (500 ppm) causes adenoma, carcinoma, and other various histopathological changes in rats. The duration of the current study was only 14 weeks, and the rats were still young. This may be why any noticeable change was not observed in DDT-exposed rats. However, the same two-year study showed that when a low concentration of DDT (5 ppm) was used, a significant difference was not observed in rats. Another study conducted by our research group investigated the steroid hormone profiles in the present rat samples. However, only estradiol showed a significant difference between male groups, whereas other hormones, including testosterone, showed no strong differences (unpublished results). Overall, no significant toxic effects of DDT were identified by the methods used in this study on rats. However, the effects of low DDT concentrations on the liver, cannot be inferred from only these findings. This study focused on only liver size, histopathological analysis, and

clinical biomarkers. Further molecular analyses are thus needed to examine DDT toxicity at low concentrations, which can be seen in DDT-sprayed regions.

5. Conclusion

In this study, rats were fed low concentrations of DDT. Hepatomegaly was observed in DDT-exposed females, but I found that the CT method still needs to be discussed and applied to other chemicals. The toxic effects of DDTs were not discovered using the method used in this study. However, every year, new studies alert the public to the risks of DDT worldwide. Further analyses are thus essential to evaluate the effects of low DDT concentrations in mammals and to compare the risks and benefits of DDT in the sprayed area.

Figures and Tables

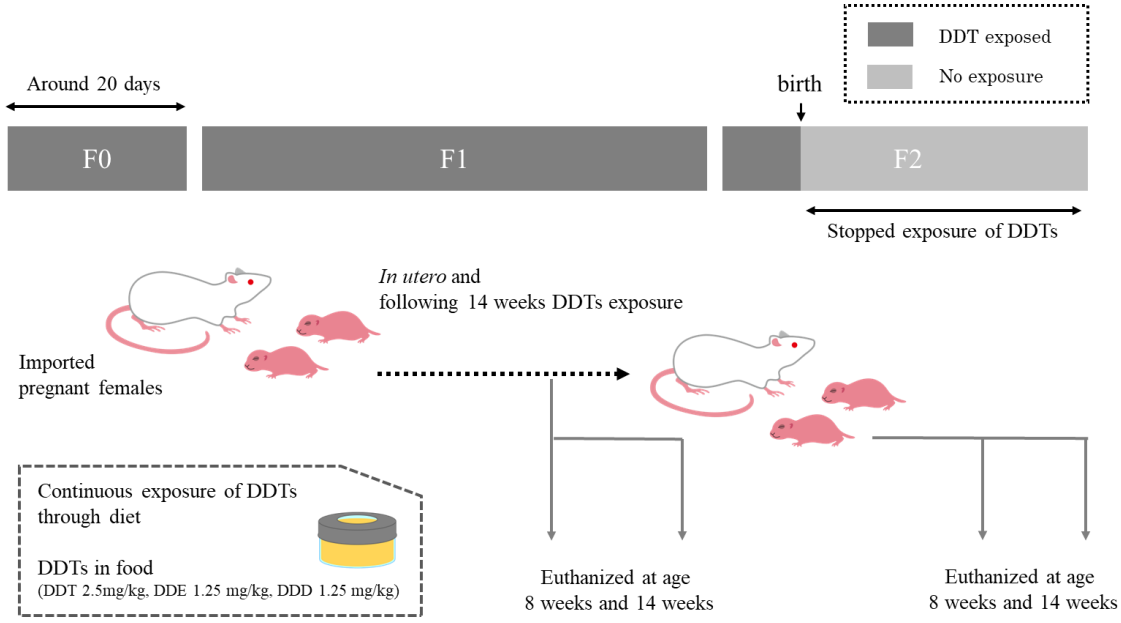

Figure 4.1. Experimental design.

Table 4.1. The number of rats in each group.

		F1		F2
		Control	Exposed	Exposed
8 weeks	Male	9	7	6
	Female	9	4	6
14 weeks	Male	6	9	6
	Female	5	5	7

Table 4.2. Physical characteristics and liver sizes in each group.

		Body weight (g)	Liver weight (g)	Liver volume (MC, mL)	Bone volume (CT, cm^3)	Liver length (CT, cm)	Liver volume (CT, cm^3)
Male	Control	306.95 (±10.95)	11.17 (±0.69)	10.67 (±0.62)	11.12 (±0.22)	3.13 (±0.20)	17.44 (±1.45)
	Exposed F1	315.48 (±8.38)	12.06 (±0.34)	11.36 (±0.52)	11.53 (±0.32)	3.29 (±0.14)	16.87 (±1.09)
	Exposed F2	340.41* (±6.94)	12.14 (±0.17)	11.71 (±0.22)	12.19* (±0.27)	3.62 (±0.20)	19.12 (±1.28)
Female	Control	189.27 (±9.14)	5.94 (±0.33)	5.75 (±0.32)	8.40 (±0.32)	2.45 (±0.16)	10.62 (±0.83)
	Exposed F1	195.93 (±3.98)	6.81 (±0.56)	6.55 (±0.50)	8.36 (±0.12)	2.71 (±0.10)	11.45 (±0.76)
	Exposed F2	201.80 (±12.00)	6.73 (±0.33)	6.68 (±0.32)	8.91* (±0.34)	2.76 (±0.10)	11.70 (±0.35)

Body and liver weights and bone and liver volumes are presented in this table. The liver volume was determined using a measuring cylinder (MC) and estimated using micro-computed tomography (CT). Brackets contain the standard deviation (SD) for each group. The differences of body weight and bone volume between each group were evaluated using the Tukey-Kramer HSD test. * indicates a significant difference from the other two groups.

Table 4.3. Normalized liver sizes in each group.

		Liver weight /Body weight	Liver volume (MC) /Body weight	Liver volume (MC) /Bone volume	Liver volume (CT) /Body weight	Liver volume (CT) /Bone volume
Male	Control	3.64 (±0.15)	3.47 (±0.15)	95.9 (±4.74)	5.68 (±0.44)	156.7 (±10.96)
	Exposed F1	3.82[ab] (±0.11)	3.60 (±0.16)	98.6 (±5.73)	5.35 (±0.39)	146.5 (±12.10)
	Exposed F2	3.57[b] (±0.05)	3.44 (±0.09)	96.1 (±2.61)	5.62 (±0.33)	156.8 (±9.01)
Female	Control	3.14 (±0.04)	3.04 (±0.06)	68.4 (±1.32)	5.61 (±0.30)	126.4 (±7.77)
	Exposed F1	3.47[a] (±0.22)	3.34 (±0.19)	78.4[a] (±6.13)	5.84 (±0.41)	136.9 (±8.31)
	Exposed F2	3.34 (±0.07)	3.31[a] (±0.07)	75.0[a] (±1.40)	5.82 (±0.41)	131.5 (±6.76)

Values are expressed in percentage (body weight- or bone volume-ratio). The superscript “a” indicates a significant difference between the control and exposed groups (F1 and F2), and “b” indicates that between the exposed groups (F1 and F2) using the Tukey-Kramer HSD test or the Steel-Dwass test ($p < 0.05$), depending on sample distribution. Brackets contain the standard deviation (SD) for each group.

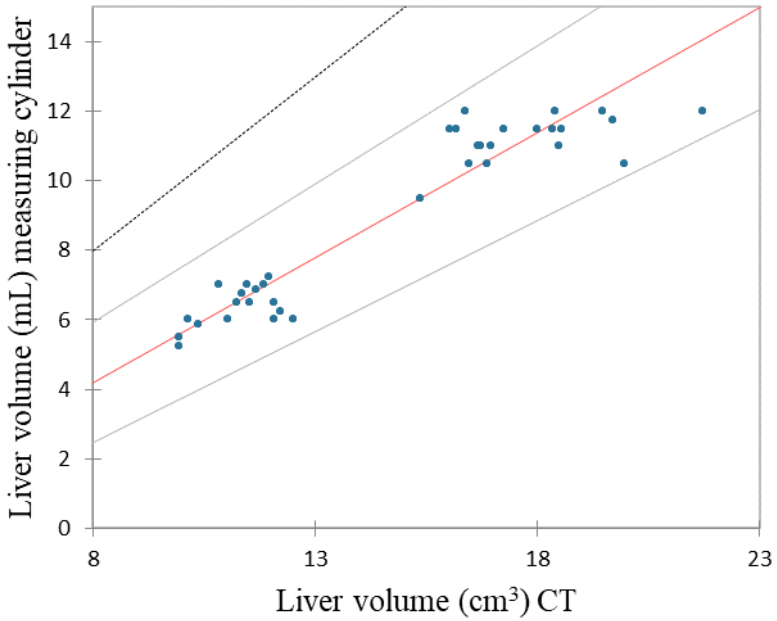

	Estimate	Lower CL (mean)	Upper CL (mean)
Intercept	-1.57	-2.62	-0.43
Slope	0.72	0.64	0.80

Figure 4.2. Regression analysis between liver sizes determined using a measuring cylinder and estimated using CT. The line was described using the Passing–Bablok regression by XLSTAT (Addinsoft, Paris, France).

Table 4.4 Correlation between liver size.

a) Both sexes	Liver weight	Liver volume (MC)	Liver volume (CT)
Liver weight	1.00	0.97	0.82
Liver volume (MC)	$p<0.01$	1.00	0.84
Liver volume (CT)	$p<0.01$	$p<0.01$	1.00

b) Male	Liver weight	Liver volume (MC)	Liver volume (CT)
Liver weight	1.00	0.83	0.17
Liver volume (MC)	$p<0.01$	1.00	0.36
Liver volume (CT)	$p=0.458$	$p=0.052$	1.0

c) Female	Liver weight	Liver volume (MC)	Liver volume (CT)
Liver weight	1.00	0.97	0.51
Liver volume (MC)	$p<0.01$	1.00	0.52
Liver volume (CT)	$p=0.037$	$p=0.032$	1.00

This table shows the Pearson correlation coefficient or Spearman's rank correlation coefficient and the *p* value. (a) both sexes, (b) males, (c) females.

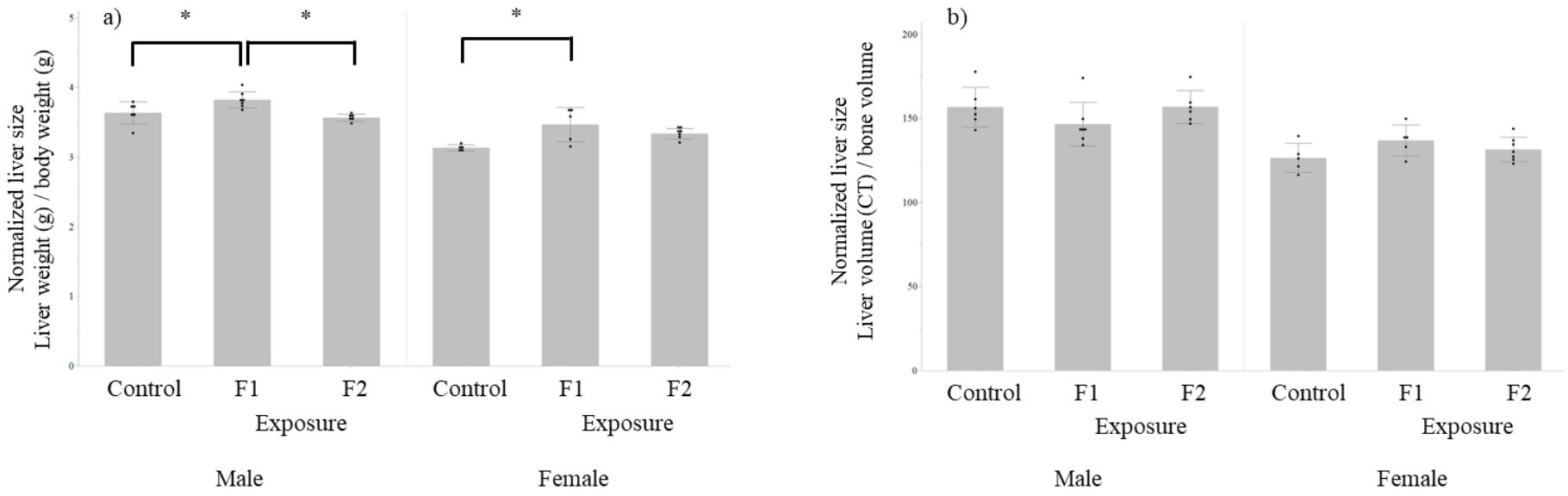

Figure 4.3. Comparison of liver size between classical and CT method. The control and exposed groups were compared using **(a)** the classical method (liver weight/body weight) and **(b)** CT method (estimated liver volume/bone volume). * indicates a significant difference between the groups analyzed using the Tukey-Kramer HSD test with $p < 0.05$. Spots and error bars indicate individual rats and standard deviation among rats, respectively.

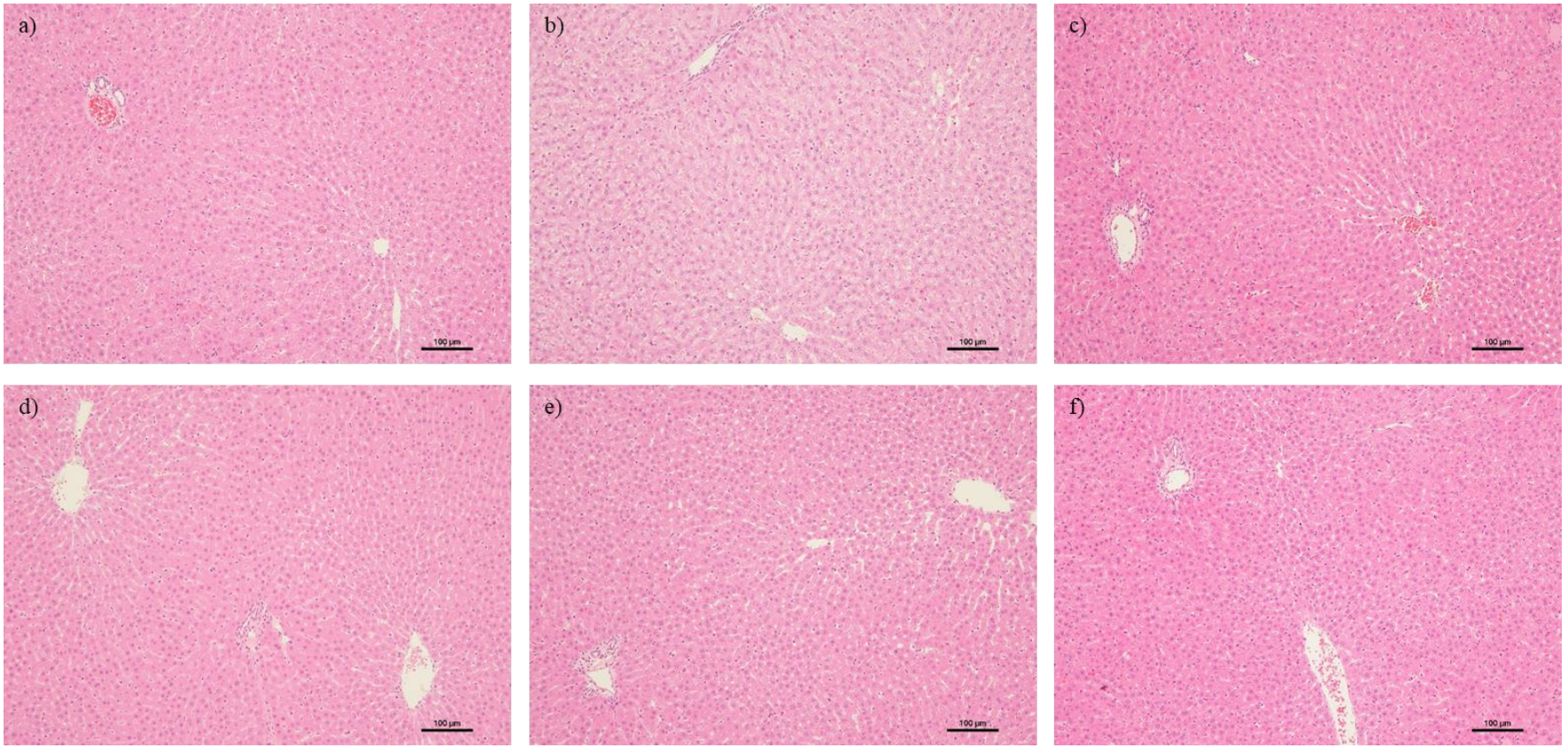

Figure 4.4 Histopathological analysis of the liver. (a) Control male, (b) DDT-exposed F1 male, (c) DDT-exposed F2 male, (d) Control female, (e) DDT-exposed F1 female, (f) DDT-exposed F2 female.

Table 4.5. Clinical biochemical parameters in each group (control and DDT-exposed and F2).

a) Female 8 weeks

	GOT	TCHO	GPT	BUN	CRE
Control	62.0 (±4.7)	83.8 (±11.6)	26.3 (±2.3)	15.8 (±1.3)	0.23 (±0.037)
F1 Exposed	64.3 (±11.0)	100.5 (±5.9)	37.8 (±13.2)	17.6 (±2.6)	0.30 (±0.076)
f2	63.3 (±7.1)	93.0 (±5.1)	27.5 (±2.9)	17.3 (±2.1)	0.36[a] (±0.026)

b) Female 14 weeks

	GOT	TCHO	GPT	BUN	CRE
Control	67.0 (±9.5)	83.4 (±11.2)	29.8 (±5.3)	19.6 (±3.1)	0.17 (±0.015)
F1 Exposed	110.6[ab] (±23.5)	114.4[a] (±17.8)	43.6[a] (±6.8)	16.7 (±0.6)	0.19 (±0.022)
f2	83.6[b] (±12.5)	98.0 (±6.8)	34.4 (±4.6)	17.7 (±1.9)	0.21[a] (±0.016)

c) Male 8 weeks

	GOT	TCHO	GPT	BUN	CRE
Control	93.1 (±35.4)	74.4 (±6.2)	41.9 (±14.5)	18.4 (±2.1)	0.29 (±0.029)
F1 Exposed	72.0 (±16.7)	76.7 (±4.5)	35.0 (±7.1)	19.2[b] (±1.3)	0.35 (±0.055)
f2	81.2 (±18.8)	68.8 (±7.2)	37.2 (±10.9)	15.7[b] (±1.8)	0.35[a] (±0.004)

d) Male 14 weeks

	GOT	TCHO	GPT	BUN	CRE
Control	95.8 (±7.5)	63.3 (±7.1)	47.7 (±6.7)	18.1 (±1.6)	0.22 (±0.029)
F1 Exposed	84.3 (±17.1)	66.3 (±13.1)	50.8 (±8.1)	20.0 (±2.8)	0.30 (±0.142)
f2	95.8 (±11.7)	63.3 (±5.5)	47.7 (±5.2)	18.1 (±1.2)	0.22 (±0.015)

The superscript "a" indicates a significant difference between the control and exposed groups (F1 and F2), and "b" indicates that between the exposed groups (F1 and F2) with the Tukey-Kramer HSD or the Steel-Dwass test ($p < 0.05$), depending on sample distribution. Brackets contain the standard deviation (SD) for each group.

(GOT: aspartate aminotransferase U/L, GPT: alanine transaminase U/L, TCHO: total cholesterol mg/dL, BUN: blood urea nitrogen mg/dL, CRE: creatinine mg/dL)

Table 4.6. Variance of liver sizes in Section 3 and 4.

	Male	Female
DDT	0.41	0.31
Phenobarbital	0.88	0.52

The variance of liver sizes in the present study (DDT) and previous study (phenobarbital) was compared using all the rats in each study.

Chapter 5:
Summary and Recommendation

DDT is a well-known organochlorine pesticide that is currently used for vector control against malaria. Recently, many insecticides such as neonicotinoids have been developed and are used widely, but malaria-endemic countries continue to use DDT. DDT provides benefits in terms of infectious disease control but also raises concerns regarding the risk of toxicity to mammals and ecosystems. In particular, because of its high environmental persistence, the effects of DDT will last for some decades even after its spraying is stopped. Therefore, considering appropriate vector control is essential by accurately assessing the risk of DDT and providing it to DDT-using countries.

First, this thesis focused on wild rodents inhabiting the DDT-sprayed areas in South Africa because they could act as sentinels for estimating the toxicity of DDT to human residents and other wild animals. This research reveals that the expression of metabolic enzymes could be perturbed because of DDT exposure. In particular, a sex-linked metabolic enzyme in rats changed its expression pattern in highly DDT-polluted areas. Unfortunately, no effective biomarker reflecting the health problems caused by DDT exposure has been discovered; however, this study did identify some potential candidates. The molecular analysis was rarely applied for field surveys in DDT-sprayed areas. This study will encourage further molecular analyses in the field and *in vivo* studies for a more accurate understanding of the effect of DDT in the field. Epidemiological and *in vivo* studies on DDT occasionally show inconsistent results. Therefore, the toxicity of DDT in the field still remains controversial. For a better understanding of the ecological effects of DDT, continuous monitoring in DDT-sprayed areas is highly recommended.

In the second half of this thesis, I discuss the development of new toxicity testing methods using CT. The current toxicity tests have several problems and need to be improved. In my research, CT clearly demonstrated phenobarbital-induced hepatomegaly in a live animal. However, CT could not adequately differentiate the size of rat livers between DDT-exposed and control animals. Although further approaches are necessary for completing the CT method, my results present a new possibility for the use of CT to evaluate chemical toxicity in the liver. Multiomics analysis was then performed to reveal the molecular process of phenobarbital-induced hepatomegaly. This thesis demonstrates that lipids in plasma can be used to estimate the mechanism of hepatomegaly. Both lipid analysis and CT can be conducted throughout an animal's lifetime. This new approach

thus enables the conduct of a continuous toxicity test using live animals, resulting in the reduction of engaged animals. This allows advocacy of a new evaluation method for toxic chemicals. This is a pioneering study; therefore, applying this approach to evaluate various chemicals is essential for developing additional effective methods.

In the last section, the effect of a low DDT concentration was evaluated using three generations of rats. However, the noticeable toxic effects of DDT were not observed in DDT-exposed rats. The life expectancy of rats in the wild is thought to be quite short, as more than half of the rats sampled in Section 2.1 were younger than those in the current exposure period (14 weeks). The present findings in this thesis did not demonstrate that wild rats suffered from the carcinogenic effects of DDT. However, the extrapolation of these findings to humans must be conducted carefully. Section 3 demonstrates the utility of multiomics analysis as well as CT analysis. Further molecular approaches should also be applied in the study of DDT to reveal the unknown toxicities and effects of low DDT concentrations in mammals. Techniques such as CT are difficult to use in DDT-sprayed areas. To assess the effects of DDT in sprayed areas, *in vivo* and field studies must be conducted together. Overall, this thesis presents the possible ecological and biological risks of DDT in Section 2, a new approach for evaluating chemical toxicity in Section 3, and the findings about DDT based on a multigenerational study on rats in Section 4. In the future, effective biomarkers reflecting the health conditions changed by DDT exposure are needed. Effective evaluation of low DDT concentration will provide a hint for considering appropriate vector control with a suitable comparison between risks and benefits.

References

Agency for Toxic Substances and Disease Registry, 2022. Toxicological Profile for DDT, DDE, and DDD.

Agency for Toxic Substances and Disease Registry, 2002. Public health statement DDT, DDE, and DDD.

Agúndez, J.A.G., Jiménez-Jiménez, F.J., Alonso-Navarro, H., García-Martín, E., 2014. Drug and xenobiotic biotransformation in the blood–brain barrier: A neglected issue. Front Cell Neurosci 8.

Alavanja, M.C.R., 2009. Introduction: Pesticides Use and Exposure, Extensive Worldwide. Rev Environ Health 24, 303–310.

Aliferis, K.A., Chrysayi-Tokousbalides, M., 2011. Metabolomics in pesticide research and development: Review and future perspectives. Metabolomics 7, 35–53.

Alsiö, J., Birgner, C., Björkblom, L., Isaksson, P., Bergström, L., Schiöth, H.B., Lindblom, J., 2009. Impact of nandrolone decanoate on gene expression in endocrine systems related to the adverse effects of anabolic androgenic steroids. Basic Clin Pharmacol Toxicol 105, 307–314.

Ament, Z., West, J.A., Stanley, E., Ashmore, T., Roberts, L.D., Wright, J., Nicholls, A.W., Griffin, J.L., 2016. PPAR-pan activation induces hepatic oxidative stress and lipidomic remodelling. Free Radic Biol Med 95, 357–368.

An, G., Kwon, D., Yoon, H., Yu, J., Bang, S., Lee, Y., Jeon, S., Jung, J., Chang, J., Chang, D., 2019. Evaluation of the radiographic liver length/11th thoracic vertebral length ratio as a method for quantifying liver size in cats. Veterinary Radiology and Ultrasound 60, 640–647.

Andrieu-Abadie, N., Gouazé, V., Salvayre, R., Levade, T., 2001. Review Article CERAMIDE IN APOPTOSIS SIGNALING: RELATIONSHIP WITH OXIDATIVE STRESS. Free Radic Biol Med 31, 717–728.

Apostolopoulou, M., Gordillo, R., Koliaki, C., Gancheva, S., Jelenik, T., de Filippo, E., Herder, C., Markgraf, D., Jankowiak, F., Esposito, I., Schlensak, M., Scherer, P.E., Roden, M., 2018. Specific hepatic sphingolipids relate to insulin resistance, oxidative stress, and inflammation in nonalcoholic steato hepatitis. Diabetes Care 41, 1235–1243.

Asaoka, Y., Sakai, H., Sasaki, J., Goryo, M., Yanai, T., Masegi, T., Okada, K., 2010.

Changes in the Gene Expression and Enzyme Activity of Hepatic Cytochrome P450 in Juvenile Sprague-Dawley Rats. Journal of Veterinary Medical Science 72, 471–479.

Astashkina, A., Mann, B., Grainger, D.W., 2012. A critical evaluation of in vitro cell culture models for high-throughput drug screening and toxicity. Pharmacol Ther 134, 82–106.

Azeredo, A., Torres, J.P.M., de Freitas Fonseca, M., Britto, J.L., Bastos, W.R., Azevedo e Silva, C.E., Cavalcanti, G., Meire, R.O., Sarcinelli, P.N., Claudio, L., Markowitz, S., Malm, O., 2008. DDT and its metabolites in breast milk from the Madeira River basin in the Amazon, Brazil. Chemosphere 73, S246–S251.

Bailey, R., 2022. Disease, DPs, and DDT: A Global Health Perspective on the History of Refugee Relief. Itinerario 46, 233–250.

Barnhoorn, I.E.J., Bornman, M.S., Jansen van Rensburg, C., Bouwman, H., 2009. DDT residues in water, sediment, domestic and indigenous biota from a currently DDT-sprayed area. Chemosphere 77, 1236–1241.

Batterman, S., Chernyak, S., Gouden, Y., Hayes, J., Robins, T., Chetty, S., 2009. PCBs in air, soil and milk in industrialized and urban areas of KwaZulu-Natal, South Africa. Environmental Pollution 157, 654–663.

Beard, J., 2006. DDT and human health. Science of the Total Environment 355, 78–89.

Benjamin Roche, Hélène Broutin, Frédéric Simard, 2018. Ecology and Evolution of Infectious Diseases: Pathogen Control and Public Health Management in Low-income Countries, 1st ed. Oxford University Press.

Benjamini, Y., Hochberg, Y., 1995. Controlling The False Discovery Rate-A Practical And Powerful Approach To Multiple Testing. Journal of the Royal Statistical Society: Series B (Methodological) 57, 289–300.

Bhushan, B., Molina, L., Koral, K., Stoops, J.W., Mars, W.M., Banerjee, S., Orr, A., Paranjpe, S., Monga, S.P., Locker, J., Michalopoulos, G.K., 2021. Yes-Associated Protein Is Crucial for Constitutive Androstane Receptor-Driven Hepatocyte Proliferation But Not for Induction of Drug Metabolism Genes in Mice. Hepatology 73, 2005–2022.

Blanco-Bose, W.E., Murphy, M.J., Ehninger, A., Offner, S., Dubey, C., Huang, W., Moore, D.D., Trumpp, A., 2008. c-Myc and its target foxM1 are critical downstream

effectors of constitutive androstane receptor (CAR) mediated direct liver hyperplasia. Hepatology 48, 1302–1311.

Bornman, M., Delport, R., Farías, P., Aneck-Hahn, N., Patrick, S., Millar, R.P., de Jager, C., 2018. Alterations in male reproductive hormones in relation to environmental DDT exposure. Environ Int 113, 281–289.

Bougarne, N., Weyers, B., Desmet, S.J., Deckers, J., Ray, D.W., Staels, B., de Bosscher, K., 2018. Molecular actions of PPARα in lipid metabolism and inflammation. Endocr Rev 39, 760–802.

Bouwman, H., Bornman, R., van den Berg, H., Kylin, H., 2013. Late lessons from early warnings: science, precaution, innovation. European Environment Agency, Copenhagen.

Bouwman, H., Kylin, H., Sereda, B., Bornman, R., 2012. High levels of DDT in breast milk: Intake, risk, lactation duration, and involvement of gender. Environmental Pollution 170, 63–70.

Bouwman, H., Yohannes, Y.B., Nakayama, S.M.M., Motohira, K., Ishizuka, M., Humphries, M.S., van der Schyff, V., du Preez, M., Dinkelmann, A., Ikenaka, Y., 2019. Evidence of impacts from DDT in pelican, cormorant, stork, and egret eggs from KwaZulu-Natal, South Africa. Chemosphere 225, 647–658.

Bouxsein, M.L., Boyd, S.K., Christiansen, B.A., Guldberg, R.E., Jepsen, K.J., Müller, R., 2010. Guidelines for assessment of bone microstructure in rodents using micro-computed tomography. Journal of Bone and Mineral Research 25, 1468–1486.

Buckley, D.B., Klaassen, C.D., 2009. Induction of mouse UDP-glucuronosyltransferase mRNA expression in liver and intestine by activators of aryl-hydrocarbon receptor, constitutive androstane receptor, pregnane X receptor, peroxisome proliferator-activated receptor α, and nuclear factor erythroid 2-related factor 2. Drug Metabolism and Disposition 37, 847–856.

Burgos-Aceves, M.A., Migliaccio, V., di Gregorio, I., Paolella, G., Lepretti, M., Faggio, C., Lionetti, L., 2021. 1,1,1-trichloro-2,2-bis (p-chlorophenyl)-ethane (DDT) and 1,1-Dichloro-2,2-bis (p, p'-chlorophenyl) ethylene (DDE) as endocrine disruptors in human and wildlife: A possible implication of mitochondria. Environ Toxicol Pharmacol.

Calzada, E., Onguka, O., Claypool, S.M., 2016. Phosphatidylethanolamine Metabolism

in Health and Disease, in: International Review of Cell and Molecular Biology. Elsevier Inc., pp. 29–88.

Campbell, G.M., Sophocleous, A., 2014. Quantitative analysis of bone and soft tissue by micro-computed tomography: applications to ex vivo and in vivo studies. Bonekey Rep 3.

Cao, Q., Shang, S., Han, X., Cao, D., Zhao, L., 2019. Evaluation on Heterogeneity of Fatty Liver in Rats: A Multiparameter Quantitative Analysis by Dual Energy CT. Acad Radiol 26, e47–e55.

Cavanaugh, D., Travis, E.L., Price, R.E., Gladish, G., White, R.A., Wang, M., Cody, D.D., 2006. Quantification of Bleomycin-Induced Murine Lung Damage In Vivo With Micro-Computed Tomography. Acad Radiol 13, 1505–1512.

Channa, K., Röllin, H.B., Nøst, T.H., Odland, J., Sandanger, T.M., 2012. Prenatal exposure to DDT in malaria endemic region following indoor residual spraying and in non-malaria coastal regions of South Africa. Science of the Total Environment 429, 183–190.

Chanyshev, M.D., Kosorotikov, N.I., Titov, S.E., Kolesnikov, N.N., Gulyaeva, L.F., 2014. Expression of microRNAs, CYP1A1 and CYP2B1 in the livers and ovaries of female rats treated with DDT and PAHs. Life Sci 103, 95–100.

Chen, F., Coslo, D.M., Chen, T., Zhang, L., Tian, Y., Smith, P.B., Patterson, A.D., Omiecinski, C.J., 2019. Metabolomic Approaches Reveal the Role of CAR in Energy Metabolism. J Proteome Res 18, 239–251.

Crist, E., Mora, C., Engelman, R., 2017. The interaction of human population, food production, and biodiversity protection. Science (1979) 356, 260–264.

Dai, Y., Huo, X., Cheng, Z., Faas, M.M., Xu, X., 2020. Early-life exposure to widespread environmental toxicants and maternal-fetal health risk: A focus on metabolomic biomarkers. Science of the Total Environment 739.

Dai, Y., Luo, J., Xiang, E., Guo, Q., He, Z., Gong, Z., Sun, X., Kou, H., Xu, K., Fan, C., Liu, J., Qiu, S., Wang, Y., Wang, H., Guo, Y., 2021. Prenatal Exposure to Retrorsine Induces Developmental Toxicity and Hepatotoxicity of Fetal Rats in a Sex-Dependent Manner: The Role of Pregnane X Receptor Activation. J Agric Food Chem 69, 3219–3231.

de Langhe, E., vande Velde, G., Hostens, J., Himmelreich, U., Nemery, B., Luyten, F.P.,

Vanoirbeek, J., Lories, R.J., 2012. Quantification of lung fibrosis and emphysema in mice using automated micro-computed tomography. PLoS One 7.

Delport, R., Bornman, R., MacIntyre, U.E., Oosthuizen, N.M., Becker, P.J., Aneck-Hahn, N.H., de Jager, C., 2011. Changes in retinol-binding protein concentrations and thyroid homeostasis with nonoccupational exposure to DDT. Environ Health Perspect 119, 647–651.

Deribe, E., Rosseland, B.O., Borgstrøm, R., Salbu, B., Gebremariam, Z., Dadebo, E., Skipperud, L., Eklo, O.M., 2013. Biomagnification of DDT and its metabolites in four fish species of a tropical lake. Ecotoxicol Environ Saf 95, 10–18.

Diwan, V., Mistry, A., Gobe, G., Brown, L., 2013. Adenine-induced chronic kidney and cardiovascular damage in rats. J Pharmacol Toxicol Methods 68, 197–207.

Eguchi, A., Sakurai, K., Watanabe, M., Mori, C., 2017. Exploration of potential biomarkers and related biological pathways for PCB exposure in maternal and cord serumA pilot birth cohort study in Chiba, Japan. Environ Int 102, 157–164.

Elrick, M.M., Kramer, J.A., Alden, C.L., Blomme, E.A.G., Bunch, R.T., Cabonce, M.A., Curtiss, S.W., Kier, L.D., Kolaja, K.L., Rodi, C.P., Morris, D.L., 2005. Differential Display in Rat Livers Treated for 13 Weeks with Phenobarbital Implicates a Role for Metabolic and Oxidative Stress in Nongenotoxic Carcinogenicity. Toxicol Pathol 33, 118–126.

Eskenazi, B., An, S., Rauch, S.A., Coker, E.S., Maphula, A., Obida, M., Crause, M., Kogut, K.R., Bornman, R., Chevrier, J., 2018. Prenatal exposure to DDT and pyrethroids for malaria control and child neurodevelopment: The VHEMBE cohort, South Africa. Environ Health Perspect 126, 047004-1-047004–11.

Feldkamp, L.A., Davis, L.C., Kress, J.W., 1984. Practical cone-beam algorithm. J. Opt. Soc. Am. A 1, 612–619.

Ferdinandusse, S., Houten, S.M., 2006. Peroxisomes and bile acid biosynthesis. Biochim Biophys Acta Mol Cell Res 1763, 1427–1440.

Fiebig, T., Boll, H., Figueiredo, G., Kerl, H.U., Nittka, S., Groden, C., Kramer, M., Brockmann, M.A., 2012. Three-dimensional in vivo imaging of the murine liver: A micro-computed tomography-based anatomical study. PLoS One 7.

Fischer, I., Milton, C., Wallace, H., 2020. Toxicity testing is evolving! Toxicol Res (Camb) 9, 67–80.

Foti, R.S., Dalvie, D.K., 2016. Cytochrome P450 and non-cytochrome P450 oxidative metabolism: Contributions to the pharmacokinetics, safety, and efficacy of xenobiotics. Drug Metabolism and Disposition 44, 1229–1245.

Fouillet, X., Tournier, H., Khan, H., Sabitha, S., Burkhardt, S., Terrier, F., Schneider, M., 1995. Enhancement of Computed Tomography Liver Contrast Using Iomeprol-Containing Liposomes and Detection of Small Liver Tumors in Rats. Acad Radiol 2, 576–583.

Fredin, M.F., Hultin, L., Hyberg, G., Rehnström, E., Hörnquist, E.H., Melgar, S., Jansson, L., 2008. Predicting and monitoring colitis development in mice by micro-computed tomography. Inflamm Bowel Dis 14, 491–499.

Gaggini, M., Sabatino, L., Vassalle, C., 2020. Conventional and innovative methods to assess oxidativestressbiomarkersintheclinicalcardiovascular setting. Biotechniques 68, 223–231.

Gährs, M., Schrenk, D., 2021. Suppression of apoptotic signaling in rat hepatocytes by non-dioxin-like polychlorinated biphenyls depends on the receptors CAR and PXR. Toxicology 464.

George, J.L., Mitchell, R.T., 1947. The Effects of Feeding DDT-Treated Insects to Nestling Birds 1. J Econ Entomol 40, 782–789.

Gerber, R., Smit, N.J., van Vuren, J.H.J., Nakayama, S.M.M., Yohannes, Y.B., Ikenaka, Y., Ishizuka, M., Wepener, V., 2016. Bioaccumulation and human health risk assessment of DDT and other organochlorine pesticides in an apex aquatic predator from a premier conservation area. Science of the Total Environment 550, 522–533.

Govere, J.M., Durrheim, D.N., Kunene, S., 2002. Malaria trends in South Africa and Swaziland and the introduction of synthetic pyrethroids to replace DDT for malaria vector control. S Afr J Sci 98, 19–21.

Graessler, J., Schwudke, D., Schwarz, P.E.H., Herzog, R., Schevchenko, A., Bornstein, S.R., 2009. Top-down lipidomics reveals ether lipid deficiency in blood plasma of hypertensive patients. PLoS One 4.

Griffin, B.R., Faubel, S., Edelstein, C.L., 2019. Biomarkers of drug-induced kidney toxicity. Ther Drug Monit 41, 213–226.

Hakkola, J., Hukkanen, J., Turpeinen, M., Pelkonen, O., 2020. Inhibition and induction of CYP enzymes in humans: an update. Arch Toxicol 94, 3671–3722.

Hall, A.P., Elcombe, C.R., Foster, J.R., Harada, T., Kaufmann, W., Knippel, A., Küttler, K., Malarkey, D.E., Maronpot, R.R., Nishikawa, A., Nolte, T., Schulte, A., Strauss, V., York, M.J., 2012. Liver hypertrophy: A review of adaptive (adverse and non-adverse) changes-conclusions from the 3rd international ESTP expert workshop. Toxicol Pathol 40, 971–994.

Hamid, M., Liu, D., Abdulrahim, Y., Liu, Y., Qian, G., Khan, A., Gan, F., Huang, K., 2017. Amelioration of CCl4-induced liver injury in rats by selenizing Astragalus polysaccharides: Role of proinflammatory cytokines, oxidative stress and hepatic stellate cells. Res Vet Sci 114, 202–211.

Harada, T., Takeda, M., Kojima, S., Tomiyama, N., 2016. Toxicity and carcinogenicity of dichlorodiphenyltrichloroethane (DDT). Toxicol Res 32, 21–33.

Harada, T., Yamaguchi, S., Ohtsuka, R., Takeda, M., Fujisawa, H., Yoshida, T., Enomoto, A., Chiba, Y., Fukumori, J., Kojima, S., Tomiyama, N., Saka, M., Ozaki, M., Maita, K., 2003. Mechanisms of Promotion and Progression of Preneoplastic Lesions in Hepatocarcinogenesis by DDT in F344 Rats. Toxicol Pathol 31, 87–98.

Hardisty, J.F., Brix, A.E., 2005. Comparative Hepatic Toxicity: PrechroniC/Chronic Liver Toxicity in Rodents. Toxicol Pathol 33, 35–40.

Harizi, H., Corcuff, J.B., Gualde, N., 2008. Arachidonic-acid-derived eicosanoids: roles in biology and immunopathology. Trends Mol Med 14, 461–469.

Hasin, Y., Seldin, M., Lusis, A., 2017. Multi-omics approaches to disease. Genome Biol 18.

Hathcock, J.T., Stickle, R.L., 1993. Principles and Concepts of Computed Tomography. Veterinary Clinics of North America: Small Animal Practice 23, 399–415.

Hemmati, M, Motamedrad, M., Shokouhifar, A., Hemmati, Mina, Moossavi, M., 2019. The regulatory effect of saffron stigma on the gene expression of the glucose metabolism key enzymes and stress proteins in streptozotocin-induced diabetic rats. Res Pharm Sci 14, 255–262.

Hernandez, J.P., Mota, L.C., Huang, W., Moore, D.D., Baldwin, W.S., 2009. Sexually dimorphic regulation and induction of P450s by the constitutive androstane receptor (CAR). Toxicology 256, 53–64.

Hirai, A., Sugio, S., Nimako, C., Nakayama, S.M.M., Kato, K., Takahashi, K., Arizono, K., Hirano, T., Hoshi, N., Fujioka, K., Taira, K., Ishizuka, M., Wake, H., Ikenaka, Y.,

2022. Ca2+ imaging with two-photon microscopy to detect the disruption of brain function in mice administered neonicotinoid insecticides. Sci Rep 12.

Hrycay, E.G., Bandiera, S.M., 2015. Involvement of Cytochrome P450 in Reactive Oxygen Species Formation and Cancer, in: Advances in Pharmacology. Academic Press Inc., pp. 35–84.

Hu, X., Li, S., Cirillo, P., Krigbaum, N., Tran, V.L., Ishikawa, T., la Merrill, M.A., Jones, D.P., Cohn, B., 2020. Metabolome Wide Association Study of serum DDT and DDE in Pregnancy and Early Postpartum. Reproductive Toxicology 92, 129–137.

Huang, S., Chaudhary, K., Garmire, L.X., 2017. More is better: Recent progress in multi-omics data integration methods. Front Genet 8.

Imaoka, S., Osada, M., Minamiyama, Y., Yukimura, T., Toyokuni, S., Takemura, S., Hiroi, T., Funae, Y., 2004. Role of phenobarbital-inducible cytochrome P450s as a source of active oxygen species in DNA-oxidation. Cancer Lett 203, 117–125.

International Agency for Research on Cancer, 2015. IARC Monographs evaluate DDT, lindane, and 2,4-D.

Issaq, H.J., Abbott, E., Veenstra, T.D., 2008. Utility of separation science in metabolomic studies. J Sep Sci 31, 1936–1947.

Jalouli, M., Carlsson, L., Améen, C., Lindén, D., Ljungberg, A., Michalik, L., Edén, S., Wahli, W., Oscarsson, J., 2003. Sex difference in hepatic peroxisome proliferator-activated receptor α expression: Influence of pituitary and gonadal hormones. Endocrinology 144, 101–109.

Jayaraj, R., Megha, P., Sreedev, P., 2016. Review Article. Organochlorine pesticides, their toxic effects on living organisms and their fate in the environment. Interdiscip Toxicol 9, 90–100.

Jellali, R., Zeller, P., Gilard, F., Legendre, A., Fleury, M.J., Jacques, S., Tcherkez, G., Leclerc, E., 2018. Effects of DDT and permethrin on rat hepatocytes cultivated in microfluidic biochips: Metabolomics and gene expression study. Environ Toxicol Pharmacol 59, 1–12.

Kalender, W.A., 2006. X-ray computed tomography. Phys Med Biol 51, R29–R43.

Kamata, R., Shiraishi, F., Nakamura, K., 2020. Avian eggshell thinning caused by transovarian exposure to o,p′-DDT: changes in histology and calcium-binding protein production in the oviduct uterus. J Toxicol Sci 45, 131–136.

Kataba, A., Nakayama, S.M.M., Yohannes, Y.B., Toyomaki, H., Nakata, H., Ikenaka, Y., Ishizuka, M., 2021. Effects of zinc on tissue uptake and toxicity of lead in sprague dawley rat. Journal of Veterinary Medical Science 83, 1674–1685.

Kato, R., Yamazoe, Y., 1992. Sex-specific cytochrome P450 as a cause of sex-and species-related differences in drug toxicity. Toxicol Lett 64165, 661–667.

Kawase, A., Fujii, A., Negoro, M., Akai, R., Ishikubo, M., Komura, H., Iwaki, M., 2008. Regular Article Differences in Cytochrome P450 and Nuclear Receptor mRNA Levels in Liver and Small Intestines between SD and DA Rats. Drug Metab. Pharmacokinet 23, 196–206.

Kazantseva, Y.A., Yarushkin, A.A., Pustylnyak, V.O., 2013. Dichlorodiphenyltrichloroethane technical mixture regulates cell cycle and apoptosis genes through the activation of CAR and ERα in mouse livers. Toxicol Appl Pharmacol 271, 137–143.

Kelce, W.R., Stone, C.R., Laws, S.C., Gray, L.E., Kemppainen, J.A., Wilson, E.M., 1995. Persistent DDT metabolite p,p'-DDE is a potent androgen receptor antagonist. Nature 375, 581–585.

Kim, S.Y., Yoon, Y.M., Hwang, T.S., Shin, C.H., Lim, J.S., Yeon, S.C., Lee, H.C., 2018. Comparison for radiographic measurements of canine liver size by left and right recumbency. Journal of Veterinary Clinics 35, 13–16.

King, S.E., McBirney, M., Beck, D., Sadler-Riggleman, I., Nilsson, E., Skinner, M.K., 2019. Sperm epimutation biomarkers of obesity and pathologies following DDT induced epigenetic transgenerational inheritance of disease. Environ Epigenet 5.

Kitamura, S., Shimizu, Y., Shiraga, Y., Yoshida, M., Sugihara, K., Ohta, S., 2002. Reductive metabolism of p, p-DDT and o, p-DDT by rat liver cytochrome P450. Drug Metabolism and Disposition 30, 113–118.

Konno, Y., Sekimoto, M., Nemoto, K., Degawa, M., 2004. Sex difference in induction of hepatic CYP2B and CYP3A subfamily enzymes by nicardipine and nifedipine in rats. Toxicol Appl Pharmacol 196, 20–28.

Koureas, M., Rousou, X., Haftiki, H., Mouchtouri, V.A., Rachiotis, G., Rakitski, V., Tsakalof, A., Hadjichristodoulou, C., 2019. Spatial and temporal distribution of p,p′-DDE (1-dichloro-2,2-bis (p-chlorophenyl) ethylene) blood levels across the globe. A systematic review and meta-analysis. Science of the Total Environment 686, 440–

451.

Krause, W., 1977. Influence of DDT, DDVP and Malathion on FSH, LH and Testosterone Serum Levels and Testosterone Concentration in Testis. Bull Environ Contam Toxicol 18, 231–242.

Krigbaum, N.Y., Cirillo, P.M., Flom, J.D., McDonald, J.A., Terry, M.B., Cohn, B.A., 2020. In utero DDT exposure and breast density before age 50. Reproductive Toxicology 92, 85–90.

Kubo, S., Hirano, T., Miyata, Y., Ohno, S., Onaru, K., Ikenaka, Y., Nakayama, S.M.M., Ishizuka, M., Mantani, Y., Yokoyama, T., Hoshi, N., 2022. Sex-specific behavioral effects of acute exposure to the neonicotinoid clothianidin in mice. Toxicol Appl Pharmacol 456.

Kubsad, D., Nilsson, E.E., King, S.E., Sadler-Riggleman, I., Beck, D., Skinner, M.K., 2019. Assessment of Glyphosate Induced Epigenetic Transgenerational Inheritance of Pathologies and Sperm Epimutations: Generational Toxicology. Sci Rep 9.

la Vecchia, C., Negri, E., 2014. A review of epidemiological data on epilepsy, phenobarbital, and risk of liver cancer. European Journal of Cancer Prevention 23, 1–7.

Lack, J.B., Greene, D.U., Conroy, C.J., Hamilton, M.J., Braun, J.K., Mares, M.A., van den Bussche, R.A., 2012. Invasion facilitates hybridization with introgression in the Rattus rattus species complex. Mol Ecol 21, 3545–3561.

Lake, B.G., 2018. Human relevance of rodent liver tumour formation by constitutive androstane receptor (CAR) activators. Toxicol Res (Camb) 7, 697–717.

Landrigan, P.J., Fuller, R., Acosta, N.J.R., Adeyi, O., Arnold, R., Basu, N. (Nil), Baldé, A.B., Bertollini, R., Bose-O'Reilly, S., Boufford, J.I., Breysse, P.N., Chiles, T., Mahidol, C., Coll-Seck, A.M., Cropper, M.L., Fobil, J., Fuster, V., Greenstone, M., Haines, A., Hanrahan, D., Hunter, D., Khare, M., Krupnick, A., Lanphear, B., Lohani, B., Martin, K., Mathiasen, K. v., McTeer, M.A., Murray, C.J.L., Ndahimananjara, J.D., Perera, F., Potočnik, J., Preker, A.S., Ramesh, J., Rockström, J., Salinas, C., Samson, L.D., Sandilya, K., Sly, P.D., Smith, K.R., Steiner, A., Stewart, R.B., Suk, W.A., van Schayck, O.C.P., Yadama, G.N., Yumkella, K., Zhong, M., 2018. The Lancet Commission on pollution and health. The Lancet 391, 462–512.

Larsson, S.C., Kumlin, M., Ingelman-Sundberg, M., Wolk, A., 2004. Dietary long-chain

n3 fatty acids for the prevention of cancer: a review of potential mechanisms 1-3.

Lcmerrill, M., Karey, E., Moshier, E., Lindtner, C., la Frano, M.R., Newman, J.W., Buettner, C., 2014. Perinatal exposure of mice to the pesticide DDT impairs energy expenditure and metabolism in adult female offspring. PLoS One 9.

Ledda-Columbano, G.M., Pibiri, M., Concas, D., Molotzu, F., Simbula, G., Cossu, C., Columbano, A., 2003. Sex difference in the proliferative response of mouse hepatocytes to treatment with the CAR ligand, TCPOBOP. Carcinogenesis 24, 1059–1065.

Lee, K.J., Wui, S.U., Heo, J., Kim, S.H., Jeong, J.Y., Lee, J. bin, 2003. DDT Reduced Testosterone and Aromatase Activity Via ER Receptor in Leydig Cell. Environmental Analysis Health and Toxicology 18, 95–100.

Li, L., Bao, X., Zhang, Q.Y., Negishi, M., Ding, X., 2017. Role of Cyp2b in phenobarbital-induced hepatocyte proliferation in mice. Drug Metabolism and Disposition 45, 977–981.

Liaset, B., Madsen, L., Hao, Q., Criales, G., Mellgren, G., Marschall, H.U., Hallenborg, P., Espe, M., Frøyland, L., Kristiansen, K., 2009. Fish protein hydrolysate elevates plasma bile acids and reduces visceral adipose tissue mass in rats. Biochim Biophys Acta Mol Cell Biol Lipids 1791, 254–262.

Lin, R.H., 2009. An intelligent model for liver disease diagnosis. Artif Intell Med 47, 53–62.

Lionetto, M.G., Caricato, R., Giordano, M.E., 2019. Pollution Biomarkers in Environmental and Human Biomonitoring. Open Biomark J 9, 1–9.

Liu, C.M., Zheng, Y.L., Lu, J., Zhang, Z.F., Fan, S.H., Wu, D.M., Ma, J.Q., 2010. Quercetin protects rat liver against lead-induced oxidative stress and apoptosis. Environ Toxicol Pharmacol 29, 158–166.

Liu, J., Yang, Ye, Yang, Yan, Zhang, Y., Liu, W., 2011. Disrupting effects of bifenthrin on ovulatory gene expression and prostaglandin synthesis in rat ovarian granulosa cells. Toxicology 282, 47–55.

Liu, L., Wu, Q., Miao, X., Fan, T., Meng, Z., Chen, X., Zhu, W., 2022. Study on toxicity effects of environmental pollutants based on metabolomics: A review. Chemosphere 286.

Liu, S., Kawamoto, T., Morita, O., Yoshinari, K., Honda, H., 2017. Discriminating

between adaptive and carcinogenic liver hypertrophy in rat studies using logistic ridge regression analysis of toxicogenomic data: The mode of action and predictive models. Toxicol Appl Pharmacol 318, 79–87.

Lopez-Clavijo, A.F., Gaud, C., C. Sousa, B., Nguyen, A., Fedorova, M., Ni, Z., O'Donnell, V.B., Wakelam, M.J.O., Andrews, S., 2021. BioPAN: A web-based tool to explore mammalian lipidome metabolic pathways on LIPID MAPS. F1000Res 10.

Lundberg, R., Jenssen, B.M., Leiva-Presa, À., Rönn, M., Hernhag, C., Wejheden, C., Larsson, S., Örberg, J., Lind, P.M., 2007. Effects of short-term exposure to the DDT metabolite p,p′-DDE on bone tissue in male common frog (Rana temporaria). Journal of Toxicology and Environmental Health - Part A: Current Issues 70, 614–619.

Luvizotto, R.A.M., Nascimento, A.F., Veeramachaneni, S., Liu, C., Wang, X.D., 2010. Chronic alcohol intake upregulates hepatic expression of carotenoid cleavage enzymes and PPAR in rats. Journal of Nutrition 140, 1808–1814.

Lv, J., Guo, L., Gu, Y., Xu, Y., Xue, Q., Yang, X., Wang, Q.N., Meng, X.M., Xu, D.X., Pan, X.F., Xu, S., Huang, Y., 2022. National temporal trend for organophosphate pesticide DDT exposure and associations with chronic kidney disease using age-adapted eGFR model. Environ Int 169.

Marouani, N., Hallegue, D., Sakly, M., Benkhalifa, M., ben Rhouma, K., Tebourbi, O., 2017. p,p'-DDT induces testicular oxidative stress-induced apoptosis in adult rats. Reproductive Biology and Endocrinology 15.

Matsuzawa, T., Nomura, M., Unno, T., 1993. Clinical Pathology Reference Ranges of Laboratory Animals. Journal of Veterinary Medical Science 55, 351–362.

Mayr, A., Klambauer, G., Unterthiner, T., Hochreiter, S., 2016. DeepTox: Toxicity prediction using deep learning. Front Environ Sci 3.

Meech, R., Hu, D.G., Mckinnon, R.A., Mubarokah, N., Haines, A.Z., Nair, P.C., Rowland, A., Mackenzie, P.I., 2019. The UDP-Glycosyltransferase (UGT) Superfamily: New Members, New Functions, And Novel Paradigms. Physiol Rev 99, 1153–1222.

Mei, Q., Richards, K., Strong-Basalyga, K., Fauty, S.E., Taylor, A., Yamazaki, M., Prueksaritanont, T., Lin, J.H., Hochman, J., 2004. Using real-time quantitative TaqMan RT-PCR to evaluate the role of dexamethasone in gene regulation of rat P-glycoproteins mdr1a/1b and cytochrome P450 3A1/2. J Pharm Sci 93, 2488–2496.

Mellert, W., Kapp, M., Strauss, V., Wiemer, J., Kamp, H., Walk, T., Looser, R., Prokoudine, A., Fabian, E., Krennrich, G., Herold, M., van Ravenzwaay, B., 2011. Nutritional impact on the plasma metabolome of rats. Toxicol Lett 207, 173–181.

Mendell, J.T., Ap Rhys, C.M.J., Dietz, H.C., 2002. Separable roles for rent1/hUpf1 in altered splicing and decay of nonsense transcripts. Science (1979) 298, 419–422.

Michihara, A., Anraku, M., Abe, A., Haruko Kinoshita, H., Kamizaki, Y., Tomida, H., Akasaki, K., 2011. Comparison of Receptors and Enzymes Regulating Cholesterol Levels in Liver between SHR/NDmcr-cp Rats and Normotensive Wistar Kyoto Rats at Ten Weeks of Age. Biol Pharm Bull 34, 1116–1119.

Miksys, S., Hoffmann, E., Tyndale, R.F., 2000. Regional and Cellular Induction of Nicotine-Metabolizing CYP2B1 in Rat Brain by Chronic Nicotine Treatment, Biochemical Pharmacology.

Ming, Y.N., Zhang, J.Y., Wang, X.L., Li, C.M., Ma, S.C., Wang, Z.Y., Liu, X.L., Li, X.B., Mao, Y.M., 2017. Liquid chromatography mass spectrometry-based profiling of phosphatidylcholine and phosphatidylethanolamine in the plasma and liver of acetaminophen-induced liver injured mice. Lipids Health Dis 16.

Miura, T., Kimura, N., Yamada, T., Shimizu, T., Nanashima, N., Yamana, D., Hakamada, K., Tsuchida, S., 2011. Sustained repression and translocation of Ntcp and expression of Mrp4 for cholestasis after rat 90% partial hepatectomy. J Hepatol 55, 407–414.

Moore, D.D., Kato, S., Xie, W., Mangelsdorf, D.J., Schmidt, D.R., Xiao, R., Kliewer, S.A., 2006. International union of pharmacology. LXII. The NR1H and NR1I receptors: Constitutive androstane receptor, pregnene X receptor, farnesoid X receptor α, farnesoid X receptor β, liver X receptor α, liver X receptor β, and vitamin D receptor. Pharmacol Rev 58, 742–759.

Motohira, K., Ikenaka, Y., Yohannes, Y.B., Nakayama, S.M.M., Wepener, V., Smit, N.J., van VUREN, J.H.J., Sousa, A.C., Enuneku, A.A., Ogbomida, E.T., Ishizuka, M., 2019. Dichlorodiphenyltrichloroethane (DDT) levels in rat livers collected from a malaria vector control region. Journal of Veterinary Medical Science 81, 1575–1579.

Mrema, E.J., Rubino, F.M., Brambilla, G., Moretto, A., Tsatsakis, A.M., Colosio, C., 2013. Persistent organochlorinated pesticides and mechanisms of their toxicity. Toxicology 307, 74–88.

Muhammad, S., Long, X., Salman, M., 2020. COVID-19 pandemic and environmental pollution: A blessing in disguise? Science of the Total Environment 728.

Müller, P.B., Taboada, J., Hosgood, G., Partington, B.P., Vansteenhouse, J.L., Taylor, H.W., Wolfsheimer, K.J., 2000. Effects of Long-Term Phenobarbital Treatment on the Liver in Dogs. J Vet Intern Med 14, 165–171.

Nguyen, A., Rudge, S.A., Zhang, Q., Wakelam, M.J., 2017. Using lipidomics analysis to determine signalling and metabolic changes in cells. Curr Opin Biotechnol 43, 96–103.

Nilsson, E., King, S.E., McBirney, M., Kubsad, D., Pappalardo, M., Beck, D., Sadler-Riggleman, I., Skinner, M.K., 2018. Vinclozolin induced epigenetic transgenerational inheritance of pathologies and sperm epimutation biomarkers for specific diseases. PLoS One 13.

Nims, R.W., Lubet, R.A., Fox, S.D., Jones, C.R., Thomas, P.E., Reddy, A.B., Kocarek, T.A., 1998. Comparative pharmacodynamics of cyP2B induction BY DDT, DDE, AND DDD In male rat liver and cultured rat hepatocytes. J Toxicol Environ Health A 53, 455–477.

Okahashi, N., Ueda, M., Yasuda, S., Tsugawa, H., Arita, M., 2021. Global profiling of gut microbiota-associated lipid metabolites in antibiotic-treated mice by LC-MS/MS-based analyses. STAR Protoc 2.

Olefsky, J.M., 2001. Nuclear Receptor Minireview Series. Journal of Biological Chemistry 276, 36863–36864.

Ozawa shogo, Gamou Toshie, Habano Wataru, Inoue Kaoru, Yoshida Midori, Nishikawa Akiyoshi, Nemoto Kiyomitsu, Degawa Masakuni, 2011. Altered expression of GADD45 genes during the development of chemical-mediated liver hypertrophy and liver tumor promotion in rats. The Journal of Toxicological Science 36, 613–623.

Padayachee, K., Reynolds, C., Mateo, R., Amar, A., 2023. A global review of the temporal and spatial patterns of DDT and dieldrin monitoring in raptors. Science of the Total Environment.

Palipoch, S., Punsawad, C., 2013. Biochemical and histological study of rat liver and kidney injury induced by cisplatin. J Toxicol Pathol 26, 293–299.

Pampori Nisar A., H.S.B.H., 1996. Feminization of Hepatic Cytochrome P450s by

Nominal Levels of Growth Hormone in the Feminine Plasma Profile. Molecular Pharmacology 50, 1148–1156.

Paradies, G., Paradies, V., Ruggiero, F.M., Petrosillo, G., 2014. Oxidative stress, cardiolipin and mitochondrial dysfunction in nonalcoholic fatty liver disease. World J Gastroenterol 20, 14205–14218.

Parasuraman, S., 2011. Toxicological screening. J Pharmacol Pharmacother 2, 74–79.

Peixoto, P., Cartron, P.F., Serandour, A.A., Hervouet, E., 2020. From 1957 to nowadays: A brief history of epigenetics. Int J Mol Sci 21, 1–18.

Pellicoro, A., van den Heuvel, F.A.J., Geuken, M., Moshage, H., Jansen, P.L.M., Faber, K.N., 2007. Human and rat bile acid-CoA:Amino acid N-acyltransferase are liver-specific peroxisomal enzymes: Implications for intracellular bile salt transport. Hepatology 45, 340–348.

Peng, Y., Ren, H., Tao, H., He, C., Li, P., Wan, J.B., Su, H., 2019. Metabolomics study of the anti-inflammatory effects of endogenous omega-3 polyunsaturated fatty acids. RSC Adv 9, 41903–41912.

Petersson, J., Schreiber, O., Steege, A., Patzak, A., Hellsten, A., Phillipson, M., Holm, L., 2007. eNOS involved in colitis-induced mucosal blood flow increase. Am J Physiol Gastrointest Liver Phys-iol 293, 1281–1287.

Phillips, J.C., Price, R.J., Cunninghame, M.E., Osimitzf, T.G., Cockbumt Karl Gabriel, A.L., Preiss, F.J., Butler, W.H., Lake, B.G., 1997. Effect of Piperonyl Butoxide on Cell Replication and Xenobiotic Metabolism in the Livers of CD-1 Mice and F344 Rats 1 Effect of Piperonyl Butoxide on Cell Replication and Xenobiotic Metabolism in the Livers of CD-I Mice and F344 Rats. Fundamental and Applied Toxicology 38, 64–74.

Pikuleva, I.A., Waterman, M.R., 2013. Cytochromes P450: Roles in diseases. Journal of Biological Chemistry 288, 17091–17098.

Pisoschi, A.M., Pop, A., 2015. The role of antioxidants in the chemistry of oxidative stress: A review. Eur J Med Chem 97, 55–74.

Raies, A.B., Bajic, V.B., 2016. In silico toxicology: computational methods for the prediction of chemical toxicity. Wiley Interdiscip Rev Comput Mol Sci 147–172.

Ramirez, T., Daneshian, M., Kamp, H., Bois, F.Y., Clench, M.R., Coen, M., Donley, B., Fischer, S.M., Ekman, D.R., Fabian, E., Guillou, C., Heuer, J., Hogberg, H.T.,

Jungnickel, H., Keun, H.C., Krennrich, G., Krupp, E., Luch, A., Noor, F., Peter, E., Riefke, B., Seymour, M., Skinner, N., Smirnova, L., Verheij, E., Wagner, S., Hartung, T., van Ravenzwaay, B., Leist, M., 2013. Metabolomics in Toxicology and Preclinical Research. ALTEX 30, 209–225.

Rando, G., Wahli, W., 2011. Sex differences in nuclear receptor-regulated liver metabolic pathways. Biochim Biophys Acta Mol Basis Dis 1812, 964–973.

Resseguie, M., Song, J., Niculescu, M.D., Costa, K.-A., Randall, T.A., Zeisel, S.H., 2007. Phosphatidylethanolamine N -methyltransferase (PEMT) gene expression is induced by estrogen in human and mouse primary hepatocytes . The FASEB Journal 21, 2622–2632.

Riegler, T., Nejabat, M., Eichner, J., Stiebellehner, M., Subosits, S., Bilban, M., Zell, A., Huber, W.W., Schulte-Hermann, R., Grasl-Kraupp, B., 2015. Proinflammatory mesenchymal effects of the nongenotoxic hepatocarcinogen phenobarbital: A novel mechanism of antiapoptosis and tumor promotion. Carcinogenesis 36, 1521–1530.

Ritman, E.L., 2004. Micro-computed tomography - Current status and developments. Annu Rev Biomed Eng 6, 185–208.

Robins, J.H., Hingston, M., Matisoo-Smith, E., Ross, H.A., 2007. Identifying Rattus species using mitochondrial DNA. Mol Ecol Notes 7, 717–729.

Rohart, F., Gautier, B., Singh, A., Lê Cao, K.A., 2017. mixOmics: An R package for 'omics feature selection and multiple data integration. PLoS Comput Biol 13.

Rooney, J.P., Oshida, K., Kumar, R., Baldwin, W.S., Corton, J.C., 2019. Chemical activation of the constitutive androstane receptor leads to activation of oxidant-induced Nrf2. Toxicological Sciences 167, 77–91.

Ross, J., Plummer, S.M., Rode, A., Scheer, N., Bower, C.C., Vogel, O., Henderson, C.J., Wolf, C.R., Elcombe, C.R., 2010. Human constitutive androstane receptor (CAR) and pregnane X receptor (PXR) support the hypertrophic but not the hyperplastic response to the murine nongenotoxic hepatocarcinogens phenobarbital and chlordane in vivo. Toxicological Sciences 116, 452–466.

Russell, D.W., 2003. The enzymes, regulation, and genetics of bile acid synthesis. Annu Rev Biochem 72, 137–174.

Safe, S., 2020. Recent advances in understanding endocrine disruptors: DDT and related compounds. Fac Rev 9.

Saigusa, D., Okamura, Y., Motoike, I.N., Katoh, Y., Kurosawa, Y., Saijyo, R., Koshiba, S., Yasuda, J., Motohashi, H., Sugawara, J., Tanabe, O., Kinoshita, K., Yamamoto, M., 2016. Establishment of protocols for global metabolomics by LC-MS for biomarker discovery. PLoS One 11.

Salihovic, S., Ganna, A., Fall, T., Broeckling, C.D., Prenni, J.E., van Bavel, B., Lind, P.M., Ingelsson, E., Lind, L., 2016. The metabolic fingerprint of p,p'-DDE and HCB exposure in humans. Environ Int 88, 60–66.

Samira, O., Kadmiri, N. el, 2021. Dichlorodiphenyltrichloroethane (DDT) and breast cancer. Health Sci J 15.

Sanderson, J.T., 2006. The steroid hormone biosynthesis pathway as a target for endocrine-disrupting chemicals. Toxicological Sciences 94, 3–21.

Schwenzer, N.F., Springer, F., Schraml, C., Stefan, N., Machann, J., Schick, F., 2009. Non-invasive assessment and quantification of liver steatosis by ultrasound, computed tomography and magnetic resonance. J Hepatol 51, 433–445.

Schymanski, E.L., Jeon, J., Gulde, R., Fenner, K., Ruff, M., Singer, H.P., Hollender, J., 2014. Identifying small molecules via high resolution mass spectrometry: Communicating confidence. Environ Sci Technol 48, 2097–2098.

Semi, Lee., Hakyoung, Yoon., Kidong, Eom., 2019. Retrospective quantitative assessment of liver size by measurement of radiographic liver area in small-breed dogs. Am J Vet Res 80, 1122–1128.

Seo, K.H., Bartley, G.E., Tam, C., Kim, H.S., Kim, D.H., Chon, J.W., Kim, H., Yokoyama, W., 2016. Chardonnay grape seed flour ameliorates hepatic steatosis and insulin resistance via altered hepatic gene expression for oxidative stress, inflammation, and lipid and ceramide synthesis in diet-induced obese mice. PLoS One 11.

Sharma, A., Shukla, A., Attri, K., Kumar, M., Kumar, P., Suttee, A., Singh, G., Barnwal, R.P., Singla, N., 2020. Global trends in pesticides: A looming threat and viable alternatives. Ecotoxicol Environ Saf.

Sharma Msc, D.R., Thapa, R.B., Manandhar, H.K., Shrestha, S.M., Pradhan, S.B., 2012. Use Of Pesticides In Nepal And Impacts On Human Health And Environment. The Journal of Agriculture and Environment 13, 67–74.

Shizu, R., Benoki, S., Numakura, Y., Kodama, S., Miyata, M., Yamazoe, Y., Yoshinari, K., 2013. Xenobiotic-Induced Hepatocyte Proliferation Associated with Constitutive

Active/Androstane Receptor (CAR) or Peroxisome Proliferator-Activated Receptor α (PPARα) Is Enhanced by Pregnane X Receptor (PXR) Activation in Mice. PLoS One 8.

Shuhendler, A.J., Pu, K., Cui, L., Uetrecht, J.P., Rao, J., 2014. Real-time imaging of oxidative and nitrosative stress in the liver of live animals for drug-toxicity testing. Nat Biotechnol 32, 373–380.

Sierra-Santoyo, A., Hernández, M., Albores, A., Cebrián, M.E., 2000. Sex-Dependent Regulation of Hepatic Cytochrome P-450 by DDT. Toxicological Sciences 54, 81–87.

Simac, J., Badar, S., Farber, J., Brako, M.O., Giudice-Jimenez, R. lo, Raspa, S., Achore, M., MacKnight, S., 2017. Malaria elimination in Sri Lanka. Journal of Health Specialties 5, 60–65.

Singh, A., Shannon, C.P., Gautier, B., Rohart, F., Vacher, M., Tebbutt, S.J., Cao, K.A.L., 2019. DIABLO: An integrative approach for identifying key molecular drivers from multi-omics assays. Bioinformatics 35, 3055–3062.

Skinner, M.K., ben Maamar, M., Sadler-Riggleman, I., Beck, D., Nilsson, E., McBirney, M., Klukovich, R., Xie, Y., Tang, C., Yan, W., 2018. Alterations in sperm DNA methylation, non-coding RNA and histone retention associate with DDT-induced epigenetic transgenerational inheritance of disease. Epigenetics Chromatin 11.

Skoda, J., Dohnalova, K., Chalupsky, K., Stahl, A., Templin, M., Maixnerova, J., Micuda, S., Grøntved, L., Braeuning, A., Pavek, P., 2022. Off-target lipid metabolism disruption by the mouse constitutive androstane receptor ligand TCPOBOP in humanized mice. Biochem Pharmacol 197.

Song, Q., Chen, H., Li, Y., Zhou, H., Han, Q., Diao, X., 2016. Toxicological effects of benzo(a)pyrene, DDT and their mixture on the green mussel Perna viridis revealed by proteomic and metabolomic approaches. Chemosphere 144, 214–224.

Sonneveld, E., Jonas, A., Meijer, O.C., Brouwer, A., van der burg, B., 2007. Glucocorticoid-Enhanced expression of dioxin target genes through regulation of the Rat aryl hydrocarbon receptor. Toxicological Sciences 99, 455–469.

Steyn, L., Hoffman, J., Bouwman, H., Maina, A.W., Maina, J.N., 2018. Bone density and asymmetry are not related to DDT in House Sparrows: Insights from micro-focus X-ray computed tomography. Chemosphere 212, 734–743.

Sugihara, K., Kitamura, S., Ohta, S., 1998. Reductive dechlorination of of DDT to DDD by rat blood. Biochemistry and Molecular Biology International 45, 85–91.

Sun, J., Fang, R., Wang, H., Xu, D.X., Yang, J., Huang, X., Cozzolino, D., Fang, M., Huang, Y., 2022. A review of environmental metabolism disrupting chemicals and effect biomarkers associating disease risks: Where exposomics meets metabolomics. Environ Int.

Tanikawa, T., 1993. An Eye-Lens Weight Curve for Determining Age in Black Rats, Rattus rattus. J. Mamm. Soc. Japan 18, 49–51.

Thangavel, C., Dworakowski, W., Shapiro, B.H., 2006. Inducibility of male-specific isoforms of cytochrome P450 by sex-dependent growth hormone profiles in hepatocyte cultures from male but not female rats. Drug Metabolism and Disposition 34, 410–419.

Thomas S. Argyris, 1968. Liver growth associated with the induction of aminopyrine demethylase activity after phenobarbital treatment in adult male rats. J Pharmacol Exp Ther 164, 405–411.

Tsugawa, H., Cajka, T., Kind, T., Ma, Y., Higgins, B., Ikeda, K., Kanazawa, M., Vandergheynst, J., Fiehn, O., Arita, M., 2015. MS-DIAL: Data-independent MS/MS deconvolution for comprehensive metabolome analysis. Nat Methods 12, 523–526.

Tsugawa, H., Ikeda, K., Takahashi, M., Satoh, A., Mori, Y., Uchino, H., Okahashi, N., Yamada, Y., Tada, I., Bonini, P., Higashi, Y., Okazaki, Y., Zhou, Z., Zhu, Z.J., Koelmel, J., Cajka, T., Fiehn, O., Saito, K., Arita, Masanori, Arita, Makoto, 2020. A lipidome atlas in MS-DIAL 4. Nat Biotechnol 38, 1159–1163.

Tudi, M., Ruan, H.D., Wang, L., Lyu, J., Sadler, R., Connell, D., Chu, C., Phung, D.T., 2021. Agriculture development, pesticide application and its impact on the environment. Int J Environ Res Public Health 18, 1–24.

Tully, D.B., Bao, W., Goetz, A.K., Blystone, C.R., Ren, H., Schmid, J.E., Strader, L.F., Wood, C.R., Best, D.S., Narotsky, M.G., Wolf, D.C., Rockett, J.C., Dix, D.J., 2006. Gene expression profiling in liver and testis of rats to characterize the toxicity of triazole fungicides. Toxicol Appl Pharmacol 215, 260–273.

Ueda, A., Hamadeh, H.K., Webb, H.K., Yamamoto, Y., Sueyoshi, T., Afshari, C.A., Urgen, J.¨, Lehmann, M., Negishi, M., 2002. Diverse Roles of the Nuclear Orphan Receptor CAR in Regulating Hepatic Genes in Response to Phenobarbital. Mol Pharmacol 61,

1–6.

van den Berg, H., da Silva Bezerra, H.S., Al-Eryani, S., Chanda, E., Nagpal, B.N., Knox, T.B., Velayudhan, R., Yadav, R.S., 2021. Recent trends in global insecticide use for disease vector control and potential implications for resistance management. Sci Rep 11.

van den Berg, H., Manuweera, G., Konradsen, F., 2017. Global trends in the production and use of DDT for control of malaria and other vector-borne diseases. Malar J 16.

van der Veen, J.N., Kennelly, J.P., Wan, S., Vance, J.E., Vance, D.E., Jacobs, R.L., 2017. The critical role of phosphatidylcholine and phosphatidylethanolamine metabolism in health and disease. Biochim Biophys Acta Biomembr 1859, 1558–1572.

Viljoen, I.M., Bornman, R., Bouwman, H., 2016. DDT exposure of frogs: A case study from Limpopo Province, South Africa. Chemosphere 159, 335–341.

VoPham, T., Bertrand, K.A., Hart, J.E., Laden, F., Brooks, M.M., Yuan, J.M., Talbott, E.O., Ruddell, D., Chang, C.C.H., Weissfeld, J.L., 2017. Pesticide exposure and liver cancer: a review. Cancer Causes and Control 28, 177–190.

Wagner, M., Halilbasic, E., Marschall, H.U., Zollner, G., Fickert, P., Langner, C., Zatloukal, K., Denk, H., Trauner, M., 2005. CAR and PXR agonists stimulate hepatic bile acid and bilirubin detoxification and elimination pathways in mice. Hepatology 42, 420–430.

Wall, R., Ross, R.P., Fitzgerald, G.F., Stanton, C., 2010. Fatty acids from fish: The anti-inflammatory potential of long-chain omega-3 fatty acids. Nutr Rev 68, 280–289.

Walter J Rogan, Aimin Chen, 2005. Health risks and benefits of bis(4-chlorophenyl)-1,1,1-trichloroethane (DDT). The Lancet 366, 763–773.

Wang, D., Zhu, W., Wang, Y., Yan, J., Teng, M., Miao, J., Zhou, Z., 2017. Metabolomics Approach to Investigate Estrogen Receptor-Dependent and Independent Effects of o,p′-DDT in the Uterus and Brain of Immature Mice. J Agric Food Chem 65, 3609–3616.

Wang, L., Wu, G., Wu, F., Jiang, N., Lin, Y., 2017. Geniposide attenuates ANIT-induced cholestasis through regulation of transporters and enzymes involved in bile acids homeostasis in rats. J Ethnopharmacol 196, 178–185.

Water J Rogan, Aimin Chen, 2005. Health risks and benefits of bis(4-chlorophenyl)-1,1,1-trichloroethane (DDT). Lancet 366, 763–773.

Waxman, D.J., 1999. P450 Gene Induction by Structurally Diverse Xenochemicals: Central Role of Nuclear Receptors CAR, PXR, and PPAR 1. Arch Biochem Biophys 369, 11–23.

Waxman, D.J., Pampori, N.A., Ram, P.A., Agrawal, A.K., Shapiro, B.H., 1991. Interpulse interval in circulating growth hormone patterns regulates sexually dimorphic expression of hepatic cytochrome P450. Proc Natl Acad Sci U S A 88, 6868–6872.

Williams, G.P., Darbre, P.D., 2019. Low-dose environmental endocrine disruptors, increase aromatase activity, estradiol biosynthesis and cell proliferation in human breast cells. Mol Cell Endocrinol 486, 55–64.

Wilson, A.L., Courtenay, O., Kelly-Hope, L.A., Scott, T.W., Takken, W., Torr, S.J., Lindsay, S.W., 2020. The importance of vector control for the control and elimination of vector-borne diseases. PLoS Negl Trop Dis.

Winkelmann, C.T., Wise, L.D., 2009. High-throughput micro-computed tomography imaging as a method to evaluate rat and rabbit fetal skeletal abnormalities for developmental toxicity studies. J Pharmacol Toxicol Methods 59, 156–165.

Wise, D.L., Winkelmann, C.T., Dogdas, B., Bagchi, A., 2013. Micro-computed tomography imaging and analysis in developmental biology and toxicology. Birth Defects Res C Embryo Today 99, 71–82.

Wishart, D.S., Feunang, Y.D., Marcu, A., Guo, A.C., Liang, K., Vázquez-Fresno, R., Sajed, T., Johnson, D., Li, C., Karu, N., Sayeeda, Z., Lo, E., Assempour, N., Berjanskii, M., Singhal, S., Arndt, D., Liang, Y., Badran, H., Grant, J., Serra-Cayuela, A., Liu, Y., Mandal, R., Neveu, V., Pon, A., Knox, C., Wilson, M., Manach, C., Scalbert, A., 2018. HMDB 4.0: The human metabolome database for 2018. Nucleic Acids Res 46, D608–D617.

Wojciechowska, A., Mlynarczuk, J., Kotwica, J., 2017. Changes in the mRNA expression of structural proteins, hormone synthesis and secretion from bovine placentome sections after DDT and DDE treatment. Toxicology 375, 1–9.

Wolmarans, N.J., Bervoets, L., Gerber, R., Yohannes, Y.B., Nakayama, S.M., Ikenaka, Y., Ishizuka, M., Meire, P., Smit, N.J., Wepener, V., 2021. Bioaccumulation of DDT and other organochlorine pesticides in amphibians from two conservation areas within malaria risk regions of South Africa. Chemosphere 274.

Wolmarans, N.J., Bervoets, L., Meire, P., Wepener, V., 2022. Sub-lethal exposure to

malaria vector control pesticides causes alterations in liver metabolomics and behaviour of the African clawed frog (Xenopus laevis). Comparative Biochemistry and Physiology Part - C: Toxicology and Pharmacology 251.

World Health Organization, 2011. Global Malaria Programme The use of DDT in malaria vector control WHO position statement.

World Health Organization, 1979. DDT and its derivatives. World Health Organization.

Xiang, E., Guo, Q., Dai, Y. guo, Sun, X. xiang, Liu, J., Fan, C. peng, Wang, Y. qing, Qiu, S. kai, Wang, H., Guo, Y., 2020. Female-specific activation of pregnane X receptor mediates sex difference in fetal hepatotoxicity by prenatal monocrotaline exposure. Toxicol Appl Pharmacol 406.

Xin, Y., Song, G., Cereda, M., Kadlecek, S., Hamedani, H., Jiang, Y., Rajaei, J., Clapp, J., Profka, H., Meeder, N., Wu, J., Tustison, N.J., Gee, J.C., Rizi, R.R., 2015. Semiautomatic segmentation of longitudinal computed tomography images in a rat model of lung injury by surfactant depletion. J Appl Physiol 118, 377–385.

Xiong, Q., Xie, P., Li, H., Hao, L., Li, G., Qiu, T., Liu, Y., 2010. Acute Effects of Microcystins Exposure on theTranscription of Antioxidant Enzyme Genes in ThreeOrgans (Liver, Kidney, and Testis) of Male Wistar Rats. J Biochem Molecular Toxicology 24, 361–367.

Xuan, R., Zhao, X., Hu, D., Jian, J., Wang, T., Hu, C., 2015. Three-dimensional visualization of the microvasculature of bile duct ligation-induced liver fibrosis in rats by x-ray phase-contrast imaging computed tomography. Sci Rep 5.

Yanagiba, Y., Ito, Y., Kamijima, M., Gonzalez, F.J., Nakajima, T., 2009. Octachlorostyrene induces cytochrome P450, UDP-glucuronosyltransferase, and sulfotransferase via the aryl hydrocarbon receptor and constitutive androstane receptor. Toxicological Sciences 111, 19–26.

Yang, J., Ward, M.D., Kahr, B., 2017. Abuse of Rachel Carson and Misuse of DDT Science in the Service of Environmental Deregulation. Angewandte Chemie 129, 10158–10164.

Yi, M.J., Fashe, M., Arakawa, S., Moore, R., Sueyoshi, T., Negishi, M., 2020. Nuclear receptor CAR-ERα signaling regulates the estrogen sulfotransferase gene in the liver. Sci Rep 10.

Yna Kostka, G.;, Palut, D., Kopec´-, J., Szle ˛zak B, K.-, Ludwicki, J.K., 2000. Early

hepatic changes in rats induced by permethrin in comparison with DDT. Toxicology 142, 135–143.

Yohannes, Y.B., Ikenaka, Y., Ito, G., Nakayama, S.M.M., Mizukawa, H., Wepener, V., Smit, N.J., van Vuren, J.H.J., Ishizuka, M., 2017. Assessment of DDT contamination in house rat as a possible bioindicator in DDT-sprayed areas from Ethiopia and South Africa. Environmental Science and Pollution Research 24, 23763–23770.

Yohannes, Y.B., Ikenaka, Y., Saengtienchai, A., Watanabe, K.P., Nakayama, S.M.M., Ishizuka, M., 2013. Occurrence, distribution, and ecological risk assessment of DDTs and heavy metals in surface sediments from Lake Awassa-Ethiopian Rift Valley Lake. Environmental Science and Pollution Research 20, 8663–8671.

Yoshinari, K., 2019. Role of Nuclear Receptors PXR and CAR in Xenobiotic-Induced Hepatocyte Proliferation and Chemical Carcinogenesis. Biol. Pharm. Bull 42, 1243–1252.

You, L., 2004. Steroid hormone biotransformation and xenobiotic induction of hepatic steroid metabolizing enzymes. Chem Biol Interact 147, 233–246.

Zhang, H., Shao, X., Zhao, H., Li, X., Wei, J., Yang, C., Cai, Z., 2019. Integration of Metabolomics and Lipidomics Reveals Metabolic Mechanisms of Triclosan-Induced Toxicity in Human Hepatocytes. Environ Sci Technol 53, 5406–5415.

Zhang, J., Pan, C., Xu, T., Niu, Z., Ma, C., Xu, C., 2015. Interleukin 18 augments growth ability via NF-κB and p38/ATF2 pathways by targeting cyclin B1, cyclin B2, cyclin A2, and Bcl-2 in BRL-3A rat liver cells. Gene 563, 45–51.

Zhang, T., Creek, D.J., Barrett, M.P., Blackburn, G., Watson, D.G., 2012. Evaluation of coupling reversed phase, aqueous normal phase, and hydrophilic interaction liquid chromatography with orbitrap mass spectrometry for metabolomic studies of human urine. Anal Chem 84, 1994–2001.

Zhang, W., Jiang, F., Ou, J., 2011. Global pesticide consumption and pollution: with China as a focus. Proceedings of the International Academy of Ecology and Environmental Sciences 1, 125–144.

Zhang, X., Yang, Y., Su, J., Zheng, X., Wang, C., Chen, S., Liu, J., Lv, Y., Fan, S., Zhao, A., Chen, T., Jia, W., Wang, X., 2021. Age-related compositional changes and correlations of gut microbiome, serum metabolome, and immune factor in rats. Geroscience 43, 709–725.

Zhu, Q., Dong, Y., Li, X., Ni, C., Huang, T., Sun, J., Ge, R.S., 2020. Dehydroepiandrosterone and Its CYP7B1 Metabolite 7α-Hydroxydehydroepiandrosterone Regulates 11β-Hydroxysteroid Dehydrogenase 1 Directions in Rat Leydig Cells. Front Endocrinol (Lausanne) 10.

Zhu, Q.N., Xie, H.M., Zhang, D., Liu, J., Lu, Y.F., 2013. Hepatic bile acids and bile acid-related gene expression in pregnant and lactating rats. PeerJ 1.

Acknowledgement

I would like to express my deepest gratitude and pray for the wild rodents and Wistar rats that sacrificed their lives for this research. Without their precious sacrifices, I could not have carried out this research. I sincerely hope that the findings of this research will be of some help to them in the future.

I am deeply indebted to my supervisors, Professor Mayumi ISHIZUKA, Professor Yoshinori IKENAKA, Associate Professor Shouta M.M. NAKAYAMA, and Specially appointed invited lecturer YARED B. Yohannes (Laboratory of Toxicology, Graduate School of Veterinary Medicine, Hokkaido University) for their greatest support, enthusiastic instruction, and supervision.

I greatly thank Professor Toshio TSUBOTA (Laboratory of Wildlife Biology, Graduate School of Veterinary Medicine, Hokkaido University) and Associate Professor Akifumi EGUCHI (Center for Preventive Medical Sciences, Chiba University) for their great advice and review of this thesis.

I thank Assistant Professor Genya SHIMBO (Veterinary Teaching Hospital, Faculty of Veterinary Medicine, Hokkaido University), Assistant Professor Yuki MIZUNO (Central Institute of Isotope Science, Hokkaido University), Professor Victor WEPENER, Professor Nico J. SMIT and Professor Johan H. J. van VEREN (Water Research Group, Unit for Environmental Sciences and Management, Potchefstroom Campus, North-West University) for their instructions and kind supports.

I thank all members of the Laboratory of Toxicology, School of Veterinary Medicine, Hokkaido University, for their support and encouragement.

I am sincerely grateful for the financial support from Grants-in-Aid for Scientific Research from the Ministry of Education, Culture, Sports, Science and Technology of Japan and Hokkaido University World-leading Innovative and Smart Education (WISE) Program. I was able to focus on my research efforts and finish this thesis as a result of these financial aids.

At last, I extend my deepest appreciation and love to my mother, father, and young sister for their constant help and love, as well as to my lovely partners (chipmunks).

Abstract

Dichlorodiphenyltrichloroethane (DDT) is a well-known organochlorine pesticide currently used for the vector control of malaria. However, DDT persists in the environment and in animals, raising concerns regarding its ecological and biological risks. Risk evaluation is crucial for the continued use of DDT. This thesis aimed to 1) evaluate the effects of DDT on wild rats in DDT-sprayed areas in South Africa, 2) develop new methods for evaluating chemical toxicities, and 3) apply the developed methods to an *in vivo* study of DDT. First, in 2014 and 2017, wild rats were collected from South Africa, and the DDT concentrations in organs and gene expression in the liver and plasma metabolome were evaluated. A sex-linked metabolic enzyme in rats was found to alter its expression pattern in highly DDT-polluted areas. Metabolomic analysis revealed a possible association between DDT and bile acids. As molecular analyses targeting wild rodents are rare, this study encourages further research to understand the ecological effects of DDT.

This thesis also discuss a new toxicity test utilizing computed tomography (CT) and multiomics analysis. Phenobarbital, a potent activator of the constitutive androstane receptor (CAR), is used as a model chemical for toxicity testing as it can induce hepatomegaly, and both DDT and phenobarbital are related to the CAR. In addition, new (multiomics) and classical (histopathology and quantitative PCR) methods were combined to identify plasma biomarkers of the molecular processes of hepatomegaly. This study demonstrated that micro-CT could be used to evaluate phenobarbital-induced hepatomegaly in live animals. Another finding was that plasma lipids, such as ceramides, are effective markers for interpreting biological reactions to phenobarbital. This new approach with combined micro-CT, multiomics, and classical methods can visualize toxic effects induced by chemicals and their molecular processes throughout an animal's lifetime.

Finally, *in vivo* DDT exposure experiments were performed on rats from three generations. A low concentration of DDT and its metabolites were exposed through food. The expression of *Cyp2b1*, regulated by CAR, was markedly upregulated in DDT-exposed rats. Although hepatomegaly was observed in the female exposure group, histopathological changes and the significant toxic effects of DDT were not observed. CT

did not adequately detect DDT-induced hepatomegaly, possible because the effects of DDT on the liver were lesser than those seen with phenobarbital. Thus, further improvements in the CT-based method and its application to the toxicity testing of other chemicals are necessary. The current analyses had some limitations, such as evaluating histopathology, clinical biomarkers, and CT analysis only. Thus, the results do not indicate that the whole toxicity of DDT in mammals. Further research is crucial to reveal the biological and ecological effects of low-dose DDT.

Overall, *in vivo* and field studies of DDT must coexist to assess the effects of DDT on the environment. This study describes the possible ecological and biological risks in DDT-sprayed areas and a new method for evaluating chemical toxicity. These findings will contribute to the re-evaluation of the effects of DDT, the comparison of its risks and benefits, and appropriate vector control.

Japanese abstract

ジクロロジフェニルトリクロロエタン（DDT）は、マラリアのベクターコントールのため、現在も使用されている有機塩素系殺虫剤である。しかしながら、DDT は環境、動物の体内に長期間、蓄積し、その生物学的、また生態学的影響が懸念されている。DDT を継続して感染症制御に利用するうえで、そのリスク評価は必要不可欠と言える。それゆえ、本研究は１）南アフリカ共和国の DDT 散布地域における、野生げっ歯類への DDT の影響評価、２）化学物質の毒性を評価する新しいアプローチの開発、そして３）そのアプローチを用い、ＤＤＴの哺乳類に対する毒性影響の再評価を目的とした。最初に、南アフリカ共和国において２０１４年、２０１７年に野生ラットを採材し、臓器中 DDT 濃度の定量、肝臓を用いた定量的 PCR、血中メタボローム解析を実施した。本研究により、シトクロームＰ４５０（CYP）などの代謝酵素がＤＤＴにより、かく乱されている可能性を明らかにした。特に、DDT 汚染がラットにおける性特異的 CYP の発現パターンを変動させる可能性を示した。さらにメタボローム解析により、DDT の蓄積と血中胆汁酸が関連している可能性を明らかにした。本研究は、これまで報告が少ない野生ラットを用いた分子学的解析を講じ、散布環境における DDT の影響解明にアプローチするものであり、ＤＤＴの生態学的影響を理解する、さらなる研究を推進すると期待できる。

次に本論文は実験ラットを用い、コンピュータ断層撮影（ＣＴ）、ならびにマルチオミクス解析を活用した新規の毒性試験法を提案した。最初に、DDT が関与することが知られている核内受容体 constitutive androstane receptor（CAR）の強力なアクチベーターであり、さらに肝腫大を引き起こすことが知られているフェノバルビタールをモデル化合物として、毒性試験の開発を行った。さらに、新規手法（マルチオミクス）と従来型の手法（病理組織学的検査、定量的 PCR）を組み合わせ、肝腫大の分子学的プロセスを推定する血中バイオマーカーの探索を行った。本研究により、マイクロ CT がフェノバルビタール誘導性肝腫大を高い精度で生前に評価できることを確認した。またセラミドなどの血中脂質が、フェノバルビタールが引き起こす生体応答を反映するマーカーとして有益であることを示した。本研究はマイクロ CT、マルチオミクス、および従来の毒性試験を組み合わせて、毒性影響とその分子学的プロセスを、動物の生前に評価にする新しい毒性試験に光をあてた。

最後に、三世代のラットを用いた DDT の曝露試験を実施した。本研究では、低濃度の DDT とその代謝物の介餌曝露を実施した。コントロールに比べ、DDT 曝露群のラットで、CAR による制御が知られている *Cyp2b1* が有意に誘導された。しかしながら、DDT 曝露群

の雌ラットで肝臓サイズの増加が見られたものの、病理学的解析からは有意な変化が見られず、今回用いた手法では DDT の目立った毒性は検出されなかった。また CT を用いた肝臓サイズの生前診断では、DDT 曝露群のラットで見られた肝腫大を、CT が十分に検出することはできなかった。これは、病理試験の結果が示唆するように、DDT による肝臓への影響が、フェノバルビタールを用いた試験と比較し、小さかったことが要因と考えられる。CT 法のさらなる手法の改善と、他の化学物質の毒性試験への応用が必要不可欠である。今回用いた解析手法は病理学的試験、CT 解析、血中生化学マーカーのみと限定的であり、本成果が哺乳類における DDT の全毒性を示しているわけではない。低濃度の DDT が引き起こす生体、生態への影響について、さらなる研究が必要である。

環境における DDT の影響を評価するためには、動物実験とフィールド研究との共同が必要不可欠である。本研究は DDT 散布地域における、DDT の生物学的、生態学的毒性の可能性を提案し、化学物質の毒性を評価する新しいアプローチを開発した。これらの成果は、DDT の毒性影響を再評価し、そのリスクとベネフィットを比較することで、適切なベクターコントロールの実現を導くと期待できる。